UNIVERSITY DUISBURG-ESSEN

DOCTORAL THESIS

Grey-box models for flood forecasting and control

Author:
Euan RUSSANO

Supervisor:
Prof. Dr. - Ing. ANDRÉ NIEMANN
Co-Supervisor:
Dr. - Ing. DIRK SCHWANENBERG

A thesis submitted in fulfilment of the requirements for the degree of Doktor-Ingenieurs (Dr.-Ing.)

in the

Fakultät Ingenieurwissenschaften / Institut für Wasserbau und Wasserwirtschaft

December 11, 2017

Date of oral examination: September 18, 2017

Declaration of Authorship

I, Euan RUSSANO, declare that this thesis titled "Grey-box models for flood forecasting and control" and the work presented in it are my own. I confirm that:

- This work was done wholly while in candidature for a research degree at this University.
- Where any part of this thesis has previously been submitted for a degree or any other qualification at this University or any other institution, this has been clearly stated.
- Where I have consulted the published work of others, this is always clearly attributed.
- Where I have quoted from the work of others, the source is always given. With the exception of such quotations, this thesis is entirely my own work.
- I have acknowledged all main sources of help.
- Where the thesis is based on work done by myself jointly with others, I have made clear exactly what was done by others and what I have contributed myself.

Signed: 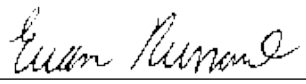

Date: 19.06.2017

UNIVERSITY DUISBURG-ESSEN

Abstract

Institut für Wasserbau und Wasserwirtschaft

Doktor-Ingenieurs (Dr.-Ing.)

Grey-box models for flood forecasting and control

by Euan RUSSANO

Flow forecasting and management are essential fields of study in hydrology to mitigate floods and droughts that can cause life or material losses. These undesired aspects arise the necessity of developing techniques to successfully control water resources. Recent developments in the control community have focused on the development of predictive control techniques, which demand computationally inexpensive models to be employed in optimization schemes. Data-driven models are well-known for low computational demand. However, their limitations, such as limited extrapolation capabilities and lack of physical meaning, arises the motivation for the development of grey-box models, which couples physically-based knowledge with a data-driven component, so as to increase the range of validity of the model, as well as to allow the physical understanding of each component of the model.
In the present work we develop two types of grey-box models for flow routing, one hydrological and the other hydraulic. The hydrological grey-box model is composed by the mass continuity equation for mass balance and the replacement of the momentum equation by an Artificial Neural Network which reproduces the discharge as a function of the storage and inflow. The hydraulic grey-box model implements also the mass-continuity component, but the momentum equation is replaced by a function which accounts for the water level upstream and downstream, enabling the reproduction of backwater effects. The hydrological model is tested in an academic and a real-world case (São Francisco River, Brazil). The hydraulic model is tested also in an academic and a real-world case (Main river, Germany). For both cases, we also implemented two control techniques: Proportional-Integral Control (PI) and Model Predictive Control (MPC). In the Main river case we tested a flood prevention event using the predictability of MPC control. Results shows that the developed techniques have similar accuracy with highly-detailed models, and the validation in the control tests shows that these models are promising as regards implementing in real-time control systems.

Keywords: Flow Routing, Grey-box Model, Artificial Neural Network.

Kurzfassung

Grey-box models for flood forecasting and control

Hochwasservorhersage und management sind wesentliche Bestandteile der Hydrologie und finden große Beachtung bei der Vermeidung von Überschwemmungen und Dürren, die Leben oder materielle Verluste kosten können. Auf Grund dieser Aspekte ergibt sich eine Notwendigkeit der entwickelten Techniken, um Wasserressourcen erfolgreich zu steuern. Aktuelle Entwicklungen auf dem Gebiet der Kontrolle konzentrierten sich auf die Entwicklung von Vorhersagesystemen, die rechnerisch einfache Modelle fordern, um diese in ein Optimierungssystem zu implementieren. Daten-gestützte Modelle sind bekannt für geringe rechnerische Anforderungen. Auf Grund von Einschränkungen, wie begrenzte Extrapolationsfähigkeiten und mangelnden physikalischen Übersetzungen, entsteht die Motivation zur Entwicklung von Grey-Box-Modellen. Diese verbinden physikalisches Wissen mit einer datengesteuerten Komponente, um den Bereich der Gültigkeit des Modells, sowie das physikalische Verständnis der einzelnen Komponenten des Modells zu erhöhen.
In der vorliegenden Arbeit wurden zwei wichtige Grey-Box-Modelle für eine hydrologische und eine hydraulische Abflussberechnung entwickelt. Das hydrologische Grey-Box-Modell besteht aus der Kontinuitätsgleichung der Masse und einem künstlichen neuralen Netz als Ersatz der Impulsgleichung, welches den Abfluss als Funktion in Abhängigkeit von der Speicherung und des Zuflusses wiedergibt. Das hydraulische Grey-Box-Modell berücksichtigt ebenfalls die Kontinuitätsgleichung, aber der Impuls wird durch eine Funktion ersetzt, welche den Wasserstand flussaufwärts und flussabwärts berechnet und es erlaubt, Rückstaueffekte abzubilden. Das hydrologische Modell wurde in einem numerischen und einem realen Fall (São Francisco Fluss - Brasilien) getestet. Das hydraulische Modell wurde ebenfalls in einer numerischen und einem realen Fall (Main - Deutschland) getestet. Für beide Fälle wurden zwei Steuerungstechniken implementiert: die Proportional-Integral Control (PI) und die Model Predictive Control (MPC). Für die Betrachtung des Mains wurde ein Hochwasservorsorge-Ereignis mit der Vorhersehbarkeit der MPC-Steuerung getestet. Ergebnisse zeigen, dass die entwickelten Techniken ähnliche Leistung wie die hochdetaillierten Modelle aufweisen, und die Validierung in den Kontrollprüfungen zeigt, dass diese Modelle in Echtzeit-Steuerungen vielversprechend in der Umsetzung sind.

Acknowledgements

Thanks at first to Jehovah God, for His support, for His love and for guiding me along the path I should walk.

I would like to express my sincere gratitude to my advisors, Prof Dr.-Ing. André Niemann and Dr.-Ing. Dirk Schwanenberg. I am sure that this work could never come to a conclusion without your support. I am also thankful for all the guidance, for the believe in this research and for the time we spent discussing and improving it together.

Thanks to CAPES, which provided the financial and organizational support, what enabled me to be fully dedicated to the development of the present work.

Thanks to the professors present on the doctoral examination, for your availability and willingness in being part of the accomplishment of this work.

Thanks to the University of Duisburg-Essen, for the opportunity of development of this work.

There are also friends and colleges made along the path of the development of this thesis, which I could never forget to be thankful for their contribution, either directly or indirectly. Especially mention to Rodolfo Alvarado Montero, for the suggestions, all the help with Matlab, Python, RTC-Tools and so many other tools...

Thanks for all the colleagues and friend in the Institute of Hydraulic Engineering and Water Resources Management, for the support, the suggestions and the nice discussions shared along this time.

At last but not least, to Elaine Ferreira Avelino, for her love and support, for understanding and for the help not only for this work, but in every aspect of my life.

Contents

List of Figures

List of Tables

List of Abbreviations

ANFIS	**A**daptive **N**eural **F**uzzy **I**nference **S**ystem
ANN	**A**rtificial **N**eural **N**etwork
ARX	**A**uto **R**egressive with E**X**ogenous input model
ARMAX	**A**uto **R**egressive **M**oving **A**verage with E**X**ogenous input model
BP	**B**ack **P**ropagation
DDM	**D**ata **D**riven **M**odelling
FNN	**F**uzzy **N**eural **N**etwork
GA	**G**enetic **A**lgorithm
IPOPT	**I**nterior **P**oint **OPT**imizer
LM	**L**evenberg **M**arquadt algorithm
MPC	**M**odel **P**redictive **C**ontrol
ODE	**O**rdinary **D**ifferential **E**quation
PDE	**P**artial **D**ifferential **E**quation
PI	**P**roportional **I**ntegral control
PID	**P**roportional **I**ntegral **D**erivative control
RR	**R**ainfall **R**unoff
RTC	**R**eal **T**ime **C**ontrol
TB-MPC	**T**ree **B**ased **M**odel **P**redictive **C**ontrol
TVD	**T**otal **V**ariation **D**iminishing

List of Symbols

A	cross-section area	m^2
A_f	flow cross-section area over hydraulic structure	m^2
C	Chezy coefficient	$\mathrm{m}^{\frac{1}{2}}/\mathrm{s}$
d	process disturbance	
e	error (difference between observed and simulated data)	
h	water level	m
K_p	proportional gain (PID control)	
K_I	integral gain (PID control)	
K_t	gain (Feed-forward control)	
L_x	reach length	m
Q	volumetric flow (discharge)	$\mathrm{m}^3\,\mathrm{s}^{-1}$
R	hydraulic radius	m
S	water volume	m^3
S_0	bottom slope	$-$
t	time	s
u	process input	
u_s	flow velocity	$\mathrm{m}\,\mathrm{s}^{-1}$
W_s	hydraulic structure width	m
x	process state vector	
y	process output vector	
z_s	crest level of hydraulic structure	m
ω_f	water surface width	m
θ_w	wind shear stress	
ε	resistance coefficient	$\mathrm{s}^2\mathrm{m}^{-5}$

Dedicated to all researches interested in innovating, not only in the field of hydraulics but in any field of science.…

Chapter 1

Introduction

1.1 Background

Throughout history, mankind has formed population cores close to water, whether rivers, seas, lakes or oceans. This occupation has been motivated mainly due to the need of drinkable water, navigation, hydropower, recreation and irrigation for agriculture.

In general, water streams are formed by the flux of underground water to the surface summed to surface runoff. The accumulation of such water forms a small watercourse, following an irregular path according to the local topography. As the water flows, it also receives contributions from smaller effluents and from precipitation. These contributions may vary in time and space and may occasionally cause floods, which potentially cause material damages and casualties, or droughts, that inhibit energy production by hydro power plants, also causing animals and human casualties by dehydration, among other losses (Van Overloop et al., 2011).

In Germany, August 2002, floods in the catchment area of the Rivers Vlatava, Elbe and Danube, in Central Europe, caused a total damage of 21.1 billion € and 37 casualties, besides affecting directly 337'000 people (Figure 1.1). The disaster underlined just how susceptible society is to extreme natural dangers. With a similar proportion, in Brazil, end of 1997, a flood in the river Doce affected riverside cities downstream Governador Valadares, leaving more than 57'000 people without home, 2 casualties and more than 7'000 affected dwellings (de Mendonça and de Souza, 2010).

FIGURE 1.1: View of Dresden main station during and after the flood, August 2002. Source: https://www.welt.de

According to a report from the United Nations and World Bank (2010), it is estimated in 3.3 millions the number of people that died from natural disasters between 1970 and 2010. From these disasters, especially in Africa, Central and Southern America, the floods account for more than 40% of the total events, as shown in Figure 1.2. Statistical tests show a low confidence level of a trend, which may show that prevention measures have likely been effective (The World Bank and United Nations, 2010).

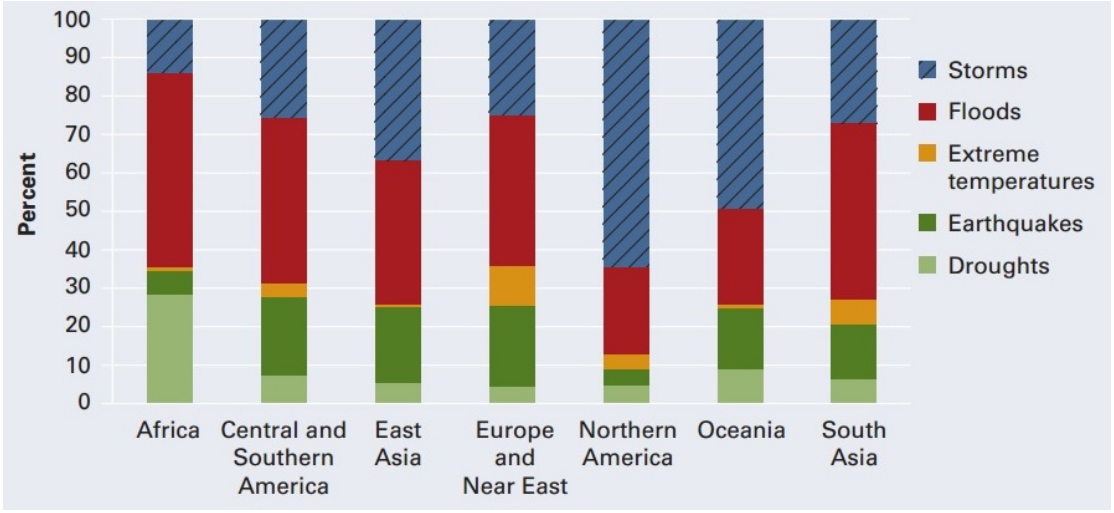

FIGURE 1.2: Worldly natural disasters distribution. Source: World Bank and United Nations, 2010

1.1.1 Flow Forecasting and Short-term Flood Management

Floods are problems that man has tried to resolve long-standing. As an example, a system of channels was developed by ancient Egyptians to protect tombs from becoming flooded before King Tutankhamen Epoch, in the area known as Valley of the Kings. Another example of great relevance was the dikes and channels built by Minister Yu in the Yellow River during Xia (BCE 2000-1500) Dynasty. These channels worked so well that later Minister Yu became Emperor Yu The Great, and the economy and society had a boost in development.

From beginning of 20^{th} century onwards, the accelerated population growth and urbanization expansion has imposed an additional pressure on government and regulatory agencies to avoid losses and damages caused by floods or droughts along watercourses, as well as make the best use of these for purposes such as navigation, recreation and energy production. For densely populated areas, there are also additional problems such as waste water management, storm water draining and pollution control.

In order to improve water resources management, there are two usual approaches. The first approach is the adoption of structural measures(Figure 1.3 a), such as the construction of dikes and dams. The second is the adoption of non-structural measures (Figure 1.3 b), such as the control of orifices and gates in real time as response to foreseen problems. Although structural measures are usually seen as safer to most people, the second approach is preferable over the first, since it may be manipulated and optimized, while the second one is static and of high cost, aside from not taking into account the actual scenario but just events envisioned at design time (Van Overloop et al., 2011).

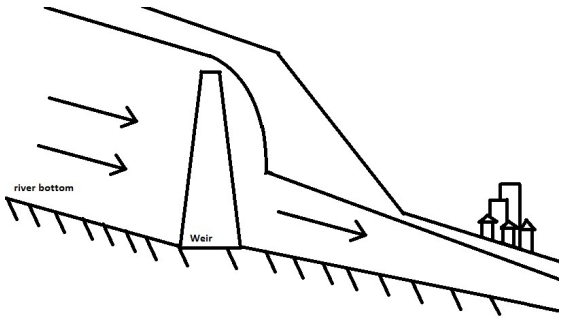

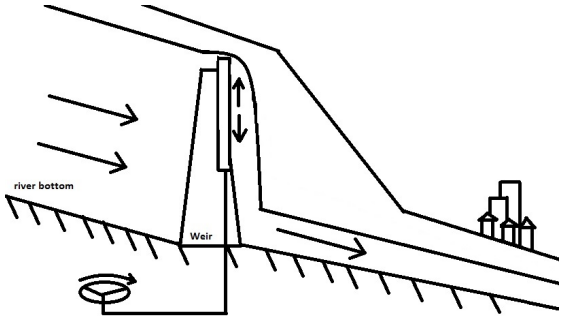

FIGURE 1.3: Example of a) Structural measure and b) non-structural measure.

Structural measures may be divided into physical and institutional interventions. As examples of traditional flood management interventions, one may cite the use of permeable pavements or artificial recharge for source control to reduce runoff, project wetlands, detention basins and reservoirs for improving storage of runoff, and construction of bypass channels for capacity enhancement of rivers (World Meteorological Organization, 2009).

The implementation of a non-structural measure involves the prediction of a scenario, in order to take necessary measures to prevent losses and damages. These predictions can besides that be used for a variety of other purposes, such as reallocation of water for navigation or human necessities during droughts, energy production optimization and flood prevention. These predictions or knowledge of future system behavior, known as forecast, may be focused in different time frames, such as short-term, medium-term and long-term forecasting. Short-term forecasting is usually centred in flood defense. Medium-term is usually applicable for reservoir operation, while long-term forecast can be important for planning and water resources management.

However, the streamflow forecasting may fall in some common related issues. Some of that may be cited are the predictability of the process and the ways it can be measured, the forecast uncertainty, which is intrinsically related to the predictability, scale and heterogeneity, which arises the question: How well the observed data represents the system behavior?

The issue related to the space is a very important one, as it may define the level of detail that will be taken into account during modeling process. For small basins which cover just a few hectares, the level of detail may consider the agriculture and urban drainage. In bigger basins, such as medium ones (up to 10^4 km^2) and big basins (bigger than 10^4 km^2), the level of detail may be

considerably less, especially depending on the objectives of the forecast, data availability and desired precision.

Another very important aspect is the way in which the dynamics of the process should be approached, as different aspects of the dynamics may be focused depending on properties of the basin under study. For an ungaged site, it may be important to take the transformation of rainfall into runoff into account. This type of approach is know as rainfall-runoff modeling. For sites regulated by hydraulic structures, the spatial translation of the discharge from an upstream location to a downstream one may be a better procedure. This approach is known as flow-routing. A brief introduction on both methods is given in the following sections.

1.1.2 Modelling of rainfall-runoff process

The process of precipitation-flow transformation is not a trivial one, and different techniques may be implemented to represent the dynamics of a specific basin. The technique to be used may depend on a series of factor, such as:

- the level of detail desired
- the range of validity of the model
- the time available for building and validating the model.
- the amount of available data (observed hydrographs or morphological data).

These are some of the factors to be taken into account when developing a model, which can fall into one of the following categories:

- physically-based model
- conceptual model
- data-driven model

In essence, a rainfall-runoff model (1.4) usually has two main components: storage elements and hydrological processes. A storage element is the main building block and it is filled or drained by the hydrological processes such as precipitation, evapotranspiration and runoff. These processes may depend on one or more parameters in the model.

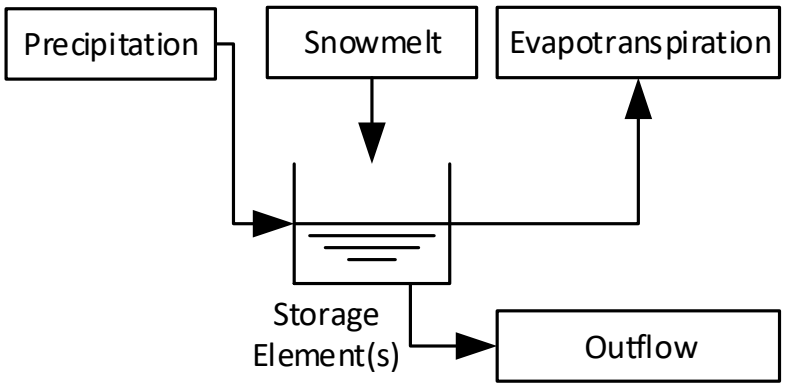

FIGURE 1.4: Simple illustration of Rainfall-Runoff model.

The level of detail of these components described inside of a model depends on the modeling approach used. A physically-based model is constituted by a high-fidelity description of each morphological characteristic of the basin, such as elevation model, land use and soil characteristics. A conceptual model, as the name suggests, is composed by components which aggregates some physical information of the catchment, but some processes are conceptualized,i.e, a heuristic technique represents the process according the desired level of fidelity that the modeler is looking for. At last, a data-driven approach is a black-box model, i.e the dynamics of the process are totally hidden under a series of parameters and functions which translates inputs into outputs, not taken into account any morphological information of the basin.

1.1.3 Modelling of open channel flow

Flow routing models (Figure 1.5) are based on the transport of the fluid from one point in space and time to another. They have special applications in the prediction of flows downstream hydro reservoirs, in which it is necessary to determine how an specific outflow originated from the reservoir will affect a city downstream. In many practical applications, rainfall-runoff models are connected to these flow routing models (as shown by the Lateral Flow node in

Figure 1.5) in order to account for the lateral inflow due to precipitation runoff along the water way.

The necessity of stream flow prediction has been overcome successfully by use of this modelling technique, which may be subdivided into three different categories, or levels of complexity: physically-based or full-dynamic models, conceptual or grey-box models and lastly empirical or data-driven models.

Dynamic models are employed extensively in the field of water resources and flood prediction, where the necessity of detailed physical information is of utmost importance. The hallmark of such models is the numerical solving of the Saint-Venant equation, with a broad range of commercial and open-source softwares available on the market, such as SAINT-VENANT (open-source), SOBEK (free), HEC-RAS (free), MIKE by DHI (commercial). Dynamic models are well-known for its accuracy, whoever they all posses the disadvantage of being computationally expensive and requiring long simulation time.

Conceptual, or grey-box models incorporate some physical knowledge and data-observations to build the model. The model structure is defined a priori by the modeler, but observed data is still necessary to calibrate parameters which represent one or more processes. This means that the continuity equation is somehow represented inside the model, explicitly (by a PDE, for example) or to a lesser extent (first-order transfer function, for example). The momentum equation is replaced by a self-defined relation. Usually a relation between flow and storage may be incorporated, as in the Muskingum-Cunge (Cunge, 1969), or Kalinin–Milyukov–Nash-cascade (Szilagyi et al., 2005).

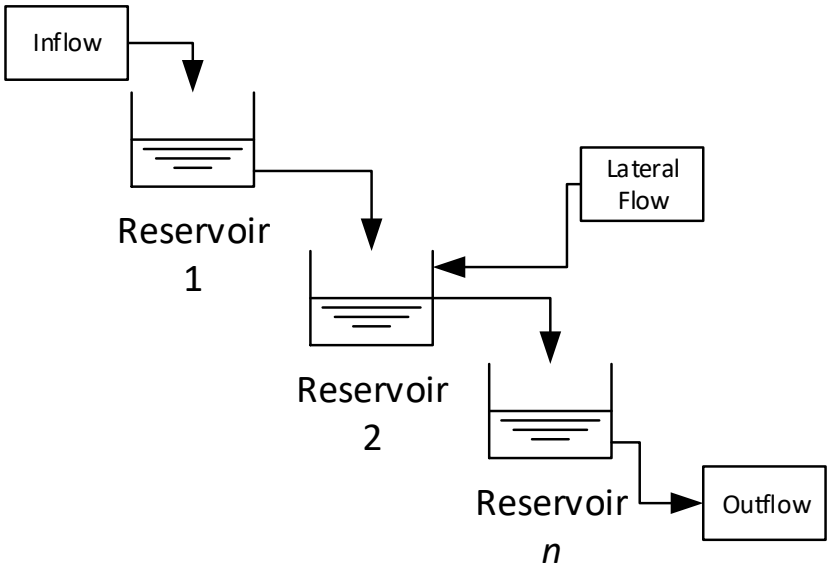

FIGURE 1.5: Simple illustration of Flow-routing model.

Such conceptual models possess the advantage of extending the accuracy and range of validity of the model, being computationally light and adding physical meaning for its components to a certain degree.

At last, empirical or data-driven models are well known for its computational efficiency and high accuracy inside of the calibration range . However, they possess some disadvantages, such as lack of physical interpretation of parameters, besides requiring a long calibration data range in order to be properly used. Its high precision also sharply decays for data outside the range. Because of these peculiarities, these type of models have limited application in control and scenario analysis. An illustrative comparison between the usual performance of these three approaches is shown in Figure 1.6.

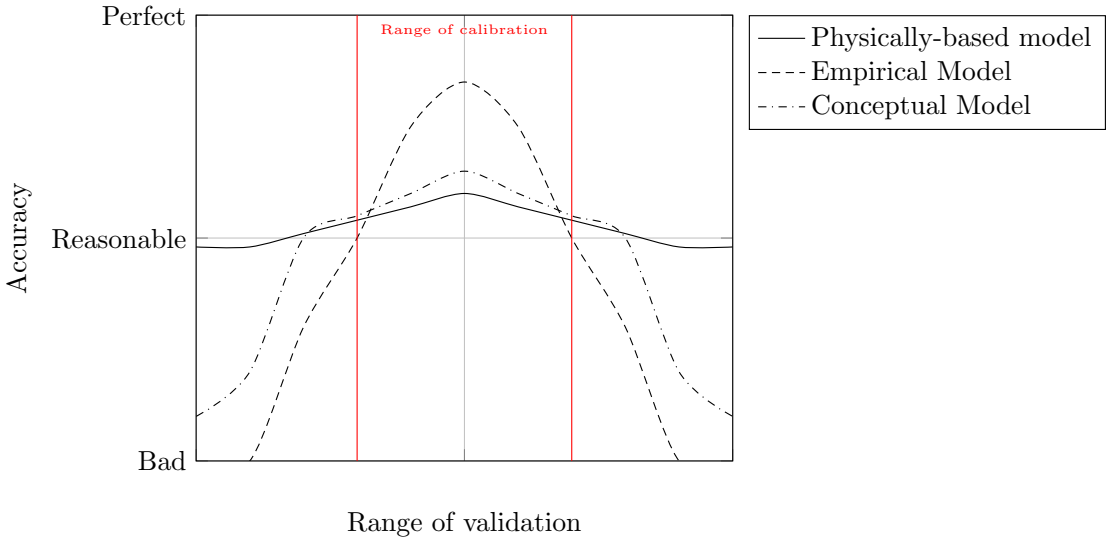

FIGURE 1.6: Illustrative performance comparison between physically-based model, empirical model and conceptual model.

The successful implementation of an accurate model allows the reliable prediction of floods or droughts, which is required to implement measures in order to protect people, environment and material in risk areas. However it is desirable, if possible, to have a well-defined methodology to know the measures necessary to prevent or at least to dampen the effects of negative effects. The use of control techniques allows the control of one or more state(s) of the water system, avoiding undesired damages.

1.1.4 Real-time control

Control techniques may be subdivided into two main branches, depending on the type of information used by the controller. The first type, called feedback, encompass controllers which react according to the degree of deviation of a variable from its desired state, or setpoint. The second type are predictive controllers, which are capable of incorporating future states and optimizing or minimizing the deviation of a controlled variable from its desired state.

A typical example of feedback controller, and extensively used in hydraulics, is the Proportional Integral (PI) or Proportional Integral Derivative (PID) controller. It has a series of advantages, such as simple and fast calibration, robust and stable performance with the right choice of its parameters. As disadvantages, it inherits the disadvantages of a feedback controller, which are the late reaction, i.e, reaction just after a deviation has already occurred, and also the fact that a PI or PID controller are linear, which means that the performance of

such controllers in highly non-linear systems are variable and may be subjected to overshoot and other undesirable effects, unless it is adapted to different situations.

One common way to partially avoid such disadvantage without losing the feedback characteristic of the controller is by incorporating a feedforward controller into the closed loop. This adds a predictive characteristic into the loop, but still a disturbance must have already occurred so to the feedforward controller takes action, but that action may be taken even before it causes a deviation into the controlled variable.

A more refined controller is the predictive control. It incorporates one or more models in its internal structure which are used to generate prediction(s) of the future states of the controlled variables, thus being able to, through some optimization algorithm, to estimate optimal control of the system to reach a determined objective.

1.2 Problem definition

The requirement for accurate and computationally inexpensive models has grown alongside the demand for hydraulic modelling coupled with spatial planning, in the integrated planning and management of economical, social and water resources. Besides, the growing necessity of different scenarios analysis and forecast demands computationally efficient models, also stable to be simulated for different scenarios.

Although this requirement is clearly defined, the solution is not simple or singular. Distinctive approaches are still computationally expensive, or lacks physical soundness as well as are restricted to a certain narrow range of validity to be used in a real application. To integrate physical concepts into a data-driven model is a challenge that has been extensively researched.

Therefore, the dominant problem is the necessity of efficient and accurate models, with reliable outcome in order to be applied into the control and optimization of hydro reservoirs.

1.3 Motivation

There is unceasing demand for computationally inexpensive models, which can be implemented into MPC schemes, in order to optimize controlled variables to satisfy particular requirements. In this sense, it stands out data-driven

models for in general, requiring few computational resources, nevertheless being able of capturing dynamics of non-linear systems. The reported disadvantages of these models are the lack of physical interpretation of model parameters, and the capabilities of extrapolation being severely limited.

Being so, we intend to overcome such limitations by integrating physical properties and data-driven techniques. This integration is commonly referred to as grey-box modelling.

1.4 Objectives

The main objective of this research is to develop grey-box models, in order to obtain computationally inexpensive models and with a broader range of validity when compared with data-driven black-box models, so as to be applied in short-term optimization of hydropower reservoir systems. As specific objectives there are two cores:

1. Development, implementation and validation of a surrogate hydrological approach for routing the flow from upstream reservoir to a downstream gauge which certain constraints must be satisfied such as maximum flow

2. Development, implementation and validation of a surrogate hydraulic model to apply model predictive control.

1.5 Structure of the Thesis

The thesis is subdivided in 6 chapters. The contents are distributed as follows.

Chapter 1 consists in a brief introduction of the topic to be addressed.

Chapter 2 focuses on the literature review and current state-of-the-art on flood management and its related issues, different modelling concepts that are currently being used in hydrology, including the different data-driven techniques and its use in a MPC scheme.

Chapter 3 covers the methodology used for each of the approaches, such as the pre-processing, model development, calibration and validation techniques.

Chapter 4 focuses on the results and discussion of each studied application. The first one is an academic experiment. The second is the application on a real-world river basin, upper São Francisco in Brazil. The third is another academic experiment, but this time it is composed by a cascade of reservoirs which can

be controlled. And at last, another real-world case, the Main River in Germany, which is also composed by a cascade of reservoirs.

Chapter 5 consists in conclusion obtained by the results and an outlook of future works. In Chapter 6 is summarized the used references throughout this thesis. An illustrative flowchart is exposed below.

Additional text with great amount of equations or graphs, are added as appendix.

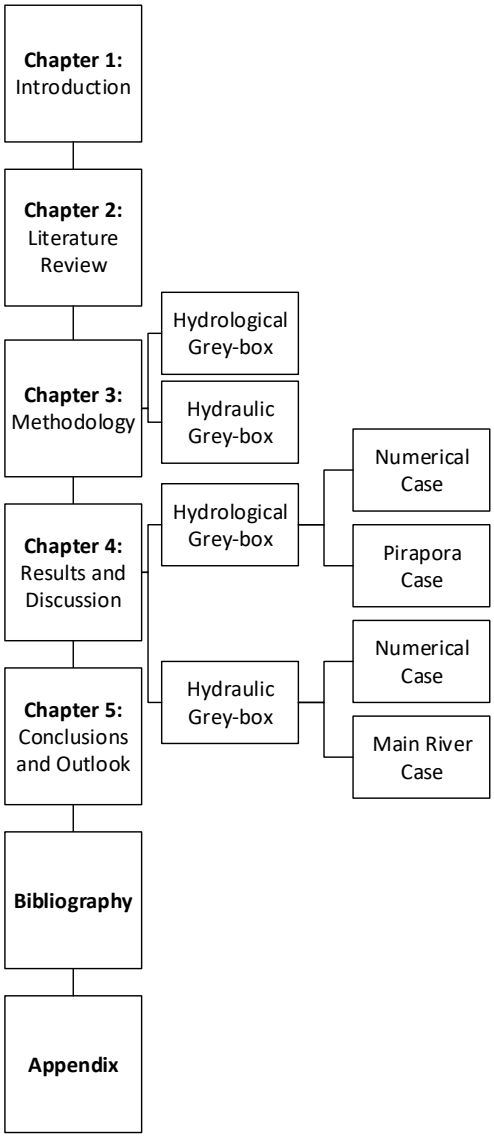

FIGURE 1.7: Thesis Structure.

Chapter 2

Literature Review

2.1 Flow Forecasting Management and Short-term Forecast

The development of systems and tools for flow forecasting in water systems is an area which embraces multiple purposes. Some that may be cited are: monitoring and allocation of water during droughts or floods, flow forecast for navigation or for energy production, among others. The accurate forecast inside a prediction horizon of days, weeks or even months can be used to take measures to avoid material and life losses. These measures may be to store water in a specific reservoir to avoid flooding downstream, or even to evacuate people in the case of a disaster and to use available hydraulic structures which can avoid or at least mitigate the occurrence of such undesired events (Van Overloop et al., 2011).

The flow forecasting management can also be used to predict and control water quality variables. Some examples of this type of application is the prediction of temperature, for a cooling purposes in a thermo plant, to control ecological aspect, or even to have an effect on trade policies among energy companies (Van Overloop et al., 2011).

Because of such broad application, flood management has became one of the most important fields of operational hydrology, and a great amount of literature has been developed during recent years. According Aqil et al. (2006), modeling of flood dynamics is performed not only to provide a warning system as a technical way to reduce flood risks but also assist in managing reservoir operation particularly during the drought periods.

According to De Bruijn (2005), flood risk management may be subdivided into flood control, flood alleviation and flood abatement. Table 2.1 shows an overview into these three different types of strategies.

TABLE 2.1: Overview of flood risk management. Source: De Bruijn (2005)

Measures	**Flood Abatement**	**Flood Control**	**Flood Alleviation**
Aim	Prevent flood waves	Prevent inundations	Reduce/ distribute flood impacts
Type	Structural	Structural	Non-structural
Examples	Reforestation,soil & water conservation	Detention areas	Flood proofing, insurance

In order to any of these strategies to work properly, an accurate forecast is of primary importance. Different techniques play a role in this context. The first to be mentioned is the modeling of a water system, or to build a predictor capable of representing the system dynamics given some inputs (rainfall, upstream discharge, evapotranspiration, etc). Besides that, other tools can be linked, such as data assimilation or uncertainty analysis. The first one have the purpose of refinement, by updating parameters, inputs, states and outputs of the model based in a series of observed data (Van Overloop et al., 2011).The second one is used to assess probability of events.

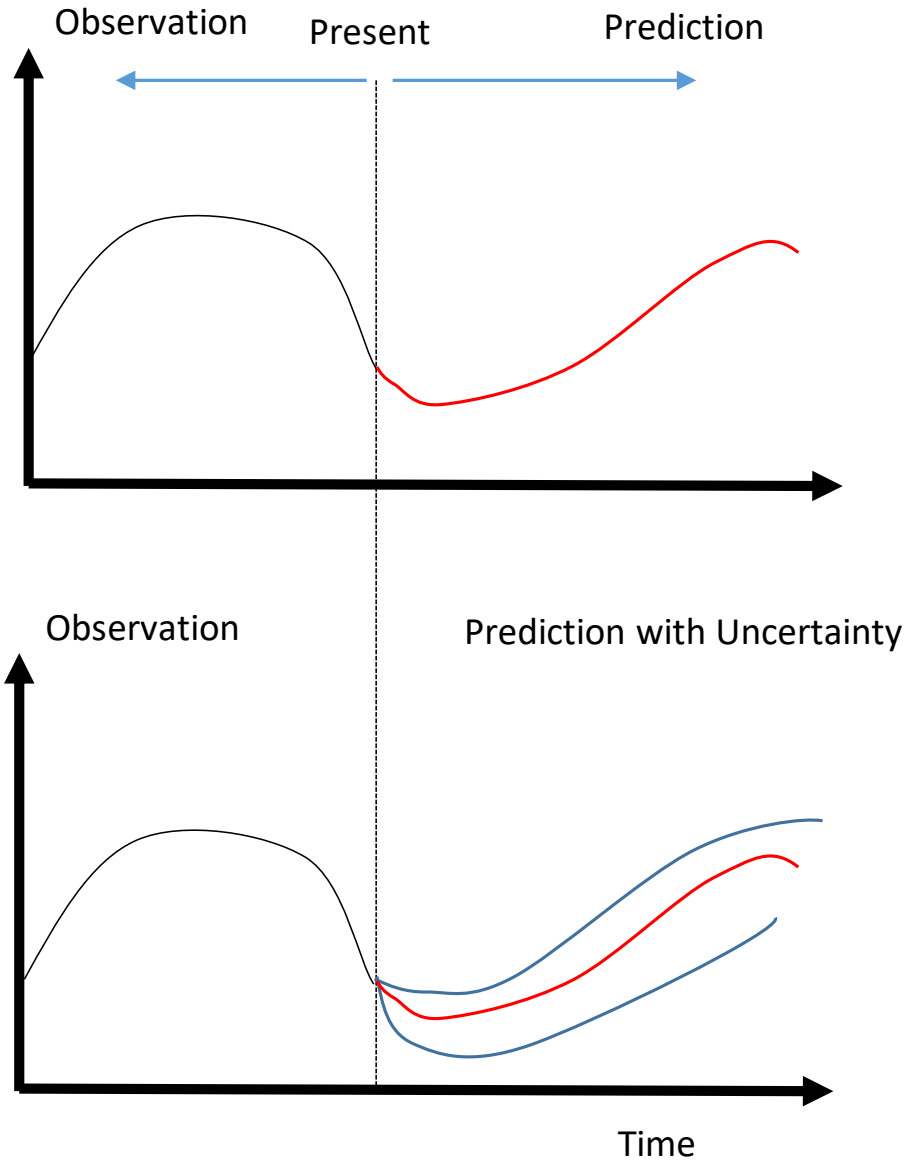

FIGURE 2.1: Differences between forecast with and without considering uncertainty.

The prediction horizon or forecast window varies according to the necessary purpose. A short-term forecast, which refers to prediction from 1 hour ahead up to a couple of days or weeks, is the usual technique for flood prevention and/or mitigation or for hydropower companies to predict production or to try to maximize it. On the other hand, a long-term forecast may refers to a forecast window of years, and it is commonly used for regulatory agencies or governments for in order to guarantee the necessary demand of water, avoiding

shortages as mentioned by Rinaudo (2015).

With respect to the modeling phase, two clear branches stand out in hydraulics area. The first modeling approach is the rainfall-runoff modeling, and the second one is flow routing modeling. The first refers to the transformation from rainfall and snow melt to discharge in a catchment, while the latter addresses the spatial and time translation of a discharge from some upstream point in a catchment to a downstream location. Both techniques are subdivided into three categories, according the amount of data necessary to calibrate them. These categories are:

- physically-based model
- conceptual model
- data-driven model

Further review on state of the art of the two main branches mentioned above and their subcategories are exposed below.

2.2 Rainfall-Runoff modeling

2.2.1 Physically-based modeling

Rainfall-runoff physically-based modeling is in its essence based on the conservation of mass, momentum and energy. With the requirement to the model to be precise, the modeling demands knowledge on how runoff is generated by the interaction between vegetation, soils and climate. Because of the spatial variability of these factors, the mathematical description of these phenomenons is done by taking into account the variation of, for example vegetation along a catchment and by subdividing the process in a system of equation or, most frequently, a system of partial differential equations capable of encapsulating this changes in space and time.

Some examples of early developments in this area may be cited. Kibler and Woolhiser (1970) implemented the numerical integration of the non-linear kinematic flow equation, where the lateral flow represents the precipitation less infiltration. The SHE model (Abbott et al., 1986), integrates a set of non-linear parabolic flow equations to describe rainfall-runoff process.

Liu and Todini (2002) developed a physically-based model called TOPKAPI (**TOP**ographic **K**inematic **A**proximation and **I**ntegration), which translates the

the rainfall-runoff and runoff routing processes as parameters in a three non-linear reservoir differential equation, which can be analytically solved, based in the kinematic wave model. Advantages reported by the authors are among others, capability of being applied at increasing spatial scales without losing model and parameter physical interpretation.

One recent development on the field of physically-based model was the semi-distributed hydrological modeling toolkit, Soil Moisture And Runoff simulation Toolkit (SMART) (Ajami et al., 2016). It is primarily conceived to be used in catchments which topography and land cover are significant drivers of rainfall-runoff transformations. One special feature of this toolkit is the use of spatially representative Equivalent Cross-Sections (ECSs), which are based on the aggregation of topographic and physiographic elements so as to reduce the number of computational elements.

2.2.2 Conceptual modeling

The motivation behind the development of the conceptual models is the assumption that the physical process of rainfall-runoff transformation may be represented by a series of mathematical components (either functions or parameters) which somehow bear physical meaning, such in a way that it would be parametrized without directly using observed data for calibration, but by using physiographic characteristics of the basin.

The development of such models is already well established in the scientific community, and a set of initial developments in this area may be cited. The Swedish Meteorological and Hydrological Institute (SMHI) developed the Hydrologiska Byrans Vattenbalansavdelning (HBV) model (Bergström, 1976), which consists in a semi-distributed conceptual model. Further improvements and modifications of this model were done by several authors. One that may be cited is the HBV-96 model (Lindström et al., 1997), which modified the spatial resolution to be based on digitized standard drainage basins, and the modified interpolation of precipitation, as well as some other improvements. Recent improvements in the model has focused on data pre and/or post-processing (van Pelt et al., 2009) or parameters estimation (Bergström et al. (2002), Lawrence et al. (2009), Abebe et al. (2010)).

Another example on early development of conceptual modeling is the ARNO model (Todini, 1996). which was named after the river with the same name. It consists on a semi-distributed conceptual model . The model is subdivided into sub-basins, according the position of the tributaries and hydrometric stations,

which defines points of interest, either because of the morphology of the basin or because of the interest of flow forecasting in a determined point. A conceptualization of the physical processes, namely the precipitation, runoff, percolation, evapotranspiration, drainage and percolation, as well as snow melt or accumulation is performed inside the modules of the model by different transfer functions, such as linear reservoir-type or linear-parabolic model. According the author, the main advantage of this model is that it is entirely driven by the total soil moisture storage, which may be analytically related to the drainage and percolation amounts. State-of-the-art developments with the Arno models involves the model calibration using genetic algorithm (Khazaei et al., 2014), as an example.

These models, although developed some years ago, are under continuous improvement. Some other well-known models that face progressive improvement are Xinanjiang (Ren-Jun, 1992) and TOPMODEL (Franchini et al. (1996); Beven and Freer (2001)).

One of the most recent developments on conceptual models for rainfall-runoff process that may be cited is the IHACRES model (Letcher et al. (2001); Croke et al. (2005));Baymani-Nezhad and Han (2014)). The main advantages of this model is its flexibility in representing large scale basins or small experiments, and to deal with different timescales. Another recent development is the improvements on MIKE-NAM model (Hafezparast, 2013), which is a lumped conceptual rainfall-runoff model and part of the MIKE 11 RR module. It was validate in different catchments, such as Strymonas River in the Balkan peninsula (Doulgeris et al., 2011) and Sarisoo River watershed in Iran (Hafezparast, 2013).

2.2.3 Data-driven modeling

In general, the application of data-driven techniques is substantially motivated by complexity and non-linearity of physical processes. The rainfall-runoff process falls in both of these categories, since the generation of flows in a catchment is highly non-linear and may be described by different physical properties, depending on the spatial and time resolution which is desired. For example, yearly streamflows may be statistically modeled, by simple cross-correlation with past years data. However, hourly streamflow is highly variable, and a poor modeling approach may represent the process in a unrealistic, and consequently inappropriate way.

Major progress in the data-driven modeling has been reached in the past decades, mainly due to computational resources availability expansion.

Although the most common application of ANNs are static or feedback mode, different authors have added different mathematical relations in order to improve performance. As an example, Sajikumar and Thandaveswara (1999) configured a Temporal Back-propagation ANN (TBP-NN), in which a finite impulse response is used to represent the input weights with a delay vector. In general this ANN structure outperformed other model structures, such as linear, second-order functional series and modified functional series model.

Comparisons between conceptual model and black-box model were performed by Toth and Brath (2002), by comparing the conceptual model ADM developed by Franchini (1996) using the ANN for pre- and post-processing of data, as well as a pure black-box static model, i.e, no feedback component. Results showed the ANN with extended training data set could outperform the conceptual model. However, when the data set was limited and did not comprehend the whole range of events possible, a better performance was obtained by the conceptual model.

Chiang et al. (2004) compared the performance of static feed-forward ANN with feedback or dynamic ANN for rainfall-runoff modeling, applied in the Lan-Yang River in Taiwan. Results show that, even though in some cases the static ANN outperformed the dynamic one, the latter captured better the peak flows. Also, in the case of a very limited training dataset, the dynamic ANN had significant better performance than the static one.

A broad evaluation of data-driven techniques in the field of rainfall-runoff was performed by Vafakhah et al. (2014). The authors evaluated the performance of different techniques, such as ARX, ARMAX, ANN, Wavelet-ANN and ANFIS. The studied case consists on the streamflow measured in Hajighoshan station from Gorgan river, Iran. The authors had better performance for the ANFIS models, while ANN and Wavelet-ANN had the worst performance in forecasting peak flows.

Another technique which has an increased popularity is the fuzzy logic. As examples, Chang and Chen (2001) has applied counter-propagation fuzzy network to streamflow forecasting in Da-cha River (Taiwan), also comparing the results with an ARMAX model. Te counter-propagation fuzzy network is basically a fusion between a feedback NN with fuzzy arithmetic in the neurons. Shiri and Kisi (2010) coupled wavelet pre-processing with neuro-fuzzy network (WNF) to predict discharges in a gauge at the river Filyos in Turkey. It was also

added periodicity to the inputs of the WNF and a simple NF network, and the model showed increased accuracy.

More recently, Kwin et al. (2016) implemented a so-called Dynamic Evolving Neuro Fuzzy (DENFIS) in which the algorithm is capable of estimating the number of clusters in a set and find the centers in the input space. The model was studied in the Sungai Kayu Ara catchment in Malaysia, in comparison with the physically-based model HEC-HMS and a linear ARX model. The results showed that the DENFIS had a very similar performance of the HEC-HMS model.

Recent developments also focuses on the use of tools from other areas of knowledge to improve modelling performance. For example, H. Kashani et al. (2016) coupled Volterra model and ANN to be able to do a non linear mapping of the rainfall process without direct application of physical characteristics of the catchment. Results showed that the developed technique had a good performance when compared with other lumped or semi-distributed models.

2.2.4 Grey-box modeling

The development of hybrid models, namely grey-box, which mixes data-driven techniques with physical properties such as mass or momentum conservation is a recent development in the field of rainfall-runoff modeling.

An application of a grey-box modeling in the Meuse river basin was developed by Corzo et al. (2009), by replacing HBV sub-basin models by ANN, coupled with a routing scheme such as Muskingum. The authors also tested the replacement of the routing scheme by ANNs, while keeping the HBV sub-basins models. The authors also addressed the fact that, the ANNs not only reproduce the generated flow, but also the noise in the system, as the model structure is not capable of differentiating one from the other. Even so, the hybrid model (ANN+conceptual) outperformed the conceptual distributed model.

Breinholt et al. (2011) developed a grey-box model based on stochastic differential equations and a noise term which is separable into process and measurement noise. The model was applied to predict one-step ahead uncertainty in a sewer system next to Copenhagen, Denmark. The uncertainty was well described by a proper diffusion term inside the model.

2.3 Flow routing modeling

2.3.1 Classical Hydraulic routing

The field of classical hydraulic modeling relates directly to the application of principles of fluid dynamics to water engineering structures, civil and environmental engineering facilities, as well as hydraulic structures (Weber, 2001).

This classical approach may be subdivided into two main categories: a full-hydrodynamic routing or a simplified hydraulic routing. The Application of both methods are widely spread in literature and references may be found up to the 70s-80s (Paiva et al., 2013). For example, Chau (1990) evaluated the application of the implicit Preissmann scheme to compute flood propagation, especially in catchments with rapid varying cross-sections, such as the Delaware Estuary and the Chincoteague Bay in the United States. Wooding (1965) introduced the kinematic wave theory, which intends to simplify the solution of mass, momentum and energy equations.

The advantage and disadvantages of classical hydraulic routing are well known as this technique has a well established foundation. A brief review on literature of this technique is given below.

Full-hydrodynamic models rely on many parameters obtained from topography-morphological data, accurate field measurements of water level, discharge, among other characteristics of the catchment under evaluation. For instance, measurements of velocity in large rivers is traditionally done using stationary or moving boats equipped with an ADCP (Acoustic Doppler Current Profiler).

However, the difficult of accessing some catchments located in dense forests, for example, may compromise the reliability of such measurements, as instrumentation may be damaged or may not settle properly installed in a location (due to animal presence, extreme weather conditions, etc). da Cunha et al. (2012), as an example, evaluated the problems and solutions to develop accurate full-hydrodynamic models in Amazon river basin, not only to forecast discharges, but also to monitor water quality parameters.

Even being so, Paiva et al. (2013) validated a full-hydrodynamic model developed by the same authors in the river Solimões, Brazil, located in the Amazon river basin. Results were mostly used to prove that effects such as backwater plays an important role in the Amazon basin.

Simplified formulation on the full-hydrodynamic model constitutes an area

of research where the necessity of models of low computational costs are demanded , such as Model Predictive Control. The three most common simplifications are the inertial, diffusive and kinematic wave. The first one neglects the convective term, while the second considers only pressure, the gravitational and friction forces and neglects the local acceleration as well as the convective acceleration. In the kinematic wave, water level gradient is assumed to be equal to the bottom slope. These models can be used as long the neglected forces are considered unimportant for the system under study.

Using one of these simplified models, Bates et al. (2010) developed an inertial formulation in the low computational cost of it allows the implementation in a variety of tools for flood forecasting and control.

Another development using inertial formulation was performed by Montero et al. (2013), who studied the application of the developed model in the control of structures for flood detention in Rhine River, Germany. The developed model was studied also in different schematizations, i.e, explicit, semi-implicit and implicit, showing accurate results and potential of future application.

Additional simplifications on the full-hydrodynamic model are also possible, which leads to the diffusive and kinematic models. One application of the diffusive model was studied by Hassan et al. (2009), who also coupled some dynamic wave components to be applied in a part of Arakawa River basin, Kanto area, Japan. The success of the implementation is endorsed by the correct estimation of water depths and discharges.

2.3.2 Classical Hydrological routing

Hydrological routing models are simplifications of the De Saint-Venant Equations, in which usually a conceptualization of one of the states (usually the discharge) is introduced, while the mass balance is maintained. Although the principle is clear, some inconsistencies may arise in the modeling procedure developed, as described below.

Two classical models that lie in this modeling technique are Muskingum and Muskingum-Cunge. According Cunge (1969), the basic assumption in the Muskingum flood wave propagation is that there is a one-to-one relationship between stage and discharge.This assumption leads to a differential equation whose analytical solution does not allow wave damping. Cunge (1969) enhanced this model by implementing time-varying parameters, accordingly a reference discharge.

These two approaches have broad applications in water systems modeling, and it has satisfied the requirements of many hydrologists. Even so, it has been reported in literature two important problems in these modeling techniques, which are mass balance inconsistency(Tang et al., 1999) and lack of agreeableness if one replaces the obtained Muskingum-Cunge parameters back in the Muskingum equations (Todini, 2007).

Todini (2007) improved the variable-parameter Muskingum-Cunge approach, by restoring the mass balance consistency and complying with the original Muskingum formulation regarding the amount of water stored in a river length. The developed methodology was tested against a full-hydrodynamic model (MIKE11) with good agreement.

An improvement on Todini (2007) was developed by Schwanenberg (2015a), which implemented a scheme known as Total Variation Diminishing (TVD) in order to improve model stability to guarantee non-negative flows as long as the TVD limiter is taken into consideration at each time step of simulation.

Another popular modeling approach is the Nash model, or Linear Reservoir. The discharge of a catchment is assumed to be linearly and directly proportional to the volume of water in the system. Initial applications were reported in the river Yangtze in China (Liang and Nash, 1988). The model was further extended by a spatial discretization, creating a set of reservoirs connected in series or parallel, the so-called cascade of linear reservoirs (Szöllösi-Nagy, 1982). Recent developments extended the model to a non-linear reservoir, which the discharge is proportional to the volume to a certain power. State-of-the-art applications of this technique are the derivation of parameters according geomorphological characteristics of the catchment (López et al., 2005), application of reservoirs in parallel to asses hydrological events (Mateo Lázaro et al., 2015), among others.

2.3.3 Data-driven routing

There is a great variety of literature regarding the use of machine-learning techniques for flow routing. Here, we briefly discuss some of them and point to different focuses that researches have tried to elucidate and investigate.

Deka and Chandramouli (2005) evaluated the use of hybrid ANN, namely FNN on the river Brahmaputra using data from gauges in different locations in India. Results showed that, besides showing flexibility and easy-to-build configuration, the fuzzy neural network shows the advantage of having transparency of the knowledge gained. Also, authors draw the attention to the fact

that the use of linguistic variables makes it relatively easy to interpret the rules and if necessary to change them.

Data-driven models may also be used to mimic more complex and time-demanding models. This technique is specially useful when it is necessary to reduce the simulation time, so the model may be integrated into an iteractive algorithm, such as an optimization. With this focus, Peters et al. (2006) used ANN to reproduce the performance of a hydrodynamic model for a streamcourse of 60 km. Results showed that ANN are highly capable of reproducing the results from more complex numerical models with a significant reduction in computation time. Roy et al. (2010) tested three different types of ANN architectures for flood routing in different sections of a river, with high performance for all the evaluated architectures ($R^2 > 0.99$).However, it is still necessary more research to give evidence on the range of applicability of the ANN in order to take full advantage of its potential, and to help to establish its limitations.

Abrahart et al. (2012) made a wide research on the application of the ANN in streamflow forecasting, as well as rainfall-runoff. It revealed that there is already a well founded research foundation in the following sub themes:

- Extending the basic model
- Neuro-fuzzy explorations
- Neuro-genetic explorations
- Neuro-wavelet explorations

Abdulkadir et al. (2013) modelled two hydro reservoirs along River Niger (Nigeria) using neural networks. The inflow, storage, reservoir level among other variables were used as input in order to simulate energy generation in the system, with reasonable linear correlation between predicted and observed energy generation for both reservoirs ($R^2 = 0.89$ and $R^2 = 0.77$).

Some fields of research are still emerging and, because of either complexity or specificity, this areas have still issues to be further researched. The areas with this characteristics mentioned by the authors are:

- ANN model structure, data handling and physical interpretation
- Data handling
- Physical interpretation

Still other areas are potential fields of research, which an increasing appearance in the field of scientific inquiry. The authors mentioned areas such as

- Modular solutions
- Ensemble solutions
- Hybrid solutions

This shows that there are still a lot of necessary research in the field of data-driven modelling, specifically the exploration of the different applications of ANN and specifically, which type of application may only be solved by a particular architecture of type of ANN.

2.3.3.1 Advantages and Disadvantages of ANNs

The main advantage of ANNs is that they are capable of modelling complex input-output relationship without the necessity of understanding the nature of the phenomena (Wang, 2006). This means that the model framework is flexible, without enforcement of constraints. Because of its flexibility and compact model structure, ANNs demand low computational efforts and can also be easily integrated with different techniques (de Vos, 2009).

A disadvantage commonly referred regarding ANNs is the difficulty of establishing theoretical ways of determining its architecture and initial values. This characteristics must be determined through a trial-and-error approach, it may also be problematic by some commonly described reason which some of them where described by de Vos (2009):

- The inability of optimization techniques to find a global optimum for high-dimensional parameters space;
- Finding minimal errors in training patterns is not a guarantee of good generalization when facing new data, as the training dataset may not be a good representative candidate for the process being studied.

One important issue when designing ANNs is the selection of the activation function. Although there has been some tentative in finding a theoretical way of defining which type is the best for each application, authors are still lacking consensus on how to implement it.

2.3.4 Grey-box routing

Developments regarding the combination of theoretical equations with data-driven modules in flow routing is a relatively recent area of scientific development, not only in the hydrology area, but in the different scientific areas in general.

Acuña et al. (2003) show different calibration techniques (direct or indirect) that can be used to obtain accurate grey-box models. Three different methodologies are mentioned by the author, which can be classified into two main approaches:

- Direct approach
- Indirect approach

The direct approach (Figure 2.2), as the name suggests, consists on the direct minimization between the current output of the black-box component and the ideal output, obtained through the available experimental data.

The indirect approach (Figure 2.3) consists into finding the optimal values of the black-box component through the minimization of the output of the whole grey-box model and the available experimental data. Through this procedure, the dynamics of the black-box component is indirectly determined and without necessity of further data processing.

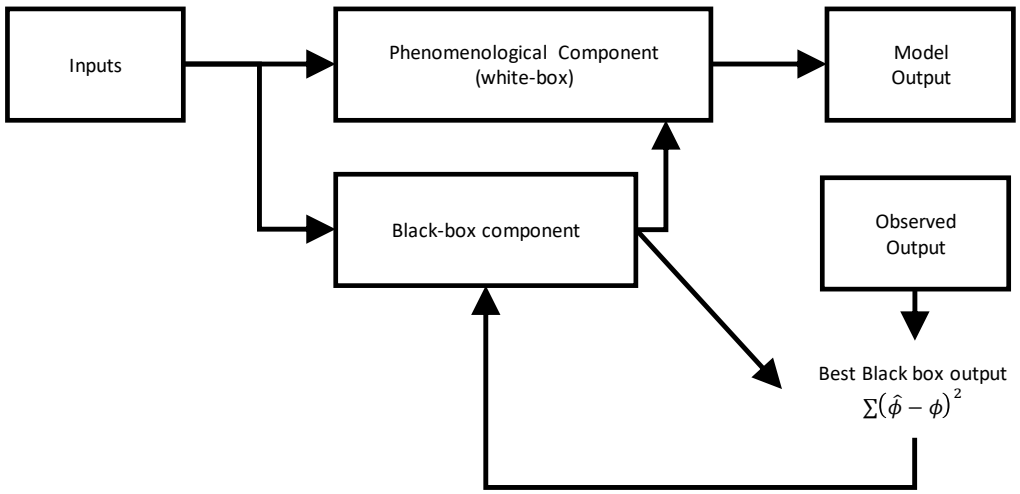

FIGURE 2.2: Grey-box Calibration - Direct Approach.

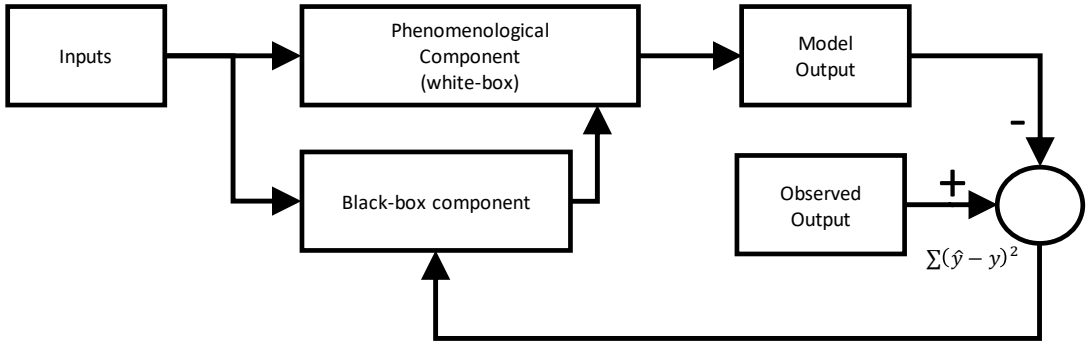

FIGURE 2.3: Grey-box Calibration - Indirect Approach.

Sohlberg and Jacobsen (2008) explain the application of grey-box modeling in a river hydro power system . The focus is the modeling of a simple hydropower plant operation through the replacement of the mass balance by an ARMAX model, and the calculated flow used to estimate the hydro power generated using a physically-based equation. The modeling procedure shows that knowledge over the process structure can be a successful way of building a grey-box model structure, in contrast with a pure trial and error procedure as it is normally done in data-driven modeling.

In his thesis, Wolfs (2016) developed two model structures, one for rivers routing and other for urban drainage systems. The author developed a modular framework, namely the Conceptual Model Developed (CMD). ANFIS and ANNs models were used to emulate complex flow dynamics in rivers, floodplains and urban drainage systems. The framework made possible to combine such model structures in a single integrated framework for modeling complex systems. The results showed high accuracy to emulate flood levels, volumes and flows, both in rivers or floodplains. The inaccuracies obtained were negligible when compared with the results for the full-hydrodynamic model used in the study.

However, both applications lack the evaluation of such grey-box models in a control scheme. Especially, what is the performance and limitations of such models in an optimization scheme? The present work addresses such implementation.

2.4 Real-time Control

The development and application of control techniques in the field of water systems became possible with the implementation of non-structural measures, such as the management of pumps, gates and orifices. Nonetheless, the controlling technique adopted depends mainly in the information usage. By this factor, three different types of controllers may be mentioned by increasingly amount of information usage: feedback control, feedforward control and model predictive control (Van Overloop et al., 2011).

2.4.1 Feedback and Feedforward control

The feedback control, as a classical technique, has been widely researched. A simple diagram of a feedback controller is shown in Figure 2.4. The illustrative implementation of feedback controllers in a river reach with a cascade of weirs is shown in Figure 2.5. This figure illustrates an important characteristic of such controllers, which is being local. That means that the control actions of the upstream weir is not taken into account into the downstream weir, which is advantageous case one of the controllers lose stability but is undesirable in general to optimize the water level of the whole reach.

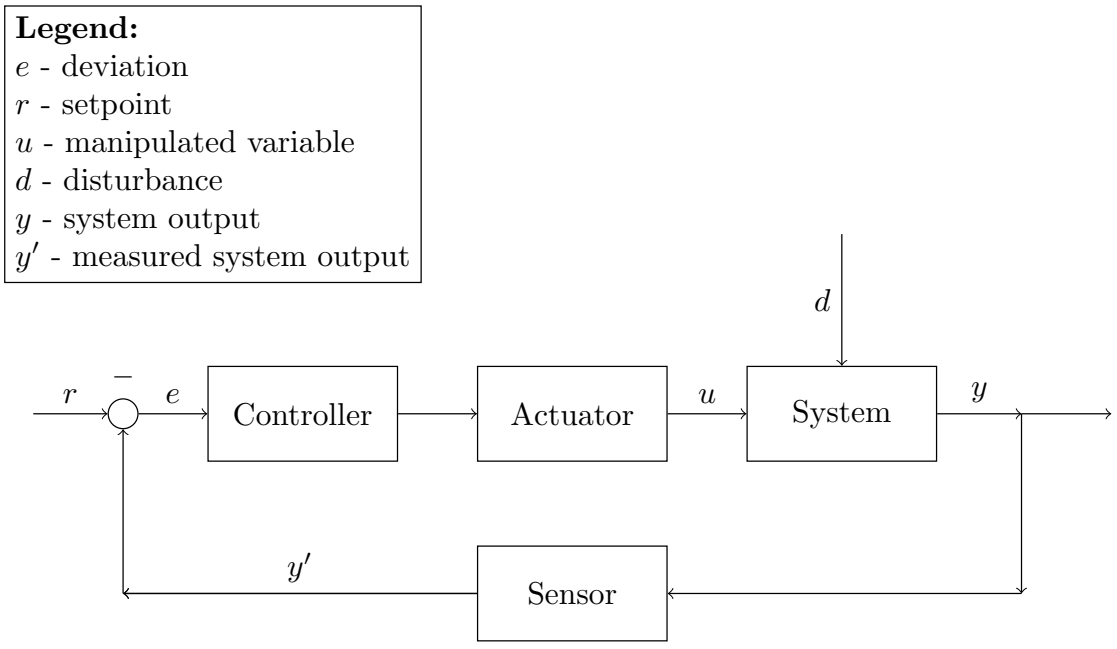

FIGURE 2.4: Closed-loop schema of a feedback controller.

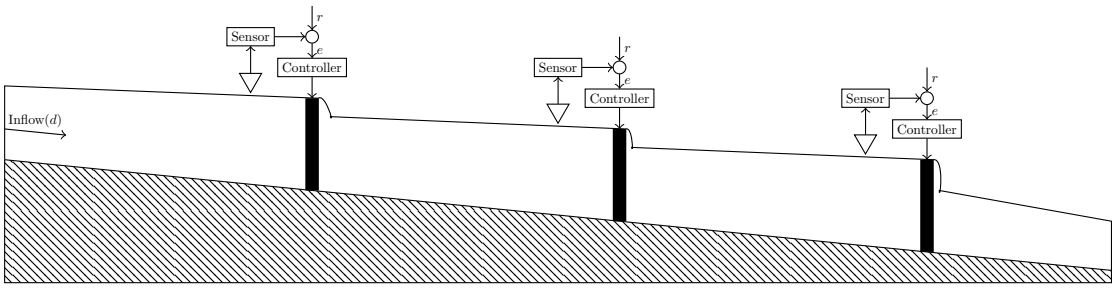

FIGURE 2.5: Feedback control of cascade of weirs.

An example of early implementation is mentioned in Litrico and Georges (1999), in which a PI controller was compared with two other controlling techniques, the Smith predictor and the pole placement controller in a river-dam case. Results showed that, although the three controllers showed robustness, the PI has the quickest response, although with a tendency to oscillation. In the case that the oscillations are filtered, it also leads to a slower response, so there is a trade-off between performance and robustness of the controllers.

Lacasta et al. (2014) studied the regulation of a irrigation channel modelled by the shallow waters equations using a PID control scheme. The model was validated by applying the data obtained in a real control application against the model showing good agreement between observed data and simulated.

Regarding general PID tuning, Dey and Ayyagari (2016) developed a technique called Fuzzy pole placement, in which the focus is to keep it robust, that is, the actuation is conservative avoiding instability margins.

As mentioned in the introduction section, one technique used to add some predictability to the feedback controller is to incorporate a feedforward component, as shown in the Figure 2.6. One example of such application in a similar reach as the example above is shown in the Figure 2.7.

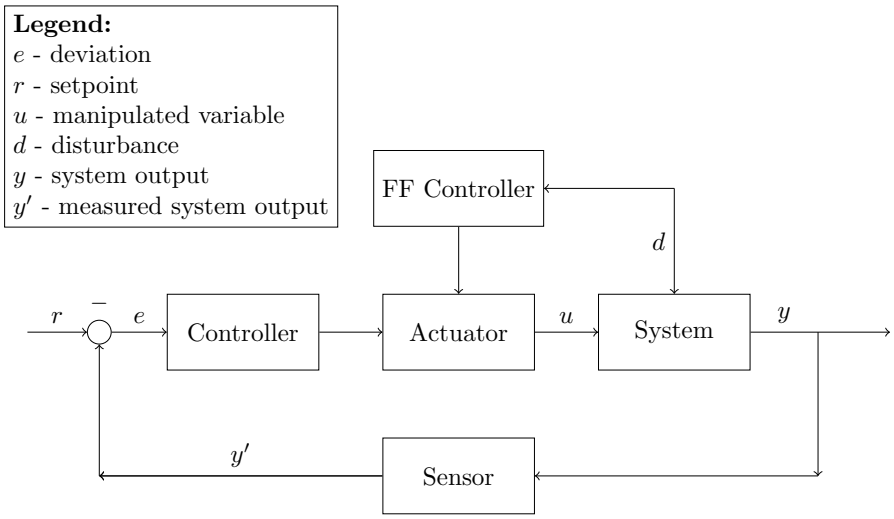

FIGURE 2.6: Closed-loop schema of a feedback controller.

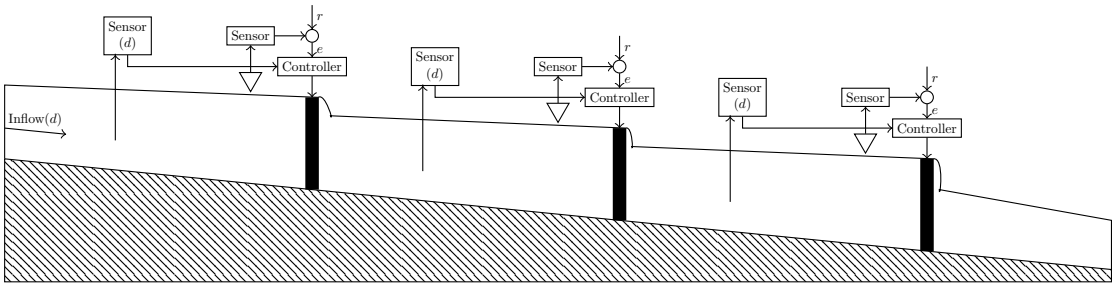

FIGURE 2.7: Feedback-feedforward control of cascade of weirs.

The feedforward control technique was investigated by Bautista et al. (2003), which related the change in performance of the controller to different states and properties of a catchment, such time needed to supply the volume, the time for the perturbation to travel down the channel, among others. A time delay parameter could compensate the time features, and the control of the hydraulic structure was performed according the desired schedule.

2.4.2 Model predictive control

A simple diagram showing the diagram of this controller is shown in Figure 2.8. Distinctly from the feedback controller, a predictive controller is usually implemented into a centralized scheme, as shown in Figure 2.9. This means that disturbances upstream the catchment can affect the control downstream or at any point. Even more, the MPC controller is capable of acknowledging

disturbances that will happen in the future, acting beforehand so as to achieve certain objective.

Legend:
r - setpoint
u - manipulated variable
d - disturbance
y - system output
y_m - model output

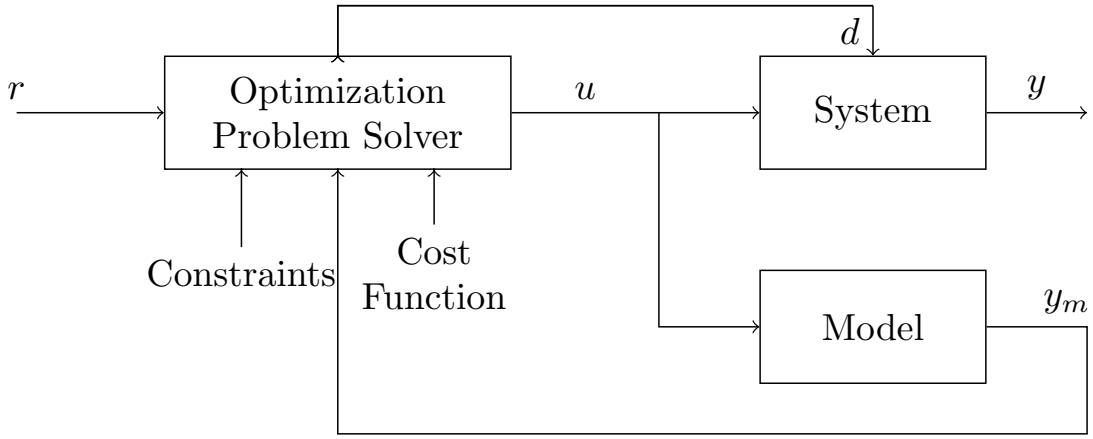

FIGURE 2.8: Model predictive control schema.

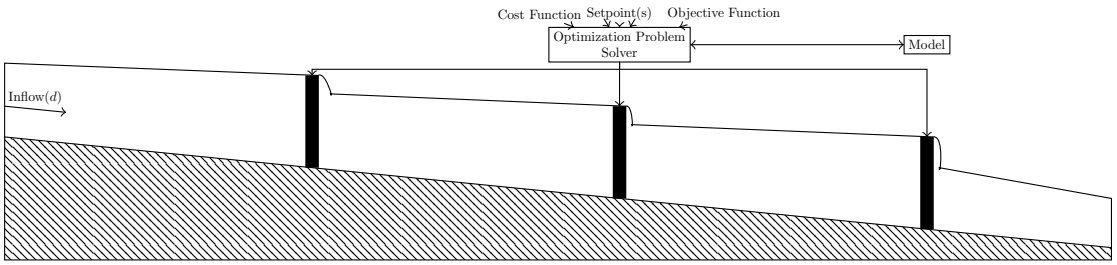

FIGURE 2.9: Model predictive control of cascade of weirs.

Inside the controller an internal model and an optimizer algorithm is capable of estimating future states of the system based on present and future inputs, thus searching an optimum trajectory so as to minimize the deviation of the controlled variable from its setpoint. Moreover, a couple of constraints and objectives can be aggregated into the controller so as to fulfil physical feasibility and still find the best control actions inside a prediction horizon. This features are illustrated in the figure below:

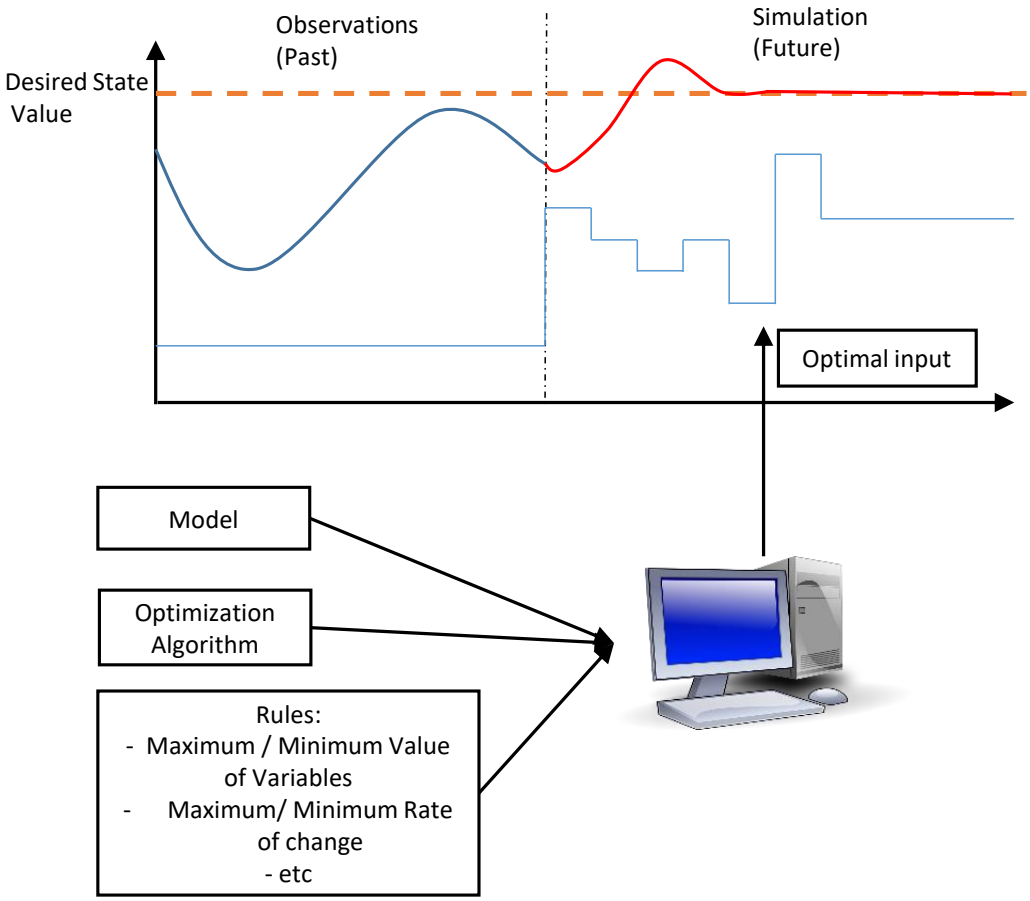

FIGURE 2.10: Illustrative example of Model Predictive Control principles.

The use of the Model Predictive Control for water systems is a relatively new field of research. Nonetheless, advantages are already clearly defined, as reported by Petrone (2010), such as:

- Relatively simple formulation and implementation, especially for complex systems.
- It can manage a high number of inputs, outputs and states.
- It integrates the system limitations such as saturations into the intern algorithm. Such limitation, in a traditional feedback scheme would have to be externally declared and the controller would not be aware of it.
- There is high flexibility in the choice of cost function and it can be defined according to the objectives of the control scheme.

Ackermann et al. (2000) applied Model Predictive Control for a system of hydro reservoirs, with the objective of meeting requirements for hydro power

generation and water level subject to narrow constraints due to the flow dynamics. The methodology was applied in the Trier reservoir of Mosel river, Germany. The authors showed that the application of this advance control technique could spare capital that was intended to be used for dredging the channel for the purpose of improved navigation.

Xu et al. (2013) assessed the possibility of coupling water quality and quantity prediction and model predictive control, showing promising results for future researches in this area.

Applying in a stochastic scenario, Raso et al. (2013) introduces a controlling technique called Tree-Based MPC (TB-MPC) for short-term management. In this method, the algorithm searches different strategies of optimum control in a set of representatives outputs of the model. These outputs have a tree structure, in the sense that at the points where two ensembles diverges significantly, a branching point is set forming two mutually exclusively subsets. The developed methodology was assessed in the Salto Grande hydro reservoir, in the border between Argentina and Uruguay.

The literature also reports applications of MPC scheme using Evolutionary Algorithm as optimizer. Van den Zegel et al. (2014) applied such a technique to control gated weirs in the river Demer, Belgium. The developed scheme could halve the floods in the river system for the studied event.

Still, the different works cited above mention either a novel modeling approach or the application of the predictive control with a classical modeling technique. There are not many researches in the application of the recently developed grey-box models inside MPC scheme. That is an issue addressed in the present work.

Chapter 3

Methodology

3.1 Classical hydrological flow routing

As a starting point for the classical hydrological routing, consider the linear reservoir model aka Nash Model (Nash, 1958). It assumes that there is a linear relation between the water volume (storage) in the reach and outflow (runoff) as shown in Equation 3.1. The mass continuity is also taken into account, according Equation 3.2.

$$s_j^t = kq_j^t \tag{3.1}$$

$$\frac{ds_j}{dt} = q_{j-1}^t - q_j^t \tag{3.2}$$

where s is the reservoir storage, q is the flow, k is a storage parameter, t is a time index and j is a spatial index.

According to Sand (1992), an stable implicit schematization of Eq. 3.2 reads

$$s^{t+\Delta t} = s^t + \Delta t.\left((1-\theta)q_{j-1}^t + \theta q_{j-1}^{t+\Delta t} - (1-\theta)q_j^t - \theta q_j^{t+\Delta t}\right) \tag{3.3}$$

Where $0.0 \leq \theta \leq 1.0$ a weighting coefficient which can fluctuate the scheme between a fully-explicit, Forward-Euler scheme ($\theta = 0.0$), passing through the second-order Crank-Nicholson method ($\theta = 0.5$), or a robust, fully-implicit first-order "Backward Euler" ($\theta = 1.0$). In the present study it is used $\theta = 1.0$, referred to as ode14x, or $\theta = 0.0$, referred to as ode1.

To solve Equation 3.3 for the outflow $q_j^{t+\Delta t}$ using $\theta = 1.0$ in Nash model, linear algebra can be used since the equation is linear. However, if it becomes non-linear (e.g k is not constant) it is necessary to apply a root-finding algorithm at each time step, since the outflow $q_j^{t+\Delta t}$ is a non-linear function of $s_j^{t+\Delta t}$ and $q_{j-1}^{t+\Delta t}$. The method used in the present work was the done inside ode14x in Simulink ©. It is a combination of Newton method and extrapolations from the

current values in order to compute the state at the next time step (Mathworks, 2014).

The Nash model can be rewritten by replacing the storage term s by Equation 3.1 in the mass balance equation to receive:

$$k\frac{dq_j}{dt} = q_{j-1}^t - q_j^t \tag{3.4}$$

A discrete-time form is derived by applying, as an example, Forward Euler time integration to the equation above, which becomes:

$$q_j^{t+1} = q_j^t + \Delta t\left(\frac{q_{j-1}^t - q_j^t}{k}\right) \tag{3.5}$$

The next step is to extend the model using matrix representation. As an example, a model with j nodes with one inflow q_{BC} at the first node and one lateral q_L at the second may be written in a matrix form as

$$Q^{t+1} = Q^t + \Delta t K^{-1}\left(Q_{BC}^t + D \cdot Q^t - Q^t\right) \tag{3.6}$$

Where Q^{t+1}, Q^t, K^{-1}, Q_{BC} and D (Connection Matrix) are defined as below:

$$Q^{t+1} = \begin{bmatrix} q_1^{t+1} \\ q_2^{t+1} \\ q_3^{t+1} \\ \vdots \\ q_j^{t+1} \end{bmatrix}, Q^t = \begin{bmatrix} q_1^t \\ q_2^t \\ q_3^t \\ \vdots \\ q_j^t \end{bmatrix}, K^{-1} = \begin{bmatrix} k_1^{-1} \\ k_2^{-1} \\ k_3^{-1} \\ \vdots \\ k_j^{-1} \end{bmatrix}, Q_{BC}^t = \begin{bmatrix} q_{BC}^t \\ q_L^t \\ 0 \\ \vdots \\ 0 \end{bmatrix}, D = \begin{bmatrix} 0 & 0 & 0 & \cdots & 0 \\ 1 & 0 & 0 & \cdots & 0 \\ 0 & 1 & 0 & \cdots & 0 \\ 0 & 0 & 1 & \cdots & 0 \\ 0 & 0 & 0 & \cdots & 0 \end{bmatrix} \tag{3.7}$$

This discrete approach is also known as a cascade of linear reservoirs.

The parameter(s) k can be calculated by different methods, such as the Moment method (Chow et al., 1988). Another technique, and is the one used in the present work, is to use numerical optimization to calibrate the values of k. According this the error between an observed outflow Q_{obs} and an simulated outflow Q_{sim} may be minimized by applying the least squares minimization algorithm, according:

$$\begin{aligned} \min_k \quad & \sum (Q_{obs} - Q_{sim})^2 \\ \text{subject to} \quad & k > k_{min} \\ & k < k_{max} \end{aligned} \tag{3.8}$$

More technical details about this modelling procedure is shown in Appendix A.

Another traditional hydrological model is the Muskingum method. In this approach, the storage s is represented as a function of both the inflow q_{j-1} and of the outflow q_j, as it reads below:

$$s_j^t = k(xq_{j-1}^t + (1-x)q_j^t) \tag{3.9}$$

where k may be physically interpreted as the travel time, while x is a weighting factor. According Chow et al. (1988), in natural streams the parameter x may vary between 0 and 0.3. Compared with the linear reservoir model, an additional variable is introduced (x), which makes it possible to represent the storage by a combination of wedge and prism as shown in the Figure 3.1.

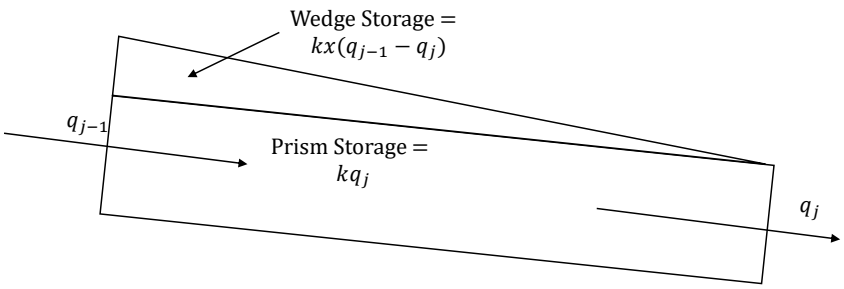

FIGURE 3.1: Representation of Muskingum channel.

A common technique used is to introduce three constants, C_0, C_1 and C_2 which are function of the parameters k, x and also of the time step Δt, as:

$$\begin{aligned} C_0 &= \frac{-kx + 0.5\Delta t}{k(1-x) + 0.5\Delta t} \\ C_1 &= \frac{kx + 0.5\Delta t}{k(1-x) + 0.5\Delta t} \\ C_2 &= \frac{k(1-x) - 0.5\Delta t}{k(1-x) + 0.5\Delta t} \end{aligned} \tag{3.10}$$

And the discharge is calculated according the following equation:

$$q_j^{t+1} = C0q_{j-1}^{t+1} + C1q_{j-1}^t + C2q_j^t \tag{3.11}$$

In a spatially discrete scheme, a complete model in matrix form with j branches reads as follows:

$$\begin{aligned} Q_1 &= DI + AQ_1 \\ Q_2 &= DQ_1 + AQ_2 \\ Q_j &= DQ_{j-1} + AQ_j \end{aligned} \tag{3.12}$$

where the matrix Q_j, I, D and A are defined as below:

$$Q^j = \begin{bmatrix} q_j^1 \\ q_j^2 \\ \vdots \\ q_j^t \end{bmatrix}, I = \begin{bmatrix} q_0^1 \\ q_0^2 \\ \vdots \\ q_0^t \end{bmatrix}, D = \begin{bmatrix} 0 & 0 & 0 & \vdots & 0 \\ C_2 & C_1 & 0 & \vdots & 0 \\ 0 & C_2 & C_1 & \vdots & 0 \\ 0 & 0 & 0 & \vdots & C_1 \end{bmatrix}, A = \begin{bmatrix} 1 & 0 & 0 & \vdots & 0 \\ C_3 & 0 & 0 & \vdots & 0 \\ 0 & C_3 & 0 & \vdots & 0 \\ 0 & 0 & 0 & \vdots & C_3 \end{bmatrix}, \tag{3.13}$$

Rearranging in the traditional form $A * X = B$:

$$\begin{aligned} (A - E)Q_1 &= -DI \\ (A - E)Q_2 &= -DQ_1 \\ (A - E)Q_j &= -DQ_{j-1} \end{aligned} \tag{3.14}$$

where E is the identity matrix. Each intermediate outflow Q_j can be solved using a stepwise linear algebraic algorithm from upstream to downstream.

These two modeling techniques were used in the present work to make comparisons between the developed grey-box modeling technique and the classical approaches.

3.2 Grey-Box for hydrological flow routing

In the former section two classical hydrological approaches are described, which are widely used, due to their simplicity and consequently low computational resources demand. However this modelling techniques may lack accuracy when compared with more detailed models which take into account physical details and which encapsulates physical characteristics. In this section, a novel approach is introduced, namely a grey-box model for hydrological flow routing.

In the grey-box hydrological scheme, it is assumed that there is a non-linear relation between the storage s, the inflow $q_{j-0.5}$ and the outflow $q_{j+0.5}$, as show in Equation 3.15. The continuity equation is the same as in Equation 3.2

$$q_{j+0.5}^t = f(s_j^t, q_{j-0.5}^t) \tag{3.15}$$

Equation 3.15 is modelled by an ANN. There are degrees of freedom in the number of layers, neurons (which defines the number of weights) in the hidden layer(s) and the selected transfer function for the ANN. The architecture and configuration of the ANN is further described in Section 3.5.

To simulate the model, Equation 3.15 is solved with the continuity equation. Applying spatial schematization using Forward-Euler time integration, the model reads:

$$\begin{aligned}
q_{1.5}^t &= f(s_1^t, q_{0.5}^t) \\
s_1^{t+1} &= s_1^t + \Delta t(q_{0.5}^t - q_{1.5}^t) \\
q_{2.5}^t &= f(s_2^t, q_{1.5}^t) \\
s_2^{t+1} &= s_2^t + \Delta t(q_{1.5}^t - q_{2.5}^t) \\
q_{j+0.5}^t &= f(s_j^t, q_{j-0.5}^t) \\
s_j^{t+1} &= s_j^t + \Delta t(q_{j-0.5}^t - q_{j+0.5}^t)
\end{aligned} \tag{3.16}$$

Another option is to solve using a implicit, Backward-Euler time integration. In this case, each equation becomes non-linear with respect to the unknown variable s_j^{t+1}, requiring a root-finding algorithm such as Newton-Raphson. The implicit scheme is accomplished as follows for one node:

$$\begin{aligned}
q_{1.5}^{t+1} &= f(s_1^{t+1}, q_{0.5}^{t+1}) \\
s_1^{t+1} &= s_1^t + \Delta t(q_{0.5}^{t+1} - q_{1.5}^{t+1})
\end{aligned} \tag{3.17}$$

Coupling the two equations above and rearranging so as to use a root-finding algorithm:

$$F = s_1^{t+1} - s_1^t - \Delta t(q_{0.5}^{t+1} - f(s_1^{t+1}, q_{0.5}^{t+1})) \tag{3.18}$$

where the storage at the next time step s_1^{t+1} is the unknown variable, and $q_{0.5}^{t+1}$ is an inflow boundary condition. Solving the above equation using Newton-Raphson algorithm is done according the recursive equation:

$$s_{i+1}^{t+1} = s_i^{t+1} - \frac{F}{F'} \tag{3.19}$$

where i is an iteration index, and F' is a finite difference according:

$$F' = \frac{F(s_i^{t+1}) - F(s_i^{t+1} + \Delta s))}{\Delta s} \tag{3.20}$$

In a spatial discrete scheme, each node upstream must be solved in order to find the inflow for the next node, until the last node is reached, repeating the procedure at each time step.

3.3 Classical hydraulic flow routing

Traditionally, a physically-based or full-hydrodynamic model computes flow and other states of a water system by solving the full De Saint Venant system of partial differential equations as shown below:

$$\frac{\partial A}{\partial t} + \frac{\partial Q}{\partial x} - q_L = 0 \tag{3.21}$$

$$\frac{\partial Q}{\partial t} + \frac{\partial}{\partial x}\left(\frac{Q^2}{A}\right) + gA\frac{\partial h}{\partial x} + \frac{gQ\,|Q|}{AC^2R} - \omega_f\frac{\theta_w}{\rho_w} = 0 \tag{3.22}$$

where $A[L^2]$ is the cross-section area of the channel,$t[T]$ is the time, $Q[L^3.T^{-1}]$ is the volumetric discharge, $x[L]$ is the position in space, $q_L[L^2.T^{-1}]$ is the lateral discharge, $g[L^2.T^{-1}]$ is the gravity acceleration, $h[L]$ is the water level, $C[-]$ is the Chezy coefficient, $R[L]$ is the hydraulic radius, $\omega_f[L]$ is he water surface width, $\theta_w[ML^{-1}T^{-2}]$ is the wind shear stress and $\rho_w[M.L^{-3}]$ is the water density.

One of the approaches used both in hydrological or hydraulics areas consists into the replacement of the momentum equation by: a) a simpler partial differential equation or b) an algebraic equation.

Besides, assumptions can be done to simplify the momentum equation for special flow conditions. For instance, the uniform flow in open channels can be calculated using the empirical Equation 3.23, developed in 1889 by Robert Manning, known as Manning Equation, which reads:

$$q = v.A = \frac{1}{n}.A.R^{\frac{2}{3}}.\sqrt{S} \tag{3.23}$$

where q is the discharge, v is flow velocity, A is the flow cross section, n is the Manning's Roughness Coefficient, R is the hydraulic radius, and S is channel slope. The coefficient n represents the roughness or friction in the channel. In uniform flow, the energy grade line, water slope and bottom slope are the same.

In hydraulic approaches, backwater effects can be taken into account in the calculation scheme, while in hydrological approaches this effect is neglect. Examples of the simplification of the momentum Equation 3.22 that may be cited are the inertial (Equation 3.24), diffusive (Equation 3.25) and kinematic (Equation 3.26) models.

$$\frac{\partial Q}{\partial t} + gA\left(\frac{\partial h}{\partial x} + \frac{Q\,|Q|}{A^2C^2R}\right) - \omega_f \frac{\theta_w}{\rho_w} = 0 \tag{3.24}$$

$$gA\left(\frac{\partial h}{\partial x} + \frac{Q\,|Q|}{A^2C^2R}\right) = 0 \tag{3.25}$$

$$gA\left(S_0 + \frac{Q\,|Q|}{A^2C^2R}\right) = 0 \tag{3.26}$$

Where S_0 is the bottom slope. From Equation 3.24 to Equation 3.26, simplifications increases as more assumptions are added, which make the solution faster but more prominent to loss of accuracy.

In the present work, full-hydrodynamic model (Equations 3.21 and 3.22) is used as the reference.

An inertial hydraulic model was developed in order to calibrate the grey-box model. For the inertial model, a fully explicit time integration using forward-Euler and central scheme is used to solve continuity and simplified momentum equation in a staggered grid (Figure 3.2), as shown in Equations 3.27 and 3.28.

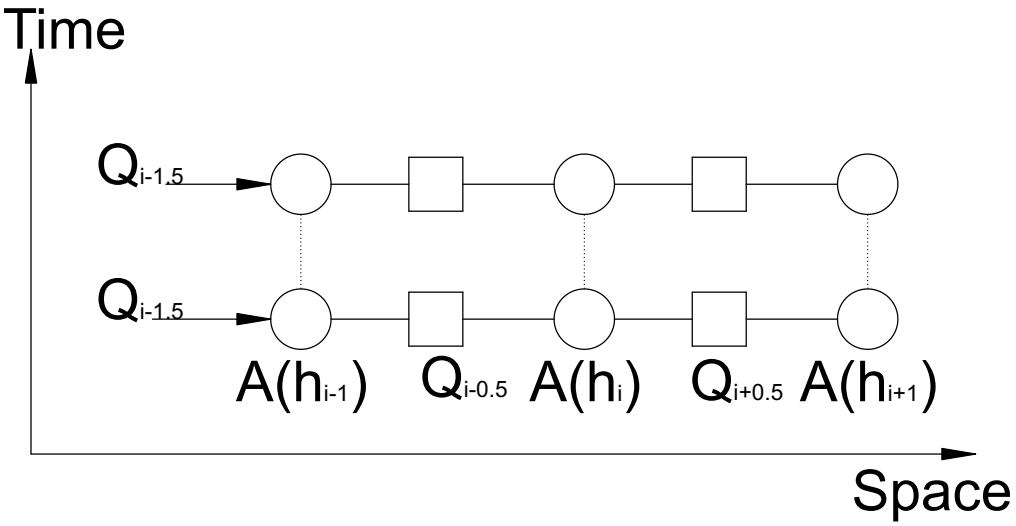

FIGURE 3.2: Staggered grid formulation.

$$A(h_i^{t+1}) = A(h_i^t) + \Delta t \left(\frac{Q_{i-0.5}^t - Q_{i+0.5}^t}{\Delta x} \right) \tag{3.27}$$

$$Q_{i+0.5}^{t+1} = Q_{i+0.5}^t + \Delta t(-gA_{i+0.5}^t \left(\frac{h_i^t - h_{i+1}^t}{\Delta x} + \frac{Q_{i+0.5}^t \left| Q_{i+0.5}^t \right|}{{A_{i+0.5}^t}^2 {C_{i+0.5}^t}^2 R_{i+0.5}^t} \right) \tag{3.28}$$

In locations where a weir is present, Equation 3.28 is replaced by an algebraic equation which represents the dynamics of the weir according Deltares (2015). Three different flow conditions may occur in a weir, which are: no flow (water level below crest level), free weir flow (tail water does not affect upstream flow) and submerged flow (high tail water affects the upstream flow). The used equations are shown below.

No flow condition: $h_i - z_s < 0$

Free weir flow condition: $h_i - z_s > \frac{3}{2}(h_{i+1} - z_s)$

$$u_s = c_e \sqrt{\frac{2}{3} g} \sqrt{h_i - z_s} \tag{3.29}$$

$$A_f = c_w W_s \frac{2}{3}(h_i - z_s) \tag{3.30}$$

$$Q = u_s A_f \tag{3.31}$$

Submerged weir flow condition: $h_i - z_s \leq \frac{3}{2}(h_{i+1} - z_s)$

$$u_s = c_e \sqrt{2g(h_i - h_{i+1})} \tag{3.32}$$

$$A_f = c_w W_s (h_{i+1} - z_s) \tag{3.33}$$

$$Q = u_s A_f \tag{3.34}$$

The model is used in a control scheme, using PI or MPC control to keep water levels upstream a weir in the setpoint by manipulating the crest level of the weirs.

The PI controller used is part of the RTC-Tools toolbox. For stability and physical feasibility, the controller output was saturated, i.e, it was limited between a maximum and a minimum value. Also the rate of change of the crest levels are limited, so as not to have abrupt changes, which could result in instability in the model and lack of physical soundness. Further description in the PI control methodology is given in Section 3.6.

The MPC control scheme is an open-loop optimization. The algorithm of optimization is IPOPT. The number of iterations were limited, and a tolerance

level was fixed to exit the optimization. Also a linear solver was used (ma57 from STFC Rutherford Appleton Laboratory (2016)). A more detailed explanation of the used control methodology is shown in Section 3.6

3.4 Grey-Box for hydraulic flow routing

Another novelty of the present work consists in a hydraulic grey-box model. Being able to account for backwater effects, it can be used to model rivers regulated by hydraulic structures.

From a hydraulic point of view, the momentum equation (Equation 3.22) is replaced by an algebraic relation in which water levels up- and downstream are taken into account. It is assumed that this equation can be modelled by an algebraic function. Knowing that the volume of water (or storage) is $s_j = A_j \Delta x$ and dividing the system in a staggered grid with position j and time t, one obtain the following system of equations in contrast with Equations 3.21 and 3.22.

$$\frac{ds_j^t(h_j^t)}{dt} = q_{j-0.5}^t - q_{j+0.5}^t \tag{3.35}$$

$$q_{j+0.5}^t = f(h_j^t, h_{j+1}^t) \tag{3.36}$$

where s is the volume of water as a function of the water level h and q is the discharge. Equation 3.35 can be solved using finite difference approximation. For this model, two explicit approaches are applied. The first one, Forward-Euler, referred to as ode1 (according naming convention from Simulink ©) is calculated according the following equation:

$$s_j^{t+1}(h_j^{t+1}) = s_j^t(h_j^t) + \Delta t \left(q_{j-0.5}^t - q_{j+0.5}^t\right) \tag{3.37}$$

A second approach, more stable, is the Runge-Kutta 4th order scheme, referred to as RK, which uses 4 estimations of the slope of the differential equation

to calculate the next time step results as a weighted result of the slopes, according the following equation:

$$\begin{aligned}
&\frac{ds_j^t(h_j^t)}{dt} = q_{j-0.5}^t - q_{j+0.5}^t = f(t, s_j^t) \\
&k_1 = f(t, s_j^t) \\
&k_2 = f(t + \frac{\Delta t}{2}, s_j^t + \frac{\Delta t}{2} k_1) \\
&k_3 = f(t + \frac{\Delta t}{2}, s_j^t + \frac{\Delta t}{2} k_2) \\
&k_4 = f(t + \Delta t, s_j^t + \Delta t k_3)
\end{aligned} \tag{3.38}$$

Regarding the procedure to calculate the discharge from Equation 3.36, a starting point is the empirical equation for uniform flow in open-channels known as Manning Equation (Equation 3.23). A corrective term $h_j - h_{j+1}$ is used to guarantee that horizontal level slope leads to zero flow. Also the roughness coefficient n may vary with flow area A and hydraulic radius R. In this case, Equation 3.23 may be rewritten as

$$q_{j+0.5}^t = \upsilon . A_{j+0.5} = f(h_j^t, h_{j+1}^t) . \sqrt{h_j^t - h_{j+1}^t} \tag{3.39}$$

The term $f(h_{j-1}^t, h_{j+1}^t)$ may be any type of function. In the present work, this term is a polynomial function of the form:

$$f(h_j, h_{j+1}) = p_n h_j^n + p_{n-1} h_j^{n-1} + ... + p_m h_{j+1}^m + pm - 1 h_{j+1}^{m-1} + .. + p0 \tag{3.40}$$

where p_{m+n+1} represents the polynomial coefficients that need to be calibrated.To adjust these coefficients, the discharges obtained using the inertial model are divided by the term $\sqrt{h_j^t - h_{j+1}^t}$, in order to obtain the "ideal values" of $f(h_j, h_{j+1})$, according:

$$f^{obs} = \frac{q_{j+0.5}^{obs}}{\sqrt{h_j^{obs} - h_{j+1}^{obs}}} \tag{3.41}$$

The data f^{obs} is then used to fit the polynomial $f(h_j, h_{j+1})$ using least squares minimization in MATLAB ©, thus becoming a data-driven approach.

At a first approach, different degrees of the Polynomial 3.40 were tested. In order to keep the polynomials in a low degree, after some trial and error procedure it was chosen the polynomial with the lowest degree which provided

reasonable performance, which was a polynomial of the form:

$$f(h_j, h_{j+1}) = p_{20}h_j^2 + p_{10}h_j + p_{01}h_{j+1} + p_{00} \tag{3.42}$$

3.5 Artificial Neural Network

The Artificial Neural Network (ANN) is a mathematical model structure originally inspired by the brain structure. It consists of simple units, called neurons, interconnected to each other forming layers (Figure 3.3). Each neuron performs weighted summation of the inputs and carries out an activation function, capable of a non-linear transformation of the result. In thesis, ANNs are capable of modelling any non-linear process, just by changing its architecture, i.e, by adding or removing layers of neurons.

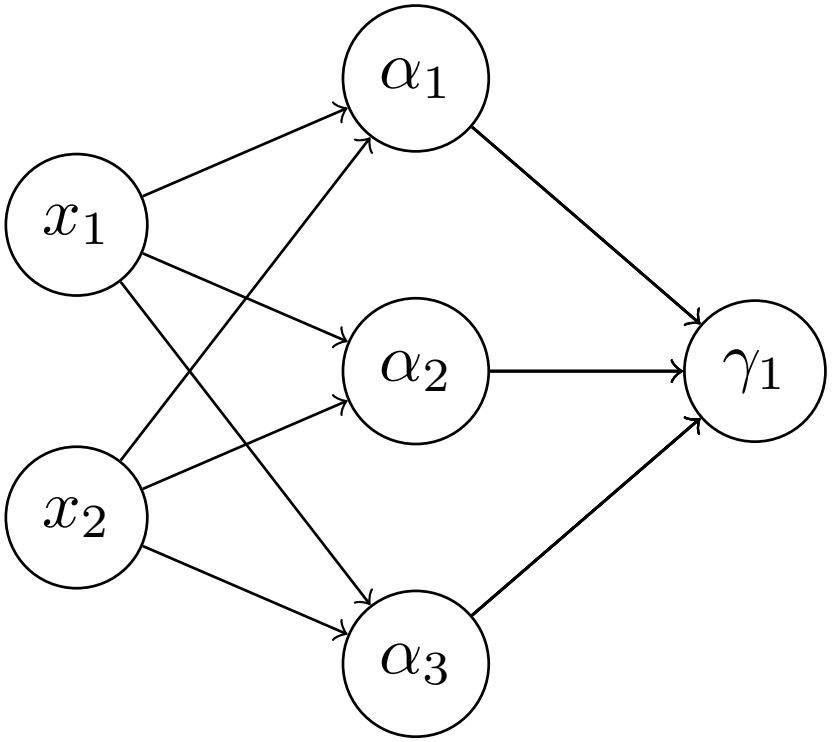

FIGURE 3.3: An Artificial Neural Network with one hidden layer and a single output.

The input signals of the network are propagated through each neuron, weighted and biased, The output of the network can be mathematically expressed by

Equations 3.44 and 3.43.

$$\alpha_j = f(\sum_{j=1}^{m} x_i \omega_{ji} + b_j) \tag{3.43}$$

$$\gamma_k = \sum_{j=1}^{m} \alpha_j \omega_{jk} + b_k \tag{3.44}$$

Where:
α_j - the output from neuron j.
x_j - input i.
ω_{ji} - weight from neuron j related to input i.
b_j) - bias of hidden layer neuron j. γ_k - the k-th output of the ANN.
ω_{jk} - weight from neuron j related to output neuron k.
b_k - bias of output neuron k.

Equation 3.43 shows that a neuron contains a (non)linear transfer function $f(.)$, which is also called activation function. This transfer function may be of any type. However there are some common types of transfer function that are generally used for ANNs. Different transfer functions were tested, the radial basis (*radbas*) and hyperbolic tangent sigmoid (*tansig*), which equations are shown below. The output layer must be a purely linear transfer function (Equation 3.47).

$$radbas(x) = e^{-x^2} \tag{3.45}$$

$$tansig(x) = \frac{2}{1 + e^{-2x}} - 1 \tag{3.46}$$

$$purelin(x) = x \tag{3.47}$$

For illustrative purpose, Figures 3.4 and 3.5 shows the profile of these evaluated transfer functions.

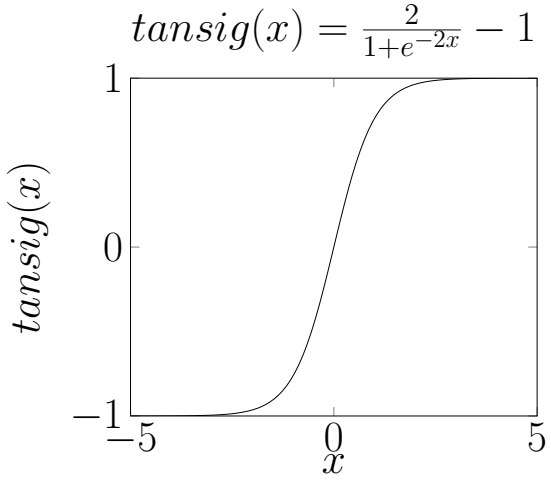

FIGURE 3.4: tansig function

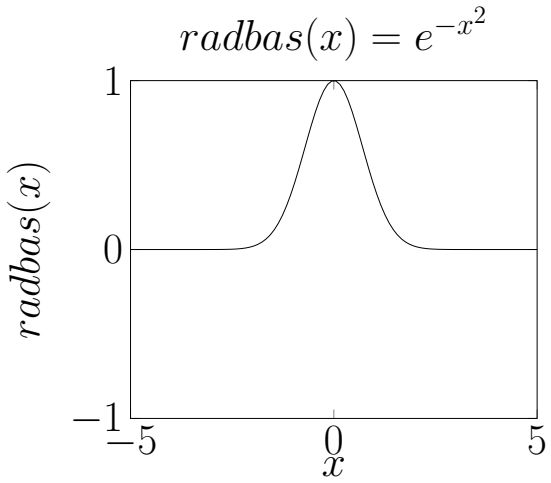

FIGURE 3.5: radbas function

After a trial and error procedure in the calibration of the model, the transfer function, number of hidden layers and the number of neurons in each hidden layer was selected for the ANNs.

3.5.1 Training

To enable an ANN to be capable of simulating a process, it must go through a process called Training. It consists on an optimization procedure of the weights (ω), in order to be capable of reproducing outputs close to observed values. This process is also commonly known as learning.

There are two common techniques of learning, namely "unsupervised learning" and "supervised learning". In the first case, there are no targets, so the networks optimizes itself to rules implicit in its design (Rojas, 1996).

In the case of supervised learning, which is the technique actually used in the present work, there is an association between the output value and the desired value, which is also called "teacher data" or "training data". These may be empirically observed value or artificially constructed time series. The expectation of such technique is that the ANN to be capable of extrapolating and modeling a time series of unknown data (Jaeger, 2005).

The most common technique for supervised learning is Back-propagation (BP), which consists in a interactive loop that the errors in the output are back-propagated to the weights and bias so as to adjust them accordingly. However, it is known as a slow technique. As an alternative, the Levenberg-Marquadt algorithm has showed to be a computational efficient optimization tool regarding ANN training (Yonaba et al., 2010) and the fastest for training ANN of moderate size, in spite of requiring a superior amount of memory compared to other algorithms (Guimarães Santos and Silva, 2014). This algorithm was developed by K. Levenberg in 1944, was a combination of two techniques, Steepest-Descent Method and Gauss-Newton Method. It has the advantage of overcoming the computationally expensive characteristic of Gauss-Newton Method, while not being limited by step size increment as in the Steepest-Descent Method. The weight adjustment according LM algorithm is done as shown in Equation 3.48.

$$\Delta\omega = -(J^T J + \lambda I)^{-1}\nabla_\omega \Psi \tag{3.48}$$

where:
$\Delta\omega$ - weight adjustment
J - Jacobian matrix.
λ - non-negative scalar.
b_k - bias of output neuron k.
I - identity matrix.
$\nabla_\omega \Psi$ - gradient of the cost function.

As an heuristic algorithm, LM may not find a global minimum of the cost function for non-linear models. Being so, it is necessary to stopping conditions to the learning, which can be:

- A performance(error) value to be met.

- A maximum number of iterations.

Or any other criteria that may be applicable for each case. Usually the training is stopped before the training optimum is found, because then the network is supposed to have learned even the noise, losing its capability of generalization, known as overtraining (de Vos, 2009).

Because of that, a common technique applied is called early stopping criteria. The training data is divided into three sets, namely:

- training set,
- cross-evaluation set or validation set,
- testing set.

The training set provides the necessary data for weights optimization of the ANN. The second dataset is used as a reference for the iteration to stop training. When the performance on cross-evaluation set starts to get higher than the training set, the minimization of weights is stopped, since a rise in the cross-evaluation set indicates lost of generalization capability. The last one is used to validate the performance of the ANN against new data.

The objective of training is to reduce the global error E (Kişi, 2007) using Bayesian Regularization, becoming

$$E = \alpha E_P + \beta E_j \tag{3.49}$$

$$E_P = \sum_{k=1}^{N} (o_k - t_k)^2 \tag{3.50}$$

$$E_j = \sum_{j=1}^{J} \omega_j^2 \tag{3.51}$$

Where:
N - number of total layers.
E_P - Error for training pattern P.
o_k - k-th output layer.
t_k - k-th training data.
P - total number of training patterns (outputs).
J - total number of weights in the ANN.
ω_j - weight of the j-th neuron or j-th input.

In Equation 3.49, $0 \leq \alpha \leq 1$, $0 \leq \beta \leq 1$ and $\alpha + \beta = 1.0$. In the special case which $\alpha = 1.0$, then there is no Bayesian Regularization. Otherwise, the ratio α/β determines the "direction" or "preference" of the training algorithm. Emphasis is given to smaller errors if $\alpha > \beta$. On the other hand, weight magnitude is reduced if $\beta > \alpha$, what leads to a smoother network response but larger errors.

3.6 Real Time Control

3.6.1 Classical Control

Classical control encompasses feedback and feedforward control. Feedback control means that the actual error, i.e, the difference between a setpoint and the the actual water level determines the magnitude of the control action. By the other side, feedforward control acts in the actual water level according the magnitude of a given disturbance.

The used control technique in the present work is the PI control with an optional feedforward component according to:

$$\begin{aligned} e(t) &= x(t) - x_{sp}(t) \\ y(t) &= K_p e(t) + K_i \int_0^t e(\tau) d\tau + K_t d(t) \end{aligned} \tag{3.52}$$

where $e(t)$ is the control error at time t, x and x_{sp} are the a selected state variable and its setpoint, $y(t)$ is the controller output, K_p and K_i are respectively, the proportional and the integral gain. The feedforward term is given by the gain K_t multiplied by the disturbance d.

For computation, one can discretize Equation 3.52 using Forward Euler, and the controller output may be limited by a upper bound ub and lower bound lb as was used in the present work, becoming:

$$\begin{aligned} e^k &= x^{k-1} - x_{sp}^{k-1} \\ E^k &= E^{k-1} + \Delta t e^k \\ y^k &= K_p e^k + K_i E^k + K_t d^k \\ lb &\leq y^k \leq ub \end{aligned} \tag{3.53}$$

This control was used in RTC-Tools to control water levels upstream weirs in the inertial model. The same technique was used to control the Grey-box hydraulic model, but using the PID controller block in Simulink/Matlab.

3.6.2 Model Predictive Control

Generally described, Model Predictive Control (MPC) is a technique which an optimization algorithm calculates the best trajectory of a control variable u subjected to constraints, so as to minimize a cost function.

The internal model may be a (non) linear state space dynamic system:

$$\begin{aligned} x^t &= f(x^{t-1}, u^t, d^t) \\ y^t &= g(x^t, u^t, d^t) \end{aligned} \tag{3.54}$$

where x is the state vector, d is the vector of disturbances to the process, y is the dependent variable and $f(.)$ and $g(.)$ are functions representing a (non)linear water resources model. This internal model is used to calculate future trajectories of the states x and dependent variable(s) y over a finite time horizon from $t = 0$ until $t = T$. The MPC optimizer is then used to find the solution of the following control optimization problem

$$\begin{aligned} \min_{\{u_t\}_{t=1}^{h}} \quad & \sum_{t=1}^{T-1} J(x_t, u_t, d_t) + E(x_T, u_T, d_T) \\ \text{subject to} \quad & x^t - f(x^{t-1}, u^t, d^t) = 0 \\ & y^t - g(x^t, u^t, d^t) = 0 \\ & c(x_t, u_t) \leq 0 \end{aligned} \tag{3.55}$$

Where J is a cost function associated with each state transition, while E is a cost function associated with the final states values. This optimization approach is also known as simultaneuous or collocated approach. The resulting optimization problem is then solved by an optimizer, such as the Interior Point Optimizer or shortly IPOPT (COIN-OR, 2016).

The IPOPT method consists on relaxing the inequality constraints using a barrier function, e.g. logarithmic function, in which the Problem 3.55 becomes

$$\begin{aligned} \min_{\{u_t\}_{t=1}^{h}} \quad & \sum_{t=1}^{T-1} J(x_t, u_t, d_t) + E(x_T, u_T, d_T) + \mu \sum_{i=1}^{n_i} [-log(-c(x_t, u_t))] \\ \text{subject to} \quad & x^t - f(x^{t-1}, u^t, d^t) = 0 \\ & y^t - g(x^t, u^t, d^t) = 0 \end{aligned} \tag{3.56}$$

which is also called the Barrier Problem (Wächter and Biegler, 2006). The procedure is to find a solution for a $\mu > 0$, and repeat it with $\mu \to 0$ until

$c(x_t, u_t) \leq \varepsilon$. As an illustrative example, Equation 3.57 shows a optimization problem with an inequality constraint, and its rewritten version as used by IPOPT in Equation 3.58. The Figure 3.6 illustrates the approximation of the solution as $\mu \to 0$.

$$\begin{aligned} &\min && x \\ &\text{subject to} && x \geq 0 \end{aligned} \tag{3.57}$$

$$\min \quad x + \mu\,(\log(x)) \tag{3.58}$$

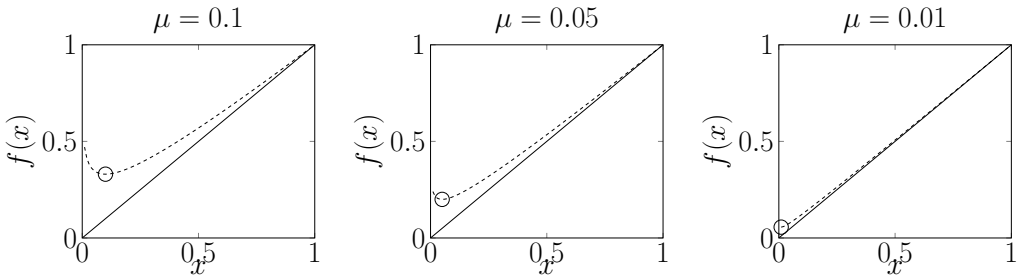

FIGURE 3.6: Illustrative example of IPOPT method. The continuous line represents the original objective function $f(x) = x$ and the dashed line is the transformed function $x + \mu\,(\log(x))$. The circle shows the location of the minimum.

In the present work, a water resources model (Inertial model and Grey-box hydraulic model) was used as the internal model in MPC for a open-loop optimization in servo-test, i.e, to keep a set of water levels in setpoint. The manipulated variable was the crest level of a set of weirs. In summary the optimization problem is:

$$\begin{aligned} \min_{z_s} \quad & \sum_{t=1}^{h-1}\sum_{n=1}^{N}(h_t^n - sp^n)^2 \\ \text{subject to} \quad & x^t - f(x^{t-1}, u^t, d^t) = 0 \\ & y^t - g(x^t, u^t, d^t) = 0 \\ & lb \leq z_s \leq ub \\ & lb_{rc} \leq \frac{dz_s}{dt} \leq ub_{rc} \end{aligned} \tag{3.59}$$

where z_s is the weir crest level, N is the number of weirs, h^n is the water level upstream a weir n, sp^n is the setpoint on the water level at n, $f(.)$ and

$g(.)$ represents the water resources model (Inertial model or Grey-box hydraulic model), lb, ub, lb_{rc}, ub_{rc} are respectively lower and upper bounds in the crest level and lower and upper bounds on the rate of change of the crest levels.

Chapter 4

Results and Discussion

4.1 Grey-box for hydrological flow routing - Academic case

4.1.1 Case description

The present case relies on an academic example provided by Todini (2007), namely a trapezoidal channel of 100 km and bottom slope of $2.5e^{-4}$, and cross section profile with a bottom width of 15m and slope ratio of 1/5, as shown in Figures 4.1 and 4.2.

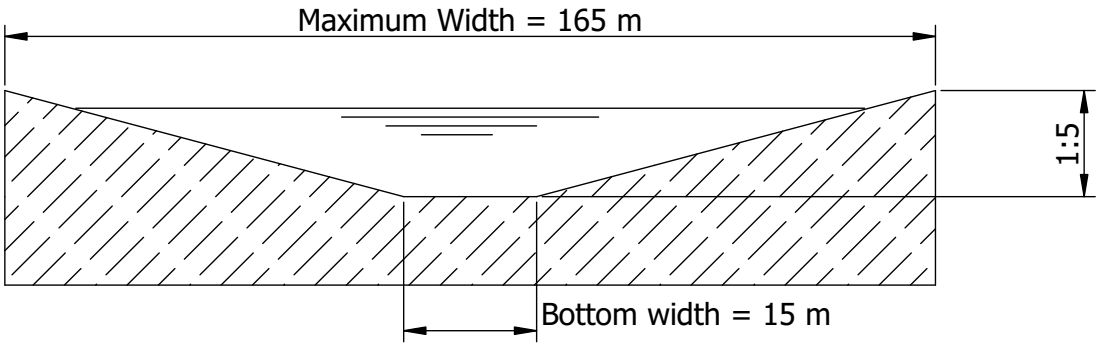

FIGURE 4.1: Academic cross section profile.

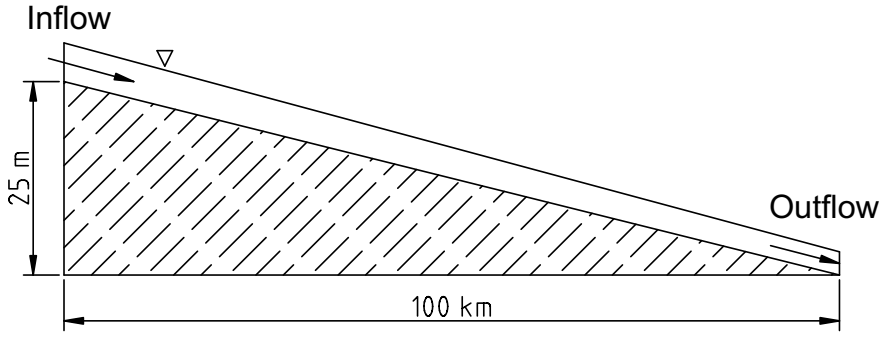

FIGURE 4.2: Academic longitudinal profile.

The inflow hydrograph was defined according Equation 4.1.

$$Q(t) = Q_{base} + (Q_{peak} - Q_{base}) \left[\frac{t}{T_P} exp(1 - \frac{t}{T_P}) \right]^{\beta} \tag{4.1}$$

where $Q_{base} = 100 m^3.s^{-1}$. The other parameters of the equation, namely Q_{peak}, T_P and β were perturbed in order to have a reasonable range of data that may be sufficient for generalization. It was generated one year of data with a time step of 5 minutes. Inflows were generated for each 240 hours (10 days), with a total of 73 peak events, as show in Figure 4.3.

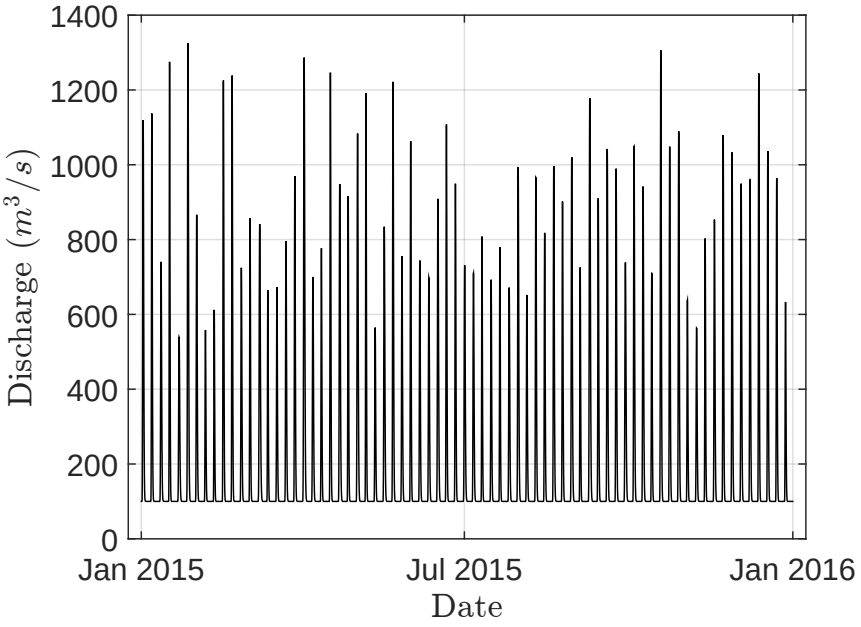

FIGURE 4.3: Synthetic Inflow Data for Academic case.

The downstream boundary condition is a stage-discharge curve generated using Manning Equation (Equation 3.23) as shown in the figure below:

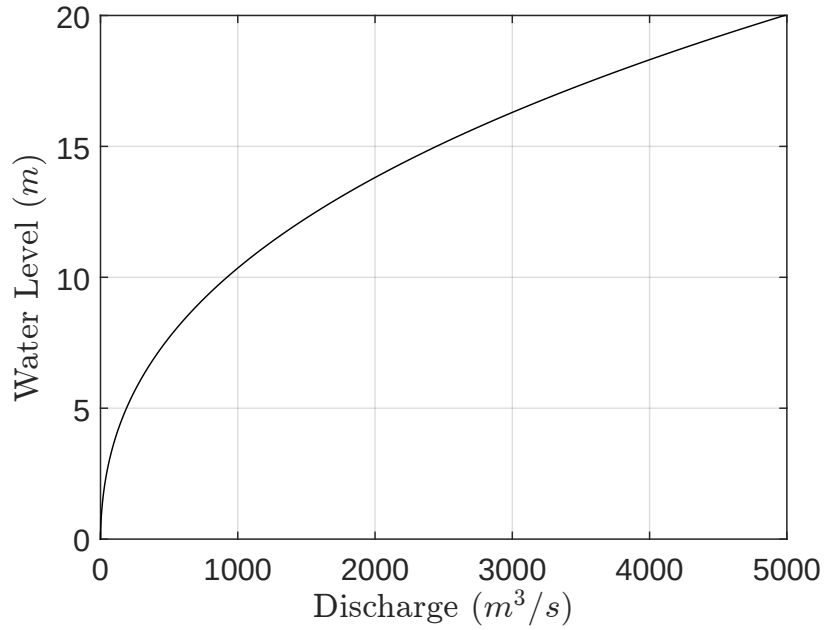

FIGURE 4.4: Downstream Boundary Condition for Academic case.

The models were also tested using 3 other upstream boundary condition. The first one, called Case 2 (Case 1 was the validation) was to apply a step in the inflow according the following equation and as illustrated in Figure 4.5 :

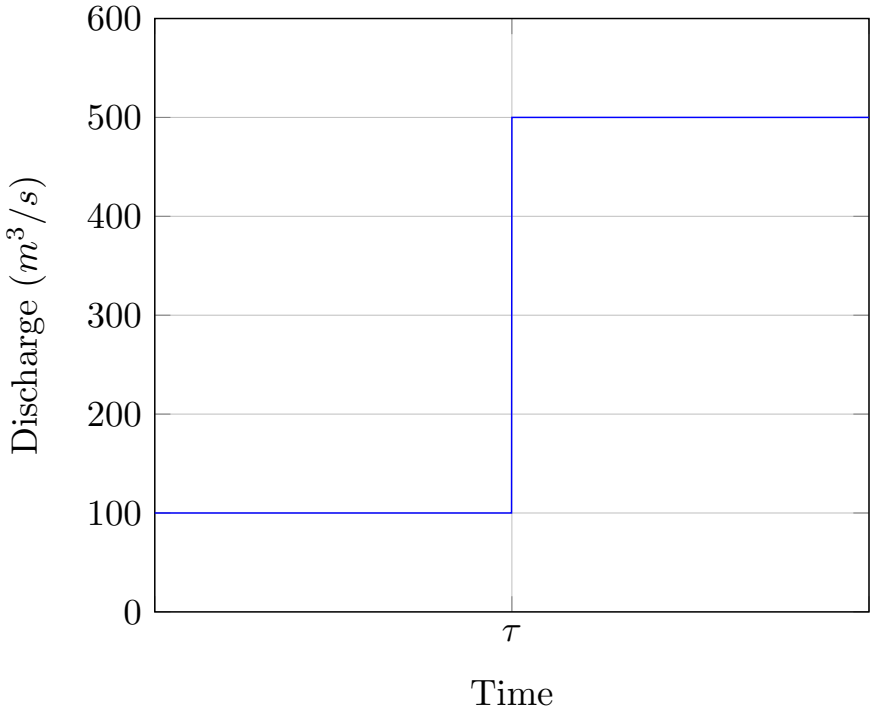

FIGURE 4.5: Case 2 upstream boundary condition.

$$Q = \begin{cases} 100\ m^3.s^{-1} \text{ if } t < \tau \\ 500\ m^3.s^{-1} \text{ if } t \geq \tau \end{cases} \tag{4.2}$$

Where τ was an arbitrary time, given enough time after the beginning of the simulation for the system to be in the steady-state. The change from 100 to 500 $m^3.s^{-1}$ was applied in a time frame of 5 minutes.

The Case 3 consisted into applying a relatively long pulse as the inflow to the catchment. This was done according the following equation:

$$Q = \begin{cases} 100\ m^3.s^{-1} \text{ if } t < \tau_1 \\ 500\ m^3.s^{-1} \text{ if } \tau_1 \leq t \leq \tau_2 \\ 100\ m^3.s^{-1} \text{ if } t \geq \tau_2 \end{cases} \tag{4.3}$$

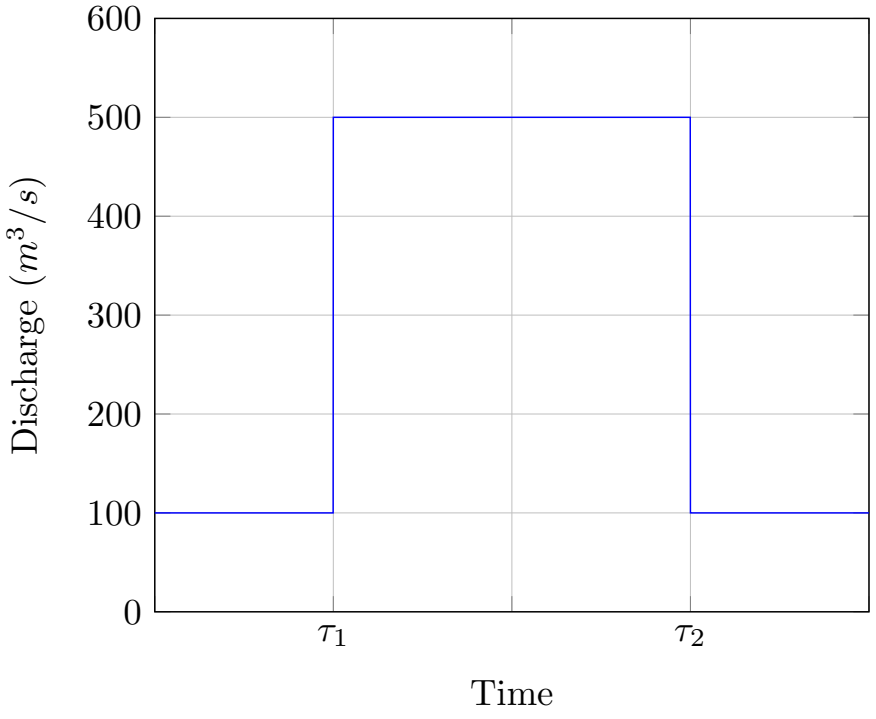

FIGURE 4.6: Case 3 upstream boundary condition.

Where τ_1, as the Case 2, was arbitrary selected, the step both increasing and decreasing took 5 minutes and $\tau_2 - \tau_1 = 3days$, as a time frame selected so the outflow have already reached the steady state when $Q = 500m^3.s^{-1}$, before returning to $Q = 100m^3.s^{-1}$.

The Case 4 consisted in a short pulse (Figure 4.7), the inflow rises and decreases even before the system showed any change. It followed the same equation as above, but in this case $\tau_2 - \tau_1 = 3hours$. The model was simulated enough time so as to observe the response of each model.

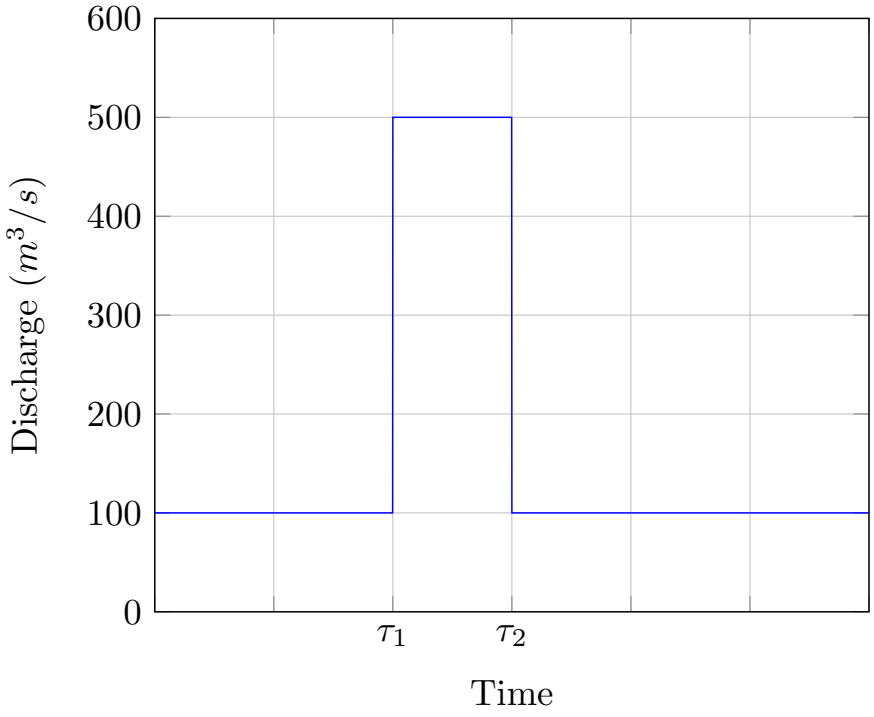

FIGURE 4.7: Case 4 upstream boundary condition.

The river reach is simulated using the software SOBEK 2.12. The generated outflow hydrograph is divided into two datasets. The first is used to calibrate the ANNs, and the second one to validate the model.

Two approaches are implemented. The first one, referred as non-discrete approach, consists of one single node where the mass balance is calculated, and one single downstream branch, where an ANN is used to calculate the outflow of the catchment.

The second approach, named discrete approach, consists of a spatially discretization of the catchment into 15 nodes, and their branches with different ANNs in between. The mass balance is calculated at each node, and the flow is propagated through the branches using ANNs trained by using the data obtained with the full-hydrodynamic model.

The model performance is assessed by two performance metrics, root mean squared error ($RMSE$) and coefficient of correlation (R^2). Each metrics contributes with different knowledge on the predictive capabilities of the model. The RMSE measures the goodness of fit especially for differences in high streamflow events. The coefficient of correlation (R^2) measures the linear correlation between the model and observed data.

4.1.2 Model implementation

The model is implemented using Simulink ©. Figure 4.8 illustrates the model for the non-discrete approach.

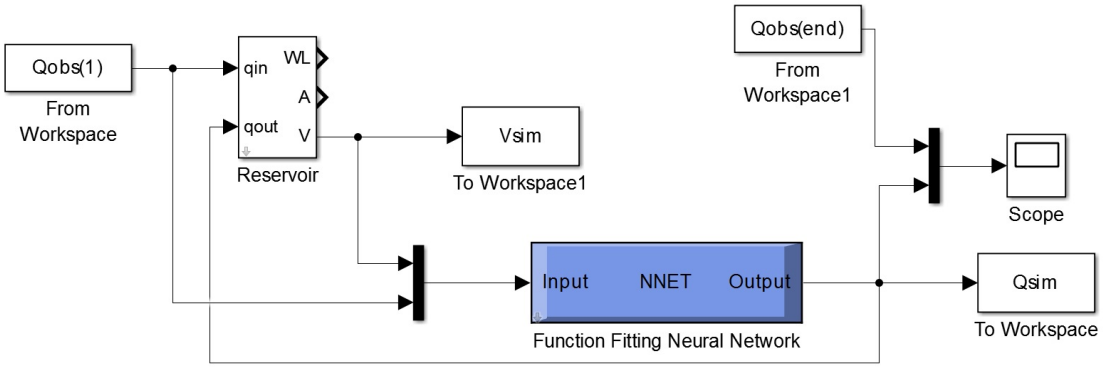

FIGURE 4.8: Simulink scheme for Grey-box Hydrological Approach

In Figure 4.8, the Function Fitting Neural Network block is the ANN (one branch). The blocks From/To Workspace represent data to be imported or exported. The block Reservoir represents the node (where mass balance is calculated). Figure 4.9 shows the block structures inside the Reservoir block. The integrator is the block which, as the name shows, perform the time integration according the solver chosen by the user.

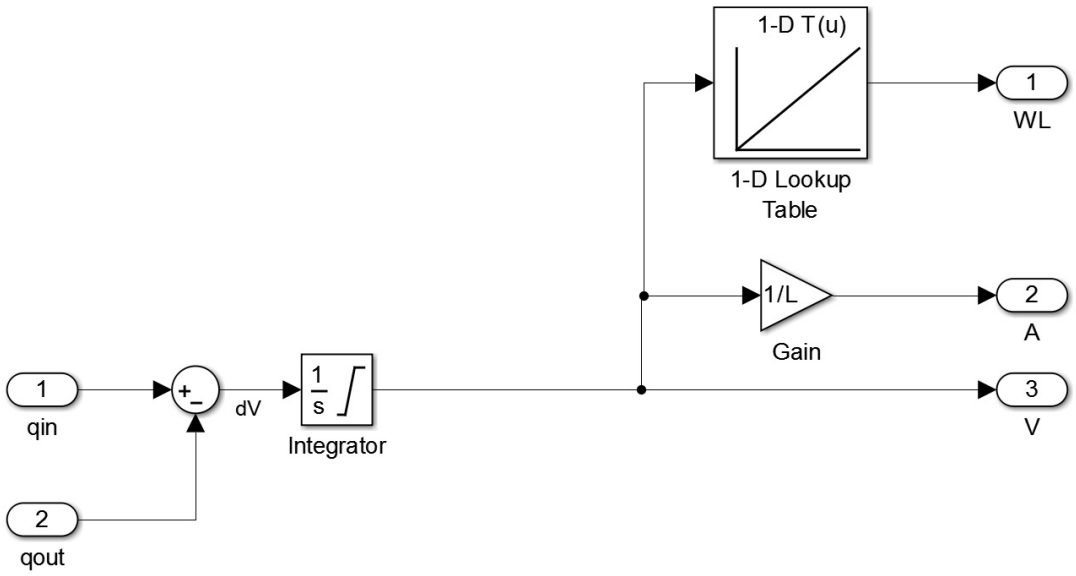

FIGURE 4.9: Simulink scheme for Grey-box Hydrological Approach -Reservoir block

The calibration of the ANNs is performed by collecting data from a simulation using the SOBEK full-hydrodynamic model. After calibration, the neural network is converted into a Simulink block (actually a collection of blocks inside a main block) and the model is tested using different solvers.

4.1.3 Results and discussion

After training the ANNs, an analysis of their outputs is performed by plotting surfaces. Figure 4.10 shows the generated 3D plots for the non-discretized approach using ANNs with 5, 10 and 15 neurons in the hidden layer. It is also plotted a 3D scatter of the training dataset, so as to better visualize the training range.

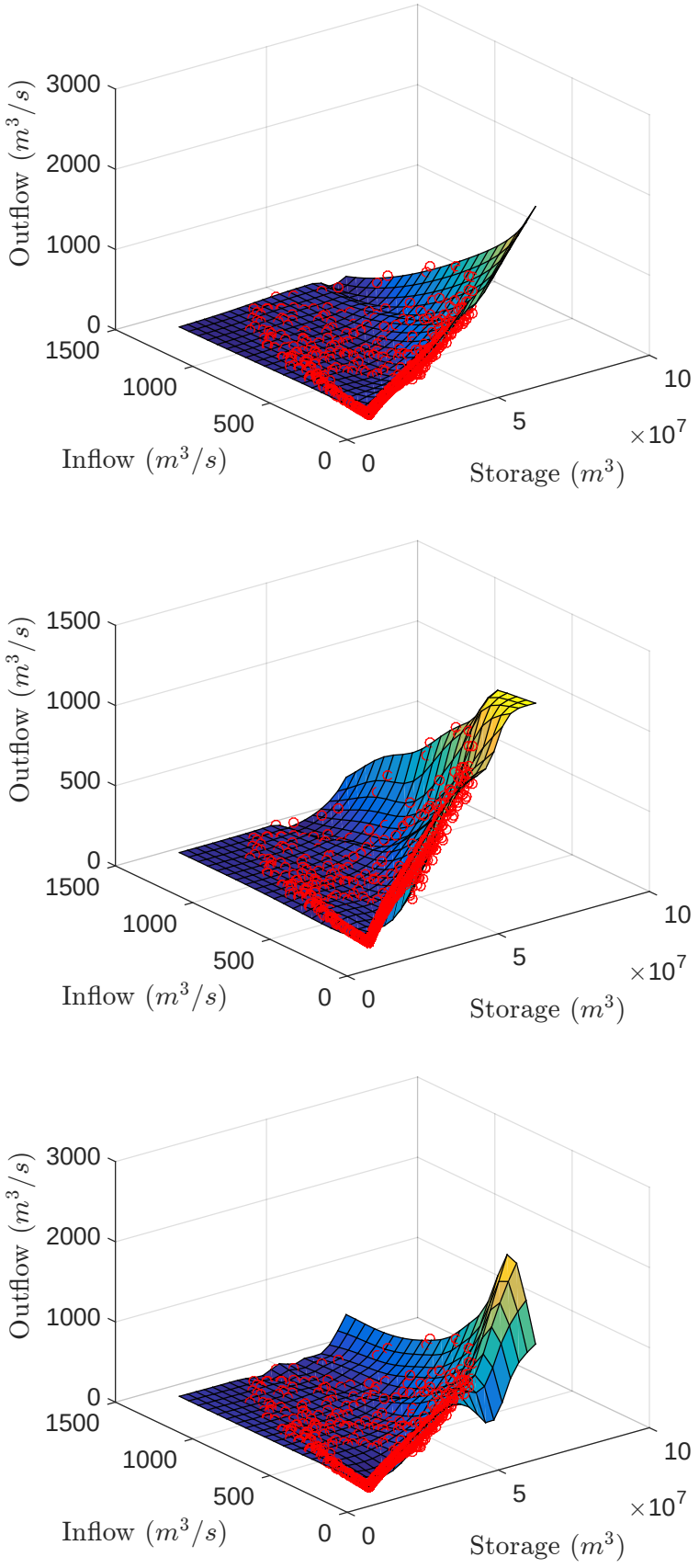

FIGURE 4.10: Plotted surface for the ANNs in the non-discretized approach, with 5, 10 and 15 neurons in the hidden layer.

It can be seen that the surfaces are similar, what shows that all of them tends to capture the dynamics of the catchment in a similar way. With the increase of neurons in the hidden layer from 5 to 15 neurons, it can be seen that the surface becomes less smooth, and there is a tendency to form more valleys and it becomes more non-linear. This is a feature reported in literature ((Hauth, 2008), (Chau and Wu, 2010), (Wolfs and Willems, 2014)), because of overfitting. As the number of neurons increase, the model tends to not only captures the dynamics of the system, but to fit every single training point. This is undesirable, so the number of neurons was limited to a maximum of 15 in the hidden layer.

The Figure 4.11 resumes the results obtained for both of the spatial used approaches using 5, 10 and 15 neurons in the hidden layer. A comparison between the performance for different solvers or time schemes is also performed, which are the forward Euler (ode1), backward Euler (ode14x) and some different time steps.

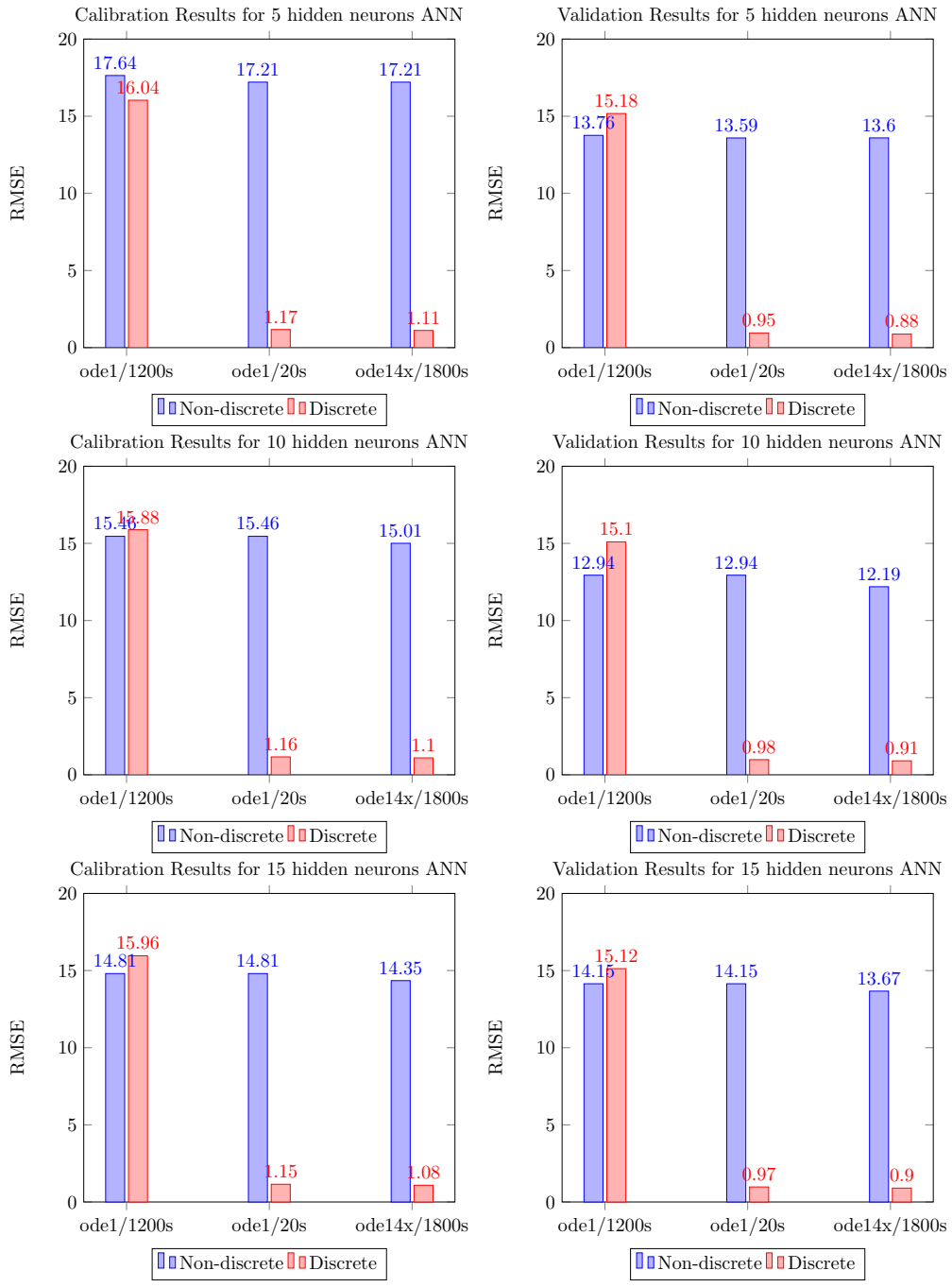

FIGURE 4.11: Performance summary for the Hydrological academic case.

From the figure above, it can be inferred that better performance is achieved by increasing the number of neurons and using an implicit time scheme (Backward Euler - ode14x) for this case. For the model with 5 neurons in hidden layer, the reduction in the time step using ode1 from 1800s to 20s improves the

results, while for the other models better performance is only achieved using the implicit solver.

The implementation of spatial discretization increases significantly the performance for all the ANN architectures and solver used, except for the case when it is used forward euler with the time step of 1800s. Regarding the time of computation, the discrete approach with 15 neurons in hidden layer takes 69.8s to simulate the whole dataset (1 year) using a time step of 20s, 2.6s using the time step of 1800s and 17.8s to compute the dataset using the implicit solver (ode14x) using the time step of 1800s.

Another observation is regarding the difference between calibration and validation results. Apparently from the figure it can be stated that the validation results are slightly better than the calibration results. However, such a small difference can be also related with the difference on the amount of peaks and the relatively shorter period used for calibration (the validation period is 66% shorter than the calibration period).

To better illustrate the results, Figure 4.12 shows the hydrographs obtained for the training data using 10 neurons, both for the non-discrete (a) as for the discrete approach (b). It was selected just part of the results, so as to be better illustrate the performance of the models when compared with the SOBEK model.

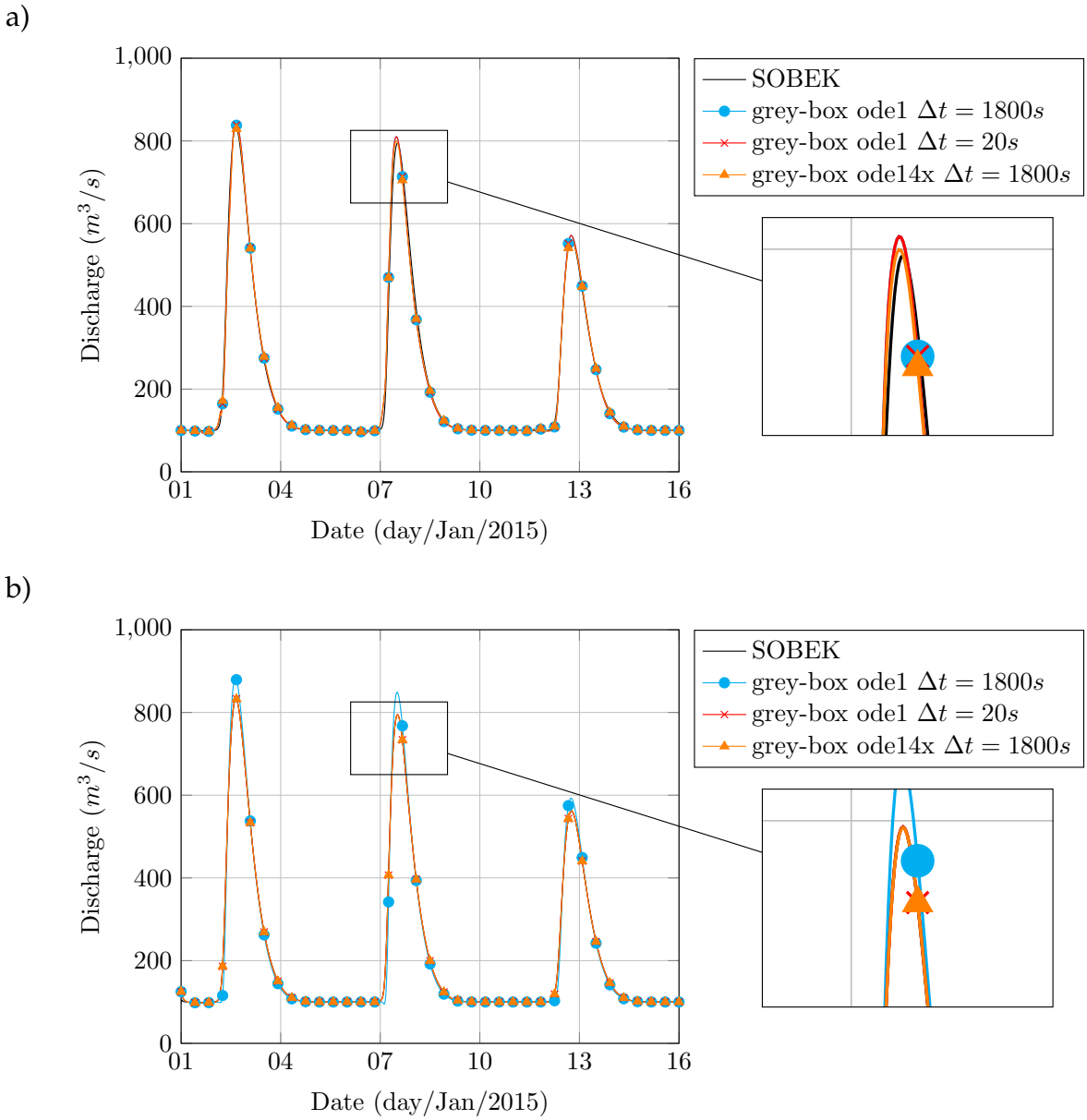

FIGURE 4.12: Hydrographs for the training dataset using ANN with 10 neurons in hidden layer using a) non-discrete approach and b) discrete approach.

The Figure 4.13 illustrates the results for the testing dataset using 15 neurons in the hidden layer, for both the discrete approach and the non-discrete one.

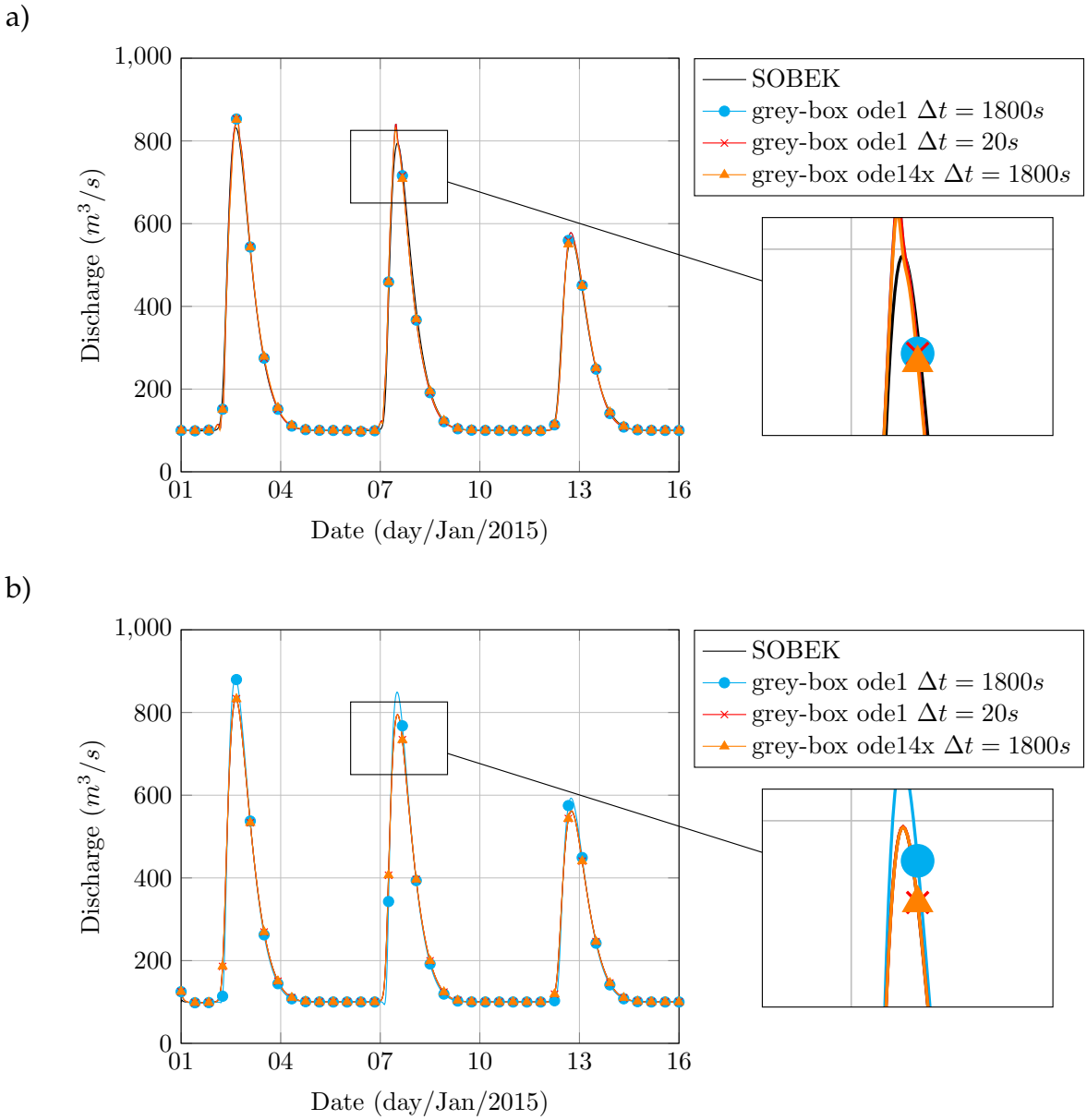

FIGURE 4.13: Hydrographs for the training dataset using ANN with 15 neurons in hidden layer using a) non-discrete approach and b) discrete approach.

It can be seen in the Figures above, that the lack of spatial discretization for the first approach introduces some small oscillations in the initial part of the rising limb of the hydrograph (Figure 4.12 a) and 4.13 a). The same phenomenon is not observable in the Figure b) part. That phenomenon raised the motivation for further investigation on the differences between the discrete approach and the non-discrete one. This was done through the 3 specific cases mentioned in the case description. In all of them, it is used the implicit solver (ode14x - Backward Euler) and a time step of 300s.

The Figure 4.14 shows the result for the Case 2. Performance metrics is measured and are exposed in Figure 4.15.

a)

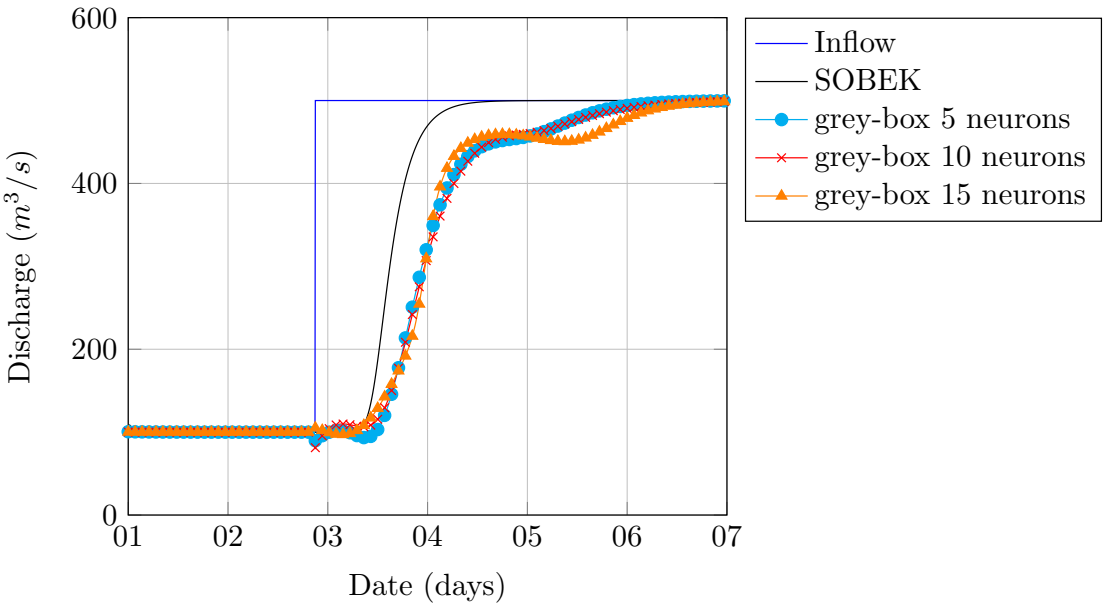

b)

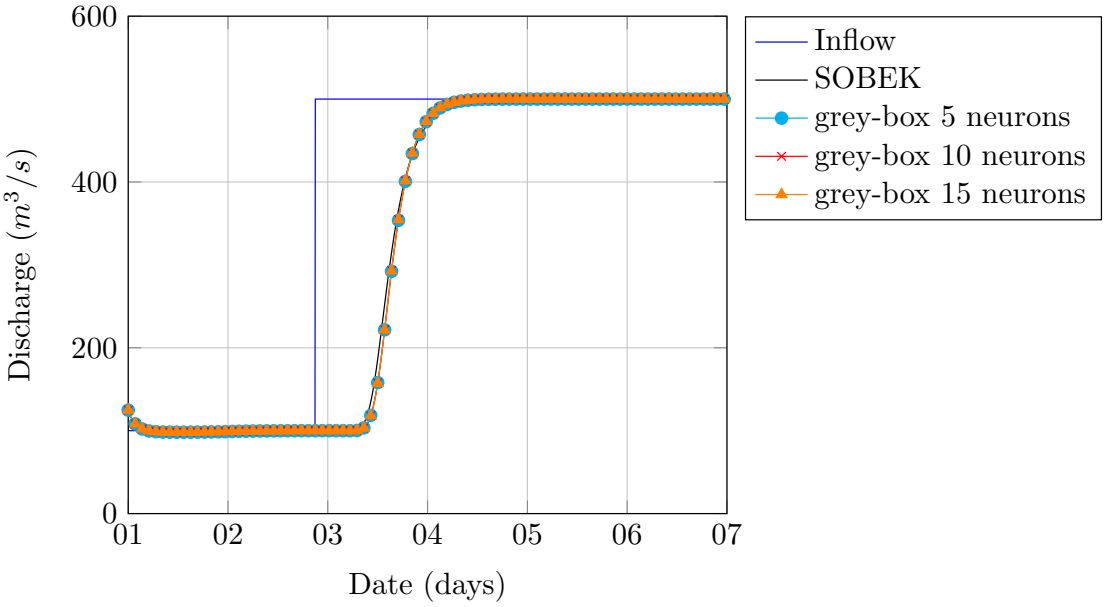

FIGURE 4.14: Case 2 Hydrographs for the (a) non-discretized approach and (b) discretized approach.

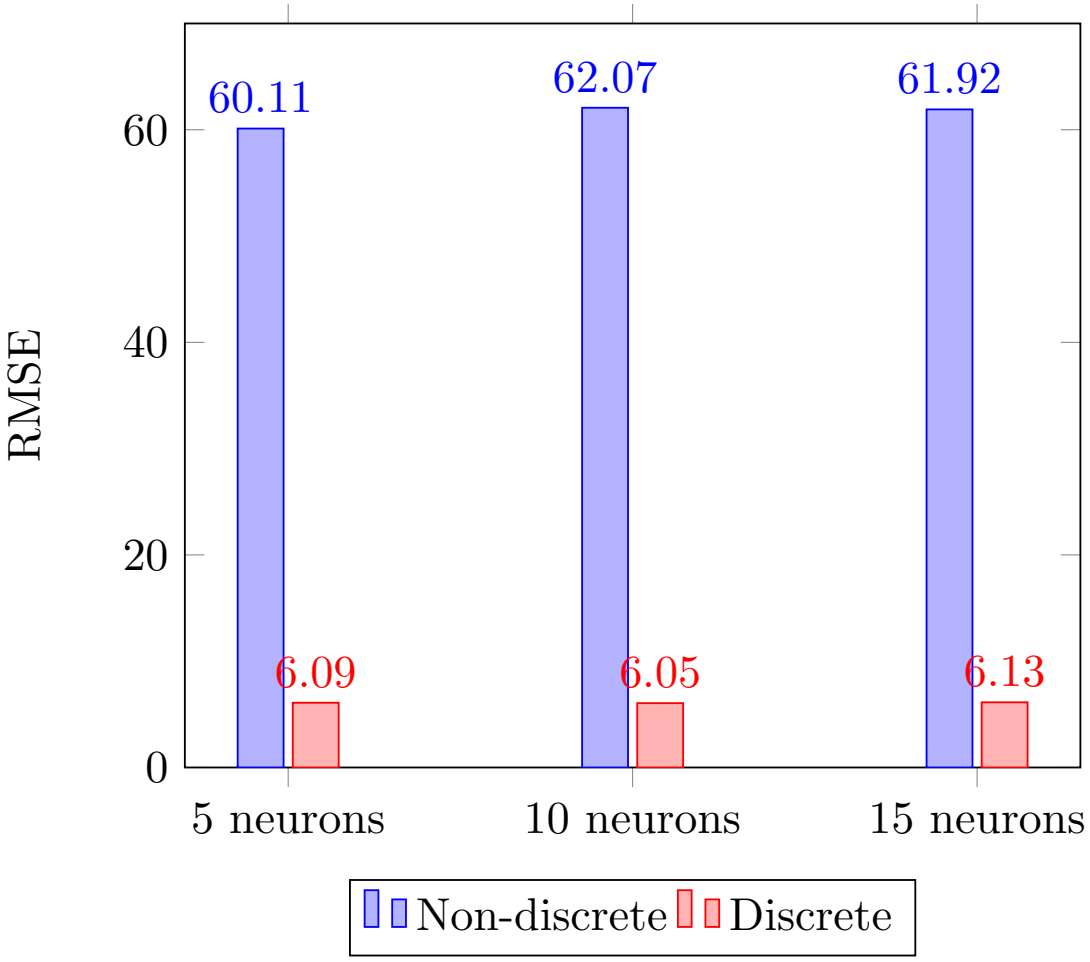

FIGURE 4.15: Performance for the 2nd Hydrological academic Case.

It was observed that all the non-discrete models have a very poor performance when compared with the full-hydrodynamic model. By the other side, the discrete approach can capture the dynamics of the response with good agreement. The non-discrete approach shows a delayed response, with some inverse response (reduction in flow before increasing) and some non-monotonic increase as the response approaches the steady-state. These phenomenons are not seen in the discrete approach.

The results for Case 3 are plotted in Figure 4.16. The performance metrics is exposed in Figure 4.17.

a)

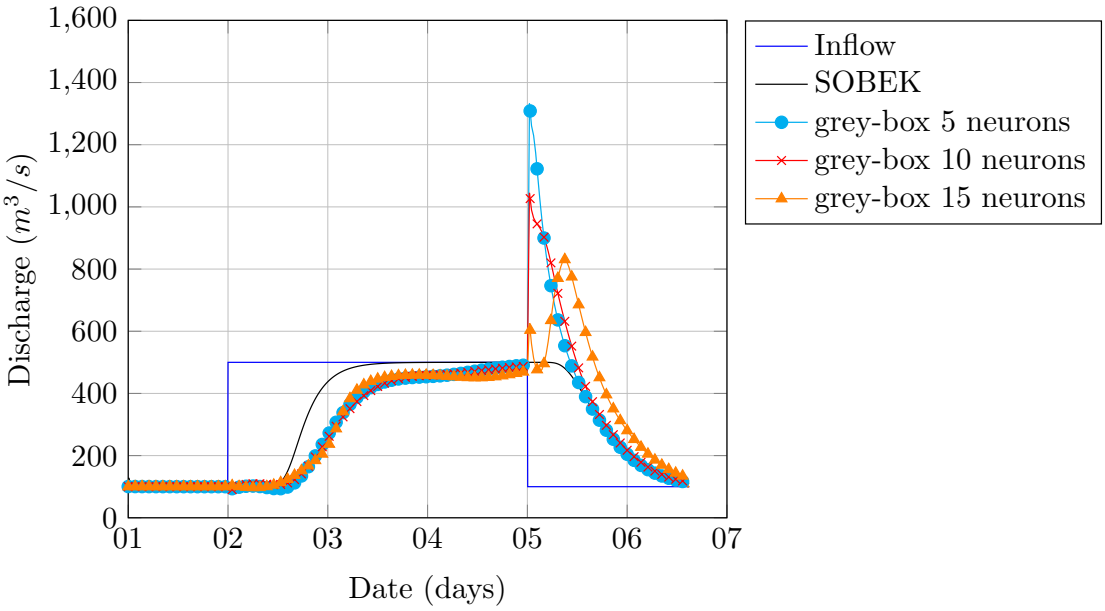

b)

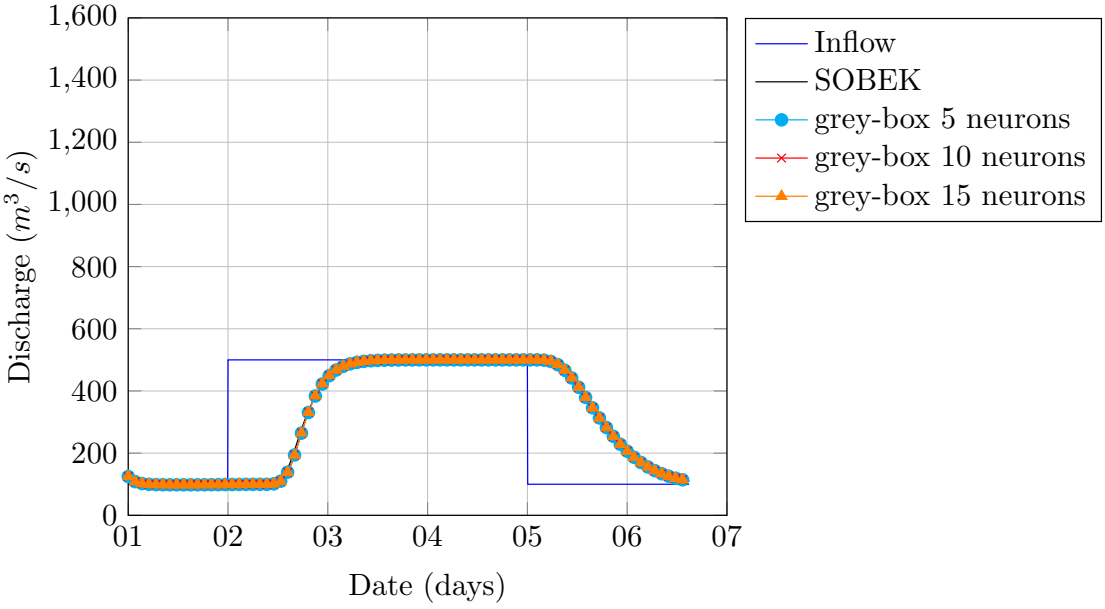

FIGURE 4.16: Case 3 Hydrographs for the (a) non-discretized approach and (b) discretized approach.

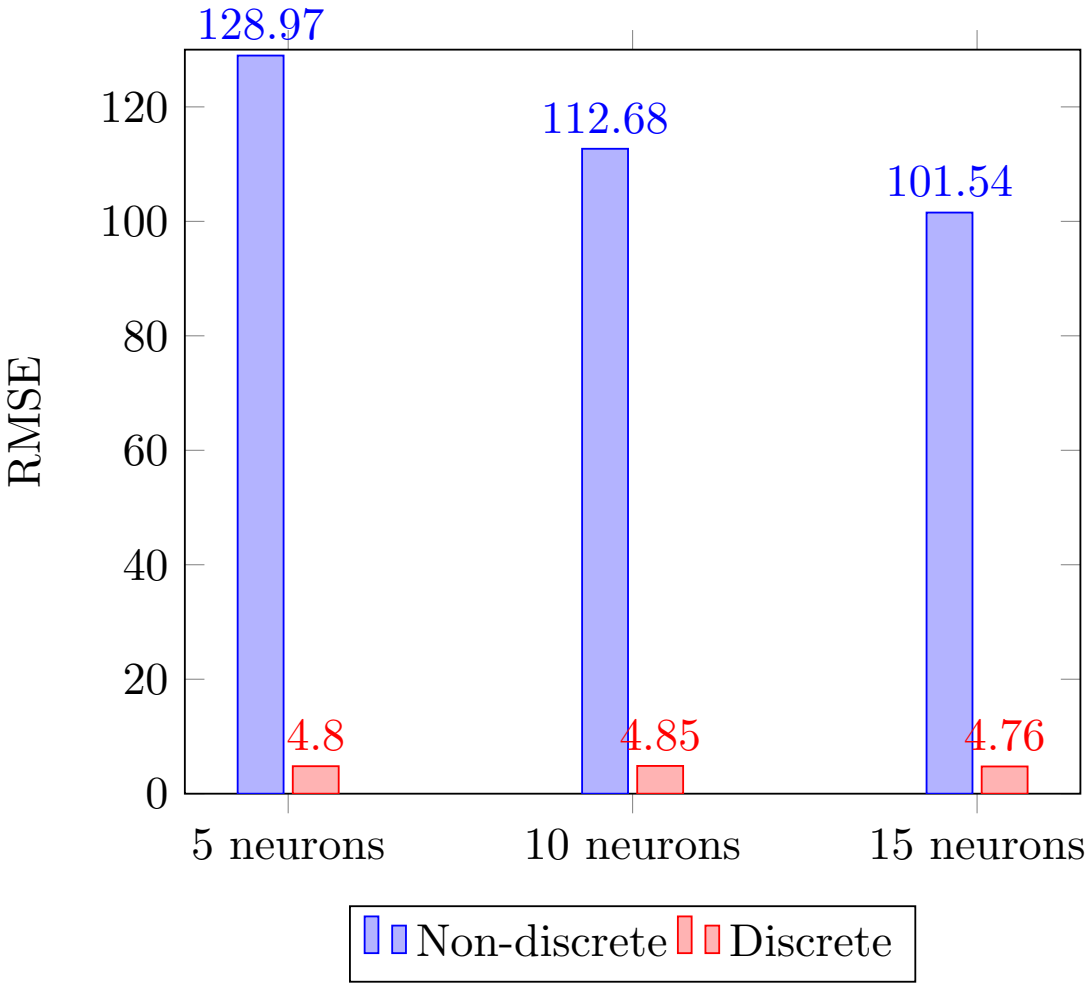

FIGURE 4.17: Performance for the 3rd Hydrological academic Case.

The non-discrete approach, as already expected (because of the results in Case 2), shows lack of agreement with the results from the full-hydrodynamic model. Especially with respect to the recession limb, the non-discrete approach shows a discontinuity in the response with the decrease pulse. On the other hand, the discrete approach shows good performance, also with respect to the delay in the response as given by the full-hydrodynamic model.

At last, the results for both approaches in the Case 4 are shown in Figure 4.18, as well as the performance metrics in the Table 4.19.

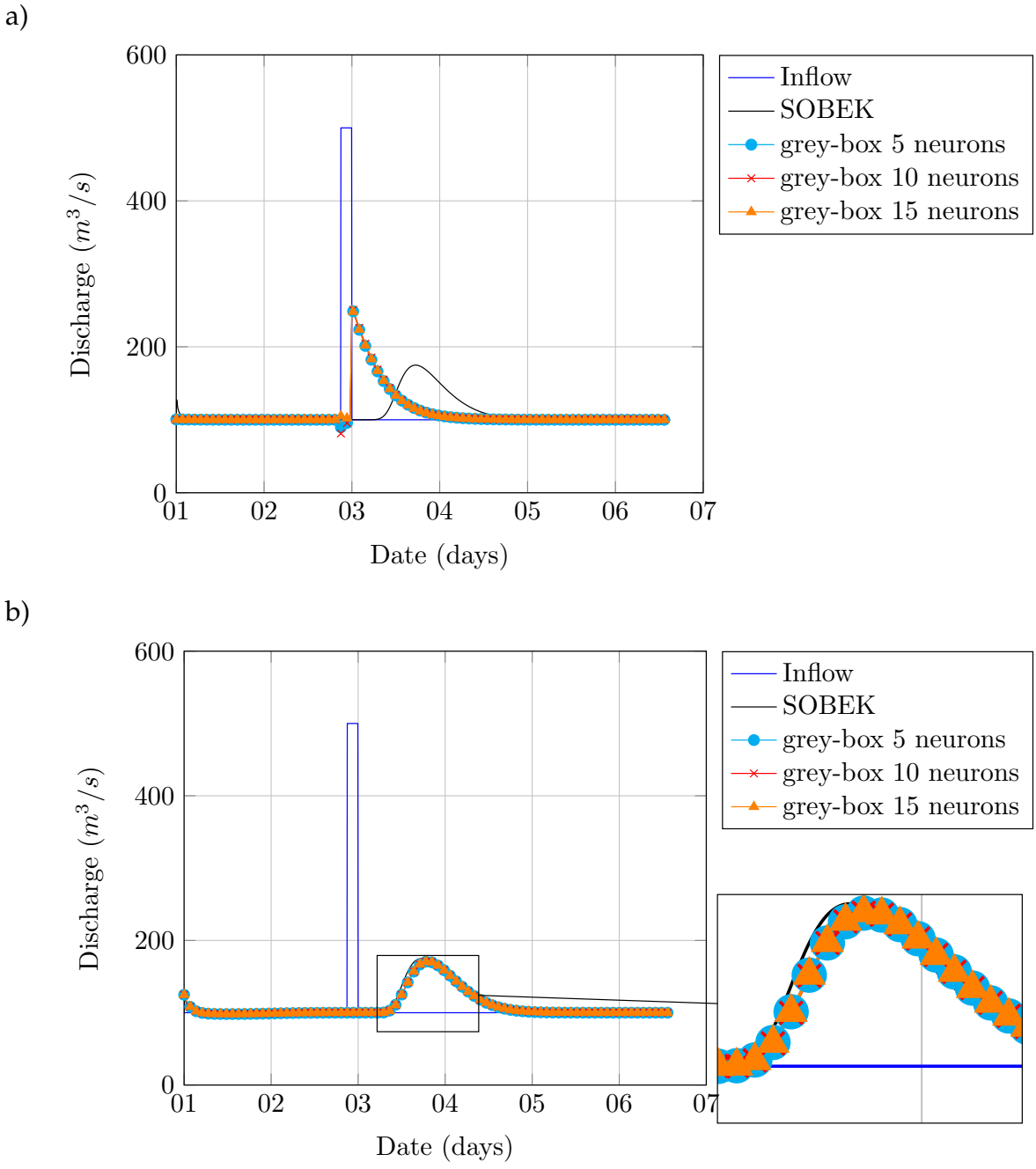

FIGURE 4.18: Case 4 Hydrographs for the (a) non-discretized approach and (b) discretized approach.

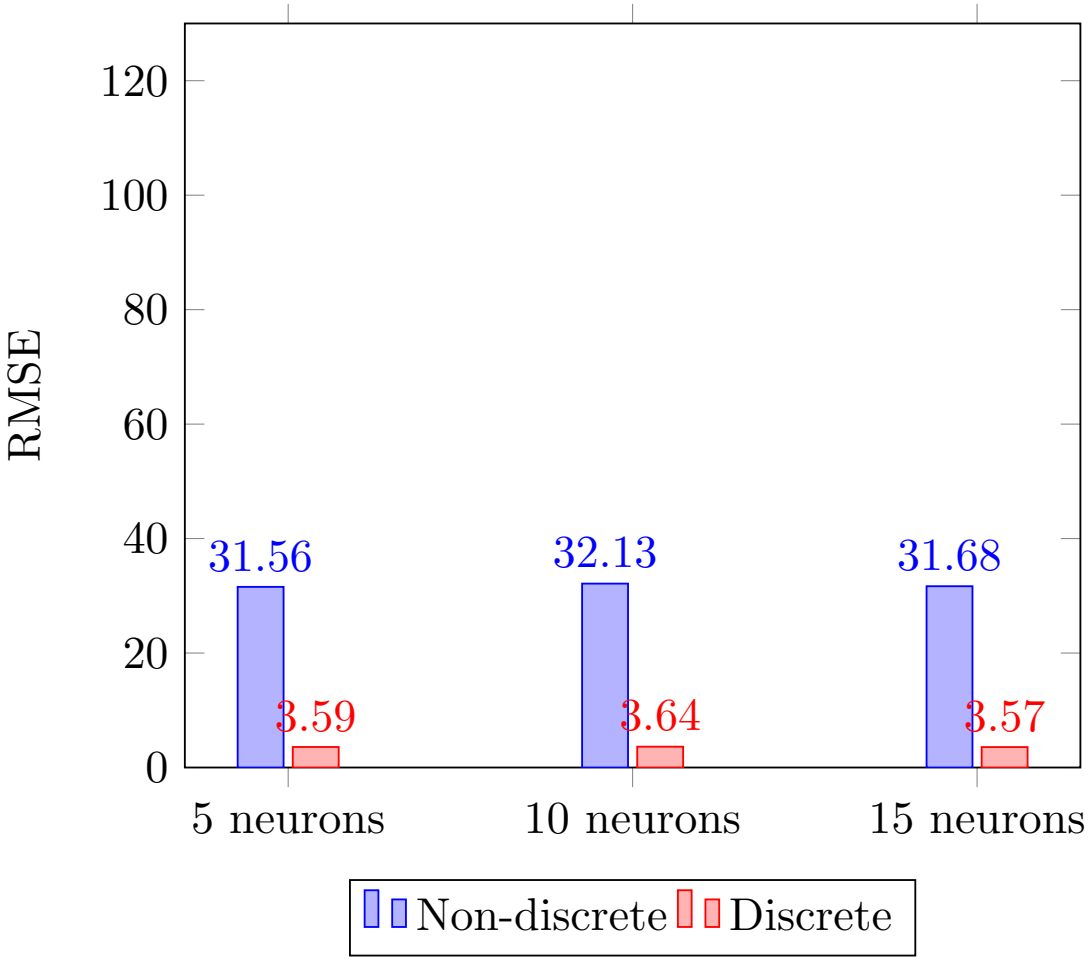

FIGURE 4.19: Performance for the 4th Hydrological academic Case.

Specially in this last case, the non-discrete approach fails to represent the "real" system, as it is not consistent with the results from the full-hydrodynamic model. Nonetheless, the discrete approach captures the dynamics and showed reasonably performance even in such case which the inflow has rapidly increased and decreased.

For a better evaluation of the performance, the model was compared with some other classical hydrological approaches, as will be shown in the next subsection.

4.1.4 Comparison with other models

The Table 4.1 shows the validation performance for the grey-box model compared with other classical hydrological approaches (Linear Reservoirs, Muskingum) against the full-hydrodynamic model. All models were calibrated with

the same data using RTC-Tools, including the grey-box model.

TABLE 4.1: Validation results.

Model	**RMSE**
Non-discrete (BE) 5N	17.208
Discrete (BE) 5N	1.113
Linear Reservoirs	29.93
Muskingum	27.41

The grey-box model shows superior performance when compared with all the other classical approaches here tested. This is expected, as it is reported in literature the capabilities of ANN technique to capture non-linearities and to have high performance when interpolating inside the training range. It capabilities are only compromised once it is requested to extrapolate, that is, to simulate data outside the training range.

To better illustrate the difference in the dynamics of each model, the Figure 4.20 illustrates the results for one flood event in the validation period.

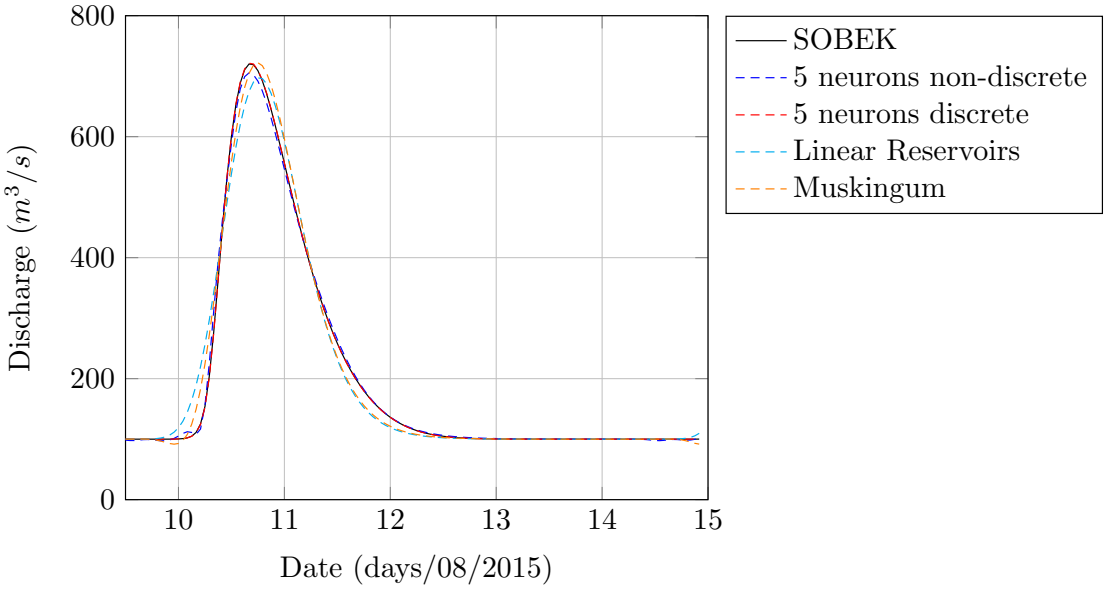

FIGURE 4.20: Comparison of grey-box model, Linear Reservoirs and Muskingum using SOBEK as standard.

It can be seen that the non-discrete grey-box model slightly sub-estimates the flood, with a small compensation for the amount of water through the introduction of a small oscillation at the beginning of the rising limb. The Linear Reservoirs model sub-estimates even more the flood, slightly shifting the peak

and creating a less steep rising limb, and after the peak flood it decreases faster than it should. The Muskingum model shows a small inverse response at the beginning of the rising limb, and also a faster recession limb. At last, the discrete grey-box model shows a very good performance, mimicking the SOBEK as it was expected.

4.2 Grey-box for hydrological flow routing - Pirapora/Brazil

4.2.1 Case description

The São Francisco basin (Figure 4.21) is located between the coordinates $7\,^{\circ}17$ to $20\,^{\circ}50$ latitude south and $36\,^{\circ}15$ to $47\,^{\circ}39$ longitude west. The whole basin is formed by coupled small basins that joins the main river São Francisco and flow into the Atlantic Ocean. The main section of the river has a total length of almost 2.700 km.

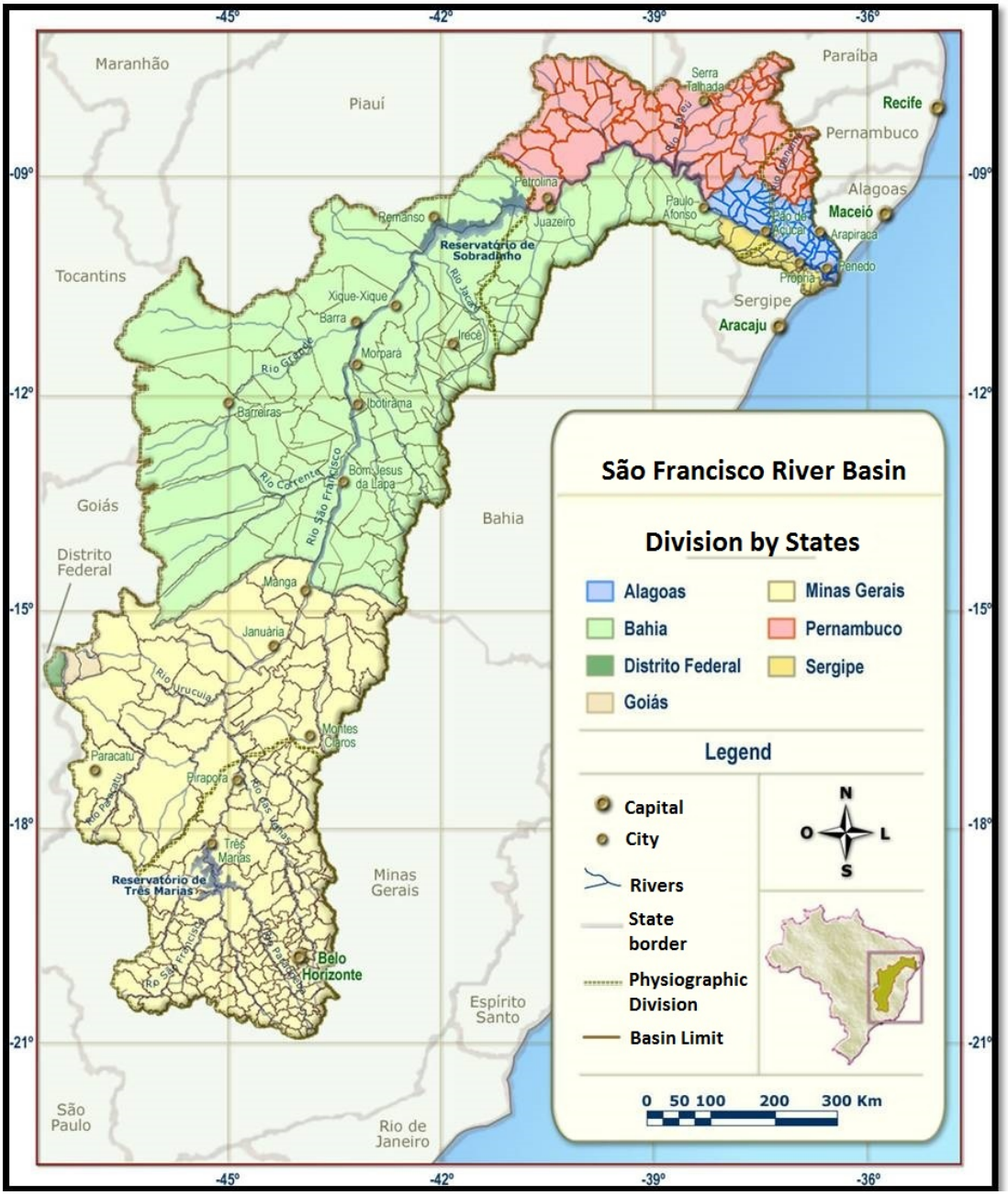

FIGURE 4.21: São Francisco Basin. Adapted from: (ANA, 2003)

The São Francisco basin occupies 638.323 km ^{2}, spread through the Brazilian states of Minas Gerais, Bahia, Goiás, Pernambuco, Sergipe, Alagoas and Distrito Federal, covering 8% of Brazil's. Currently, the basin is subdivided in four regions according to PNRH (National Plan of Hydro Resources). These parts are the upper São Francisco, which covers the source until Pirapora. The middle and submiddle São Francisco, from Pirapora to Remanso, and at last the low São Francisco, from Paulo Afonso until the river mouth (Renováveis, 2006).

The climate conditions of the basin varies along it. The Table 4.2 shows some characteristics of the upper part of the basin, which is the one under investigation in the present study.

TABLE 4.2: Hydroclimatic characteristics of the Upper São Francisco basin.

Characteristic	**Upper**
Predominant climate	Humid and temperate rain altitude
Average Annual Rainfall(mm)	2.000 to 1.100
Average Temperature (°C)	23 °C
Average Annual Insolation(h)	2400
Average Annual Evapotranspiration (mm)	1000
Main patch length (km)	702
Main river declivity(m/km)	0,7 to 0,2
Contribution of average natural flow (%)	42,0
Specific Flow (L.s^{-1}.km^{-2})	11,89

The hydro energy potential is estimated as 26300 MW, and the installed capacity is 10380 MW, which represents 16 % of the Brazilian energy matrix, with 33 plants in operation. The reservoirs are also used for water supply, recreation and irrigation (CEMIG, 2012).

One of the major reservoirs in the São Francisco river is the Três Marias hydro reservoir. It is a multipurpose reservoir, i.e, it is used for flood mitigation, energy production, irrigation and for smoother navigation along the São Francisco river. The starting point for the construction of the reservoir was in 1958. Its operation began in 1962, with 2 main energy production cores, each one with 66 MW. Actually it possess 4 generation units, with a total installed potential of 396 MW, feeding a electric network capable to support 1.1 million people (CEMIG, 2012). Some data from the reservoir is summarized in Table 4.3.

TABLE 4.3: Três Marias reservoir characteristics

Total Area	1090 km^2
Maximum Volume	19528 hm^3
Maximum Usable Volume	15278 hm^3
Minimum Water level	549.2 m
Maximum Water level	572.5 m
Installed Potential	396 MW
Nº of generators	6 MW
Type of turbines	Kaplan

The operation of the reservoir is regulated by ANA (National Water Agency), and there are a series of regualatory constraints in the operation of the reservoir, such as the outflow minimum or maximum, both at the turbines outlet, as well as downstream, as in the Pirapora gauge, named after the city at the same location. Figue 4.22 shows a schematic overview of the reach downstream Três Marias hydro reservoir up to the Pirapora gauge.

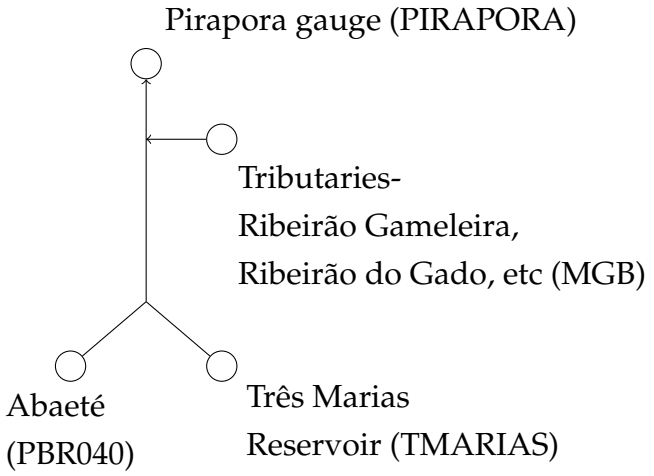

FIGURE 4.22: Overview of Upper Sao Francisco Basin - path between Três Marias Reservoir, PBR040 and Pirapora gauge.

This river section was modelled using the grey-box hydrological routing technique. For simpler referencing, the flow at the Abaeté river gauge is named PBR040 (which means "bridge over the road BR040"), the outflow from Três Marias Reservoir is TMARIAS and the flow at Pirapora gauge is PIRAPORA.

The tributaries and additional rainfall that contributes to PIRAPORA are obtained using a set of inflows generated using MGB (Modelo de Grandes Bacias) model.

The data obtained for PIRAPORA has resolution of one hour. The input data for the model are TMARIAS, PBR040 and MGB (this last one is a series of discharges along the catchment). The period of available data corresponds to 10.07.2008 until 22.06.2012, with 34651 hourly data records. Table 4.4 shows some statistics of the available data.

TABLE 4.4: Dataset statistics.

Inflow Boundaries	**Mean ($m^3.s^{-1}$)**	**Maximum ($m^3.s^{-1}$)**	**Minimum ($m^3.s^{-1}$)**	**Standard Deviation**
MGB(total)	273.892	2578.709	233.718	95.556
TMARIAS	71.587	1368.6	7.6	101.917
PBR040	724.749	3125.39	39.44	412.947
PIRAPORA	819.324	3557.5	415.0	429.381

As in the academic hydrological case described above, two approaches here were also tested, a non-discrete approach and a discrete one. The discrete grey-box hydrological model for this case consisted in 15 sequential nodes. A full-hydrodynamic model (SOBEK) was used to calibrate the grey-box model. The period for calibration was from 10.07.2008 00:00:00 to 27.06.2011 23:00:00. The validation data was from 27.06.2011 23:00:00 until 22.06.2012 21:00:00.

4.2.2 Model implementation

The model implementation of the Pirapora case follows the same procedures for the academic case, described in the section above.

4.2.3 Results and discussion

The obtained results for the calibration and validation periods are summarized in Figures 4.23, 4.24 and 4.25. As shown in the Figures, different schemes were tested, a Forward-Euler (FE) scheme with a time step of 20 seconds and a Backward-Euler scheme (BE), using a time step of 1800 seconds.

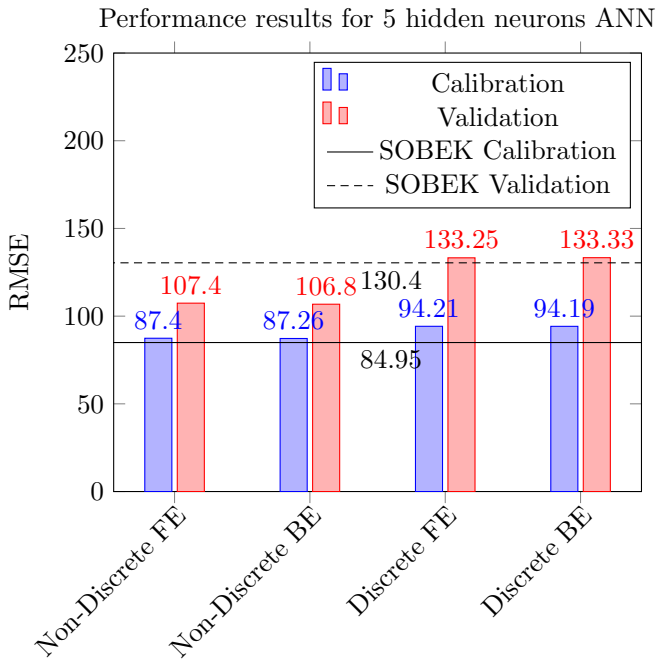

FIGURE 4.23: Performance for Pirapora case - 5 neurons in hidden layer.

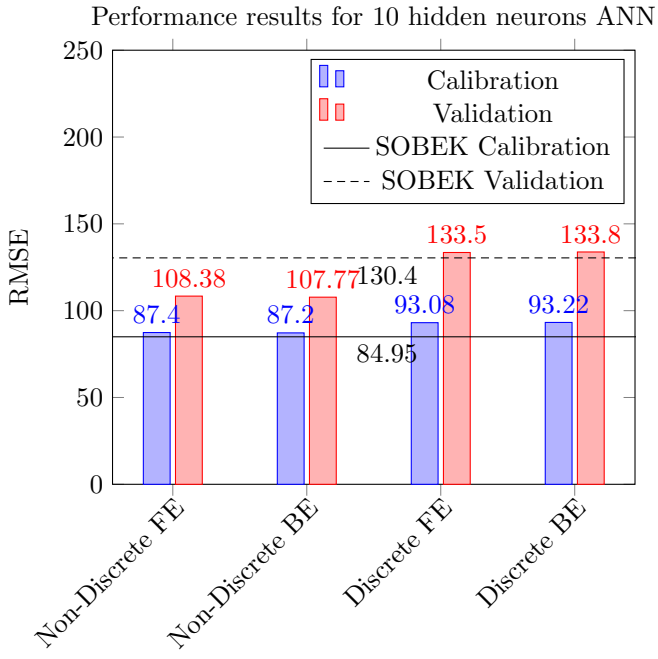

FIGURE 4.24: Performance for Pirapora case - 10 neurons in hidden layer.

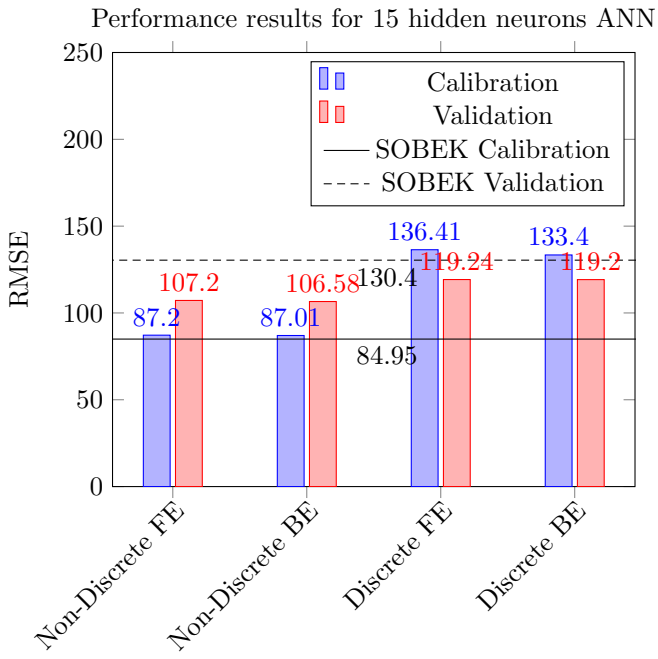

FIGURE 4.25: Performance for Pirapora case - 15 neurons in hidden layer.

The results show that better performance is achieved by using an implicit scheme (Backward-Euler) with a non-discrete approach. The discrete approached shows instabilities using a time step of 1800 seconds. It was expected that the spatial discretization would provide better performance, but that was not the case. This fact may be attributed to the accumulation of errors in the routing downstream, resulting in a worst performance when compared with the non-discrete which used a single ANN to route the flow upstream the catchment to downstream. Also, for the non-discrete approach the performance gets better with the increase on the number of the neurons in the hidden layer of the ANN, as expected. However, the discrete approach shows a inverse relation, i.e the performance got worst for a higher number of neurons, which can be again correlated with the accumulation of errors and also due to the elevated non-linearity of using a cascade of ANN with 15 neurons in the hidden layer.

The Figures below illustrate the results for calibration and training using both approaches. For simplicity, it is plotted the results for the implicit scheme. The figures visualize that, although the performance for the discrete approach was worst, it was accurate and could capture the dynamics of the catchment with good agreement. Comparing time consumed and performance, the forward-euler scheme has a similar performance when compared with the backward euler scheme, and the simulation time increased severely, around 490% (from 68.8

seconds (BE) to 338.7 seconds).

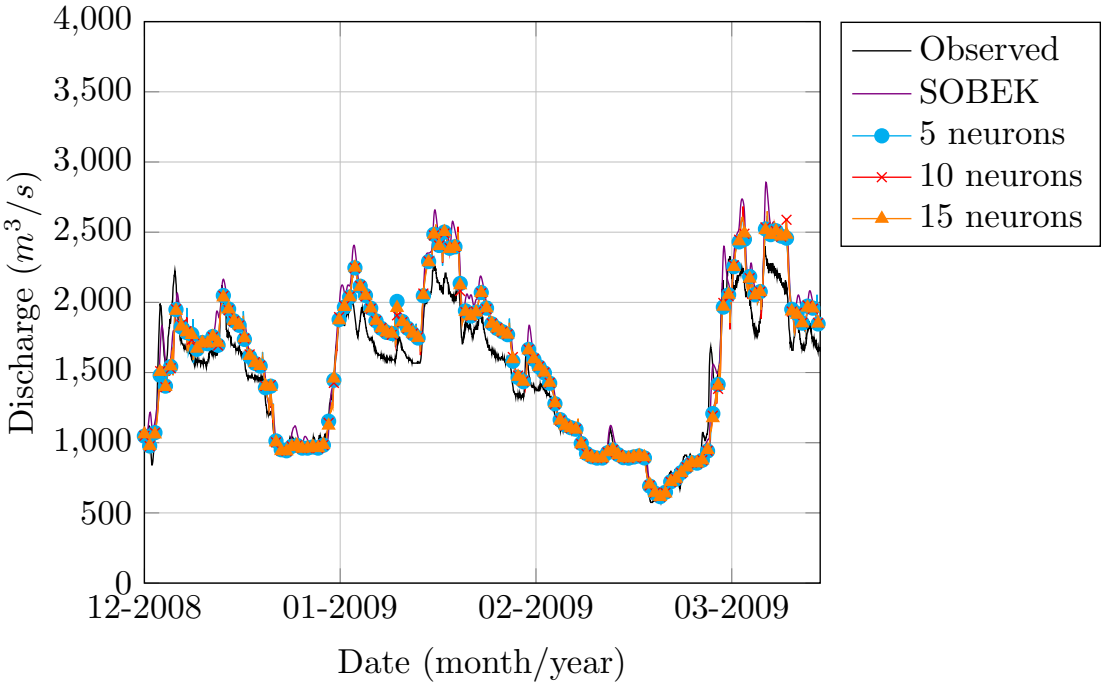

FIGURE 4.26: Training results for the non-discrete approach - Pirapora case.

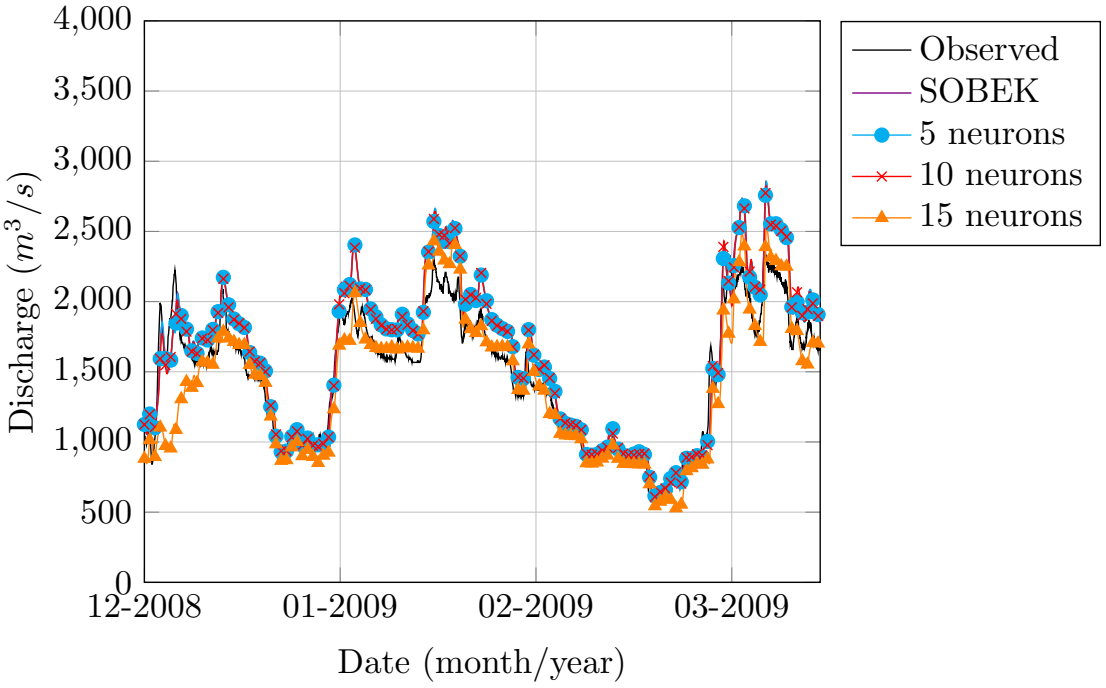

FIGURE 4.27: Training results for the discrete approach - Pirapora case.

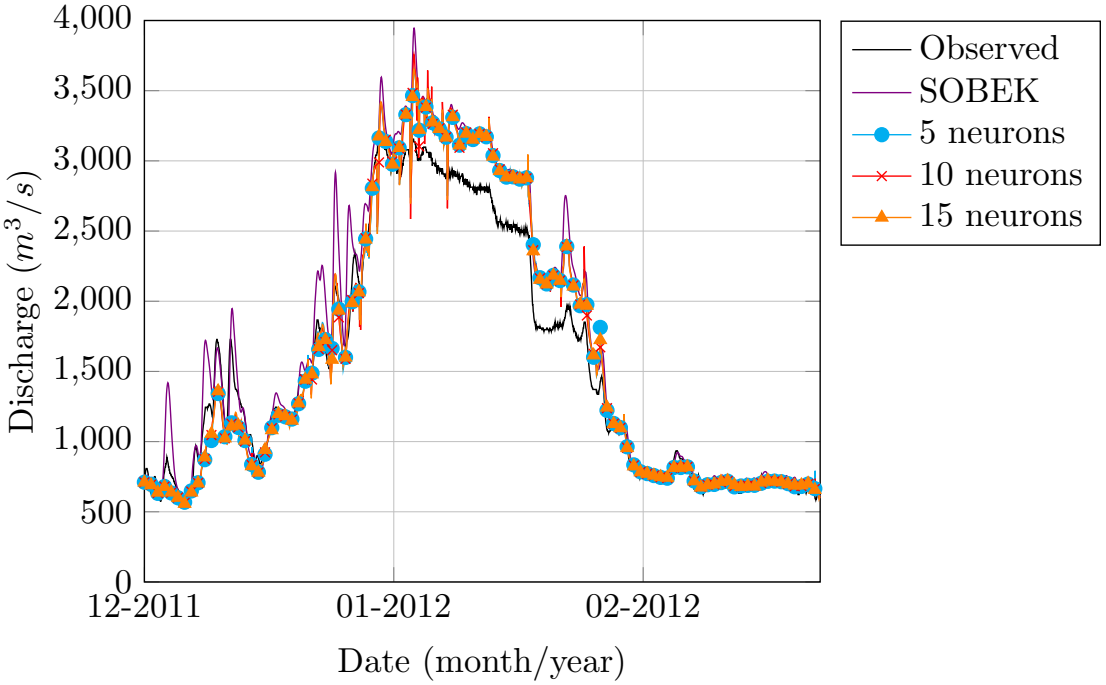

FIGURE 4.28: Validation results for the non-discrete approach - Pirapora case.

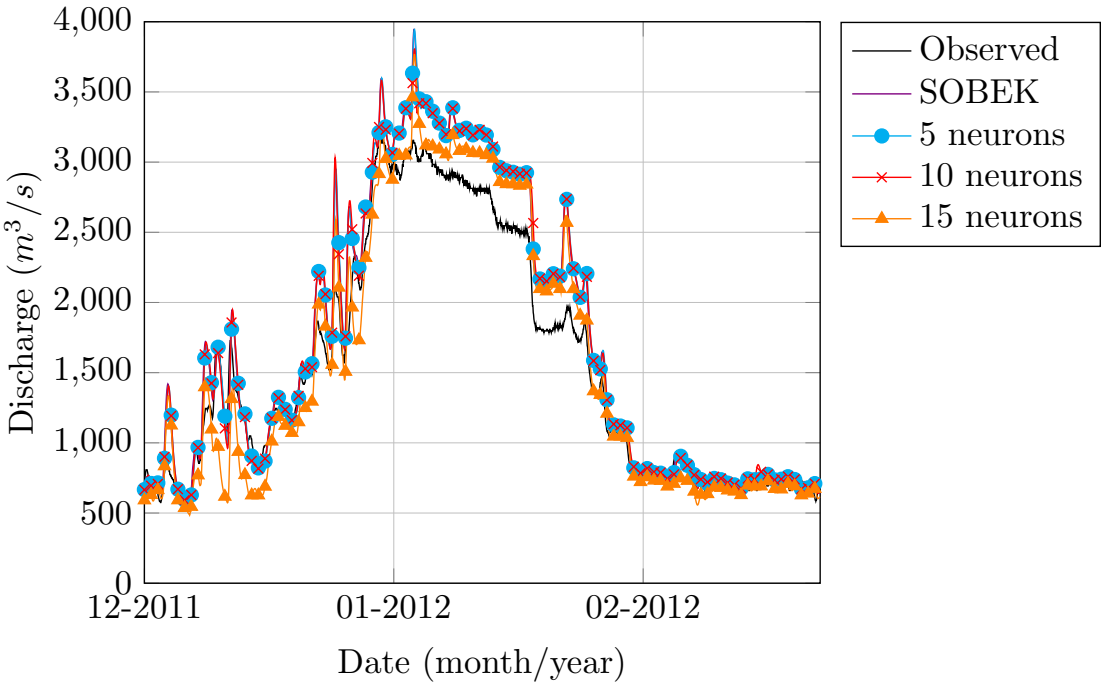

FIGURE 4.29: Validation results for the discrete approach - Pirapora case.

It is interesting to observe that, in the validation data, the grey-box outperforms the SOBEK, and the reason can be seen in the Figure 4.28 and 4.29. There is a flood event which the observed outflow is much less than simulated by the full-hydrodynamic model. Because the non-discrete grey-box models, in this case, has a tendency to sub estimate the peaks in flood events, it could have a better agreement with the observed data. Nonetheless, this is unexpected, as the grey-box models were calibrated using the data obtained by the full-hydrodynamic model.

As supplementary comparison, the next section shows a comparison in performance for the developed models with some other classical approaches.

4.2.4 Comparison with other models

Additional validation is done for the developed grey-box model, by comparing the results with some classical hydrological approaches ((Linear Reservoirs and Muskingum) as well as the full-hydrodynamic model agains the observed data. The performance metrics is seen in Table 4.5.

TABLE 4.5: Validation results.

Model	**RMSE**
SOBEK	130.4
Non-discrete (BE) 15N	106.58
Discrete (BE) 15N	119.2
Linear Reservoirs	134.62
Muskingum	134.98

In the results, the performance of the grey-box is significantly superior to the classical hydrological approaches. This is expected, as the ANN possesses great flexibility due to its high number of parameters and transfer functions, which makes them capable of capturing non-linear dynamics with great efficiency. Nonetheless, the fact that the performance of the grey-box is superior to the SOBEK model is not expected, since the latter is used to calibrate the grey-box model. This superior performance occurs because there is a sub estimation of the peak flows attributed to a decrease in flow at the boundaries of the calibration range of the Artificial Neural Networks.

The following figures illustrates those results. Figure 4.30 shows the results for the different models during high flood season (summer in South Hemisphere). The discrete grey-box model had a discrepant result, due to sub-estimation of the flows. The Muskingum and Linear Reservoirs almost overlap each other, and they showed similar results with the full-hydrodynamic model, but with some anticipation. The non-discrete grey-box could follow more closely the full-hydrodynamic one.

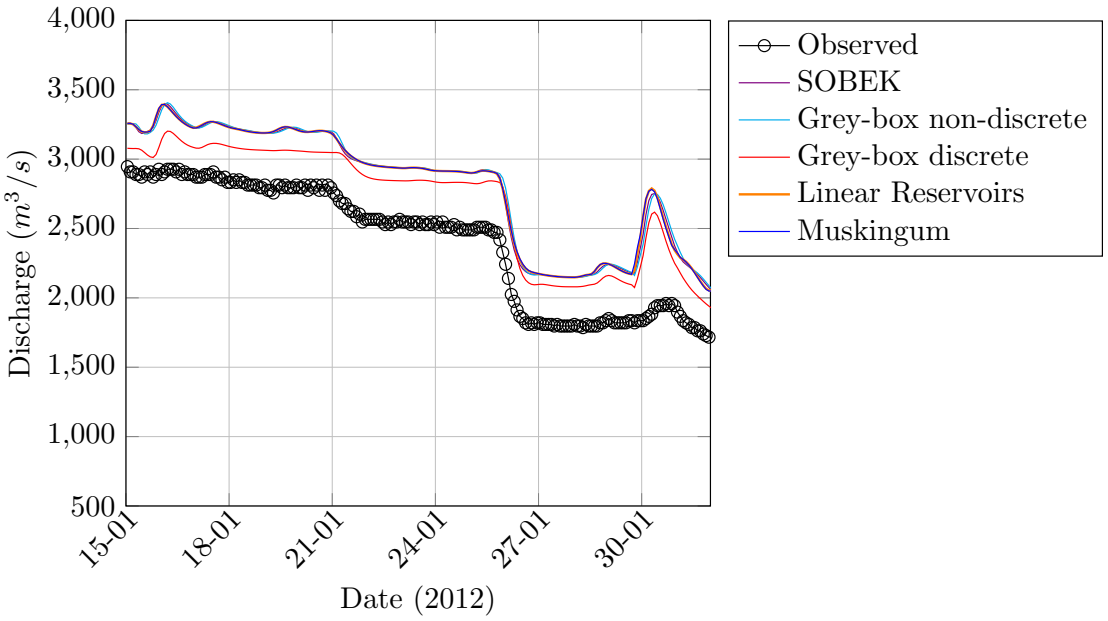

FIGURE 4.30: Comparison of different models for Pirapora case during high flood season.

The obtained results for the low flood season are compared, as shown in Figure 4.31. Again, the sub-estimation of the flows provided by the grey-box model aided it in obtaining a good performance. Even during low flood conditions, the linear models (Muskingum and Linear Reservoirs) anticipate the flow, while the non-discrete grey-box model follows more closely the full-hydrodynamic model.

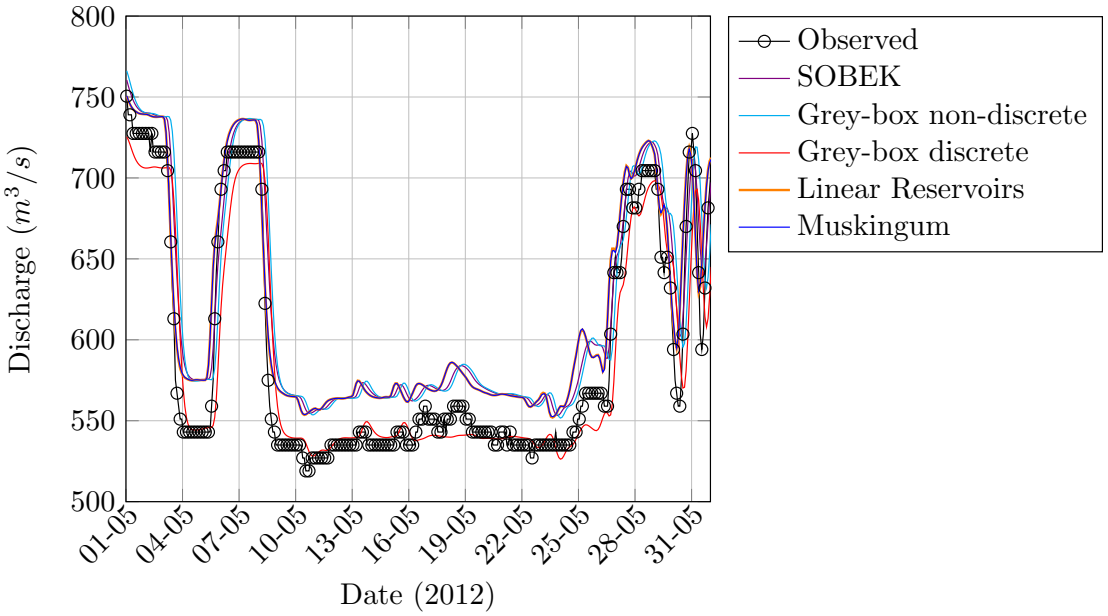

FIGURE 4.31: Comparison of different models for Pirapora case during low flood season.

4.3 Grey-box for hydraulic flow routing - Academic case

4.3.1 Case description

The river morphology, as well as the boundary conditions for the hydraulic academic case refers to the same as the hydrological academic case, as described in subsection 4.1.1. The additional components inserted in this case were a set of 5 weirs, which are capable of controlling the upstream water levels through the manipulation of crest levels. The characteristics of the weirs is shown in Table 4.6. An illustrative profile is shown in Figure 4.32

TABLE 4.6: Characteristics of the weirs.

Weir	**Width**	**Minimum crest level**	**Maximum crest level**
1st	165	23	28
2nd	165	18	23
3rd	165	13	18
4th	165	8	13
5th	165	3	8

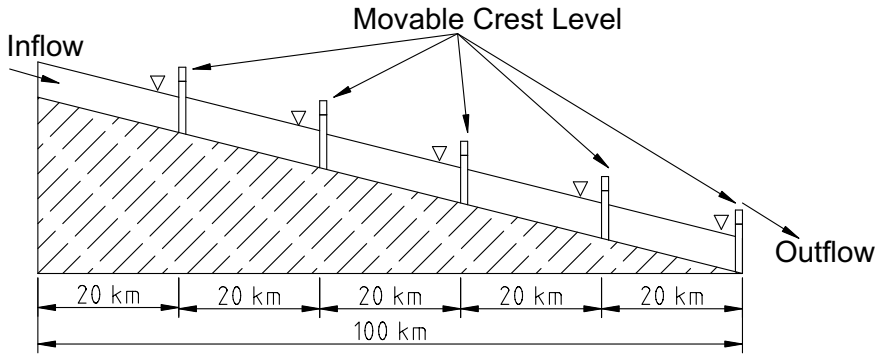

FIGURE 4.32: Illustrative profile of the Hydraulic academic case.

The whole dataset refers to a period of 1 year (hypothetically from 01.01.2015 00:00:00 until 01.01.2016 00:00:00). The dataset is subdivided into training (75% of the period, from 01.01.2015 00:00:00 until 01.09.2015 00:00:00) and validation data (the remaining 25% or 01.09.2015 00:00:00 until 01.01.2016 00:00:00). For a broader range of validity of the model, the crest levels of all the weirs are varied randomly, so as to create fluctuations. The Figure 4.33 shows the crest levels values for the calibration and validation data.

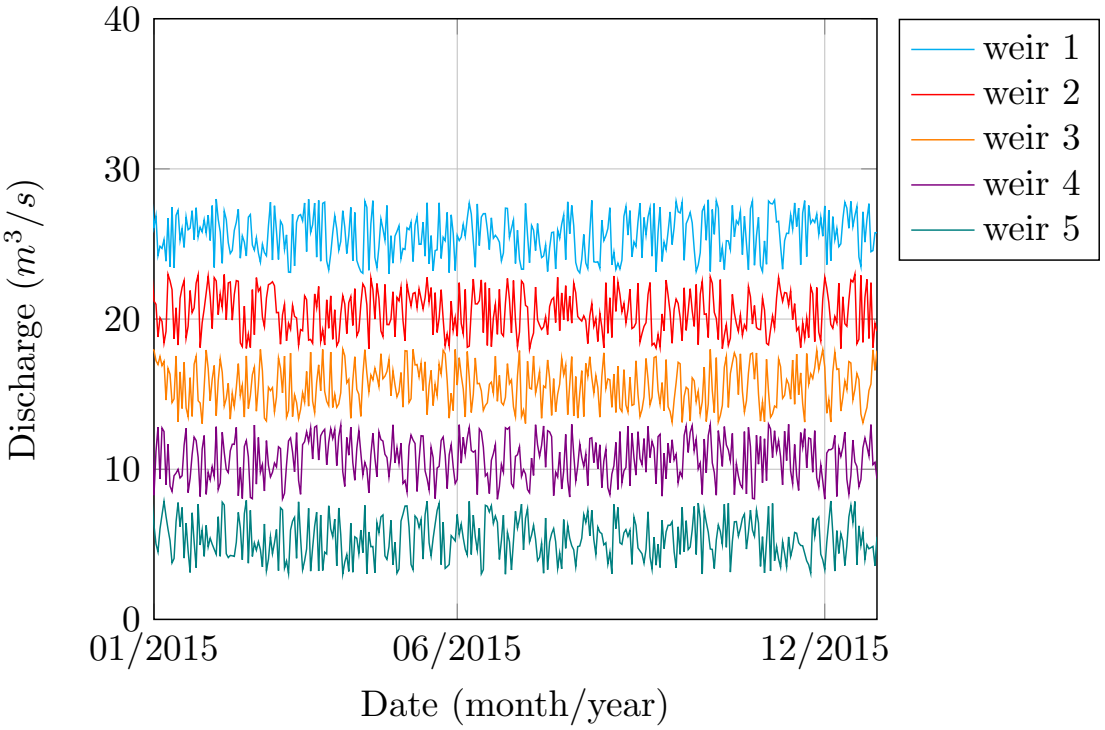

FIGURE 4.33: Crest Levels for the 5 weirs for the calibration and validation period.

The model was simulated in SOBEK, and a simplified inertial model was derived from it.

The SOBEK model is used in this case as an "observed" dataset. The inertial model was used to calibrate the grey-box model, and the performance of both was compared with the SOBEK model.

4.3.2 Model implementation

The model is implemented using Simulink ©. Figure 4.34 shows the scheme for calculating the discharge of one single branch.

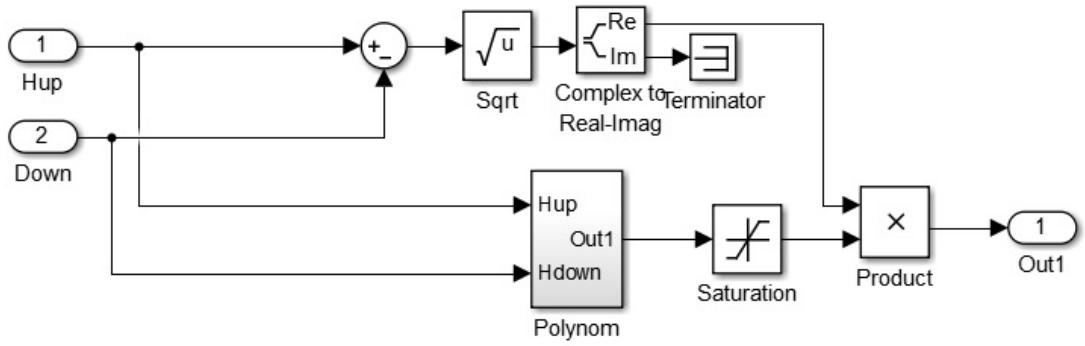

FIGURE 4.34: Simulink scheme for Grey-box Hydraulic Approach - Branch.

For locations where one or more weirs are located, the calculations are made by by replacing the branch by a Matlab Function Block that uses a weir equation as stated in SOBEK manual (Deltares, 2015)

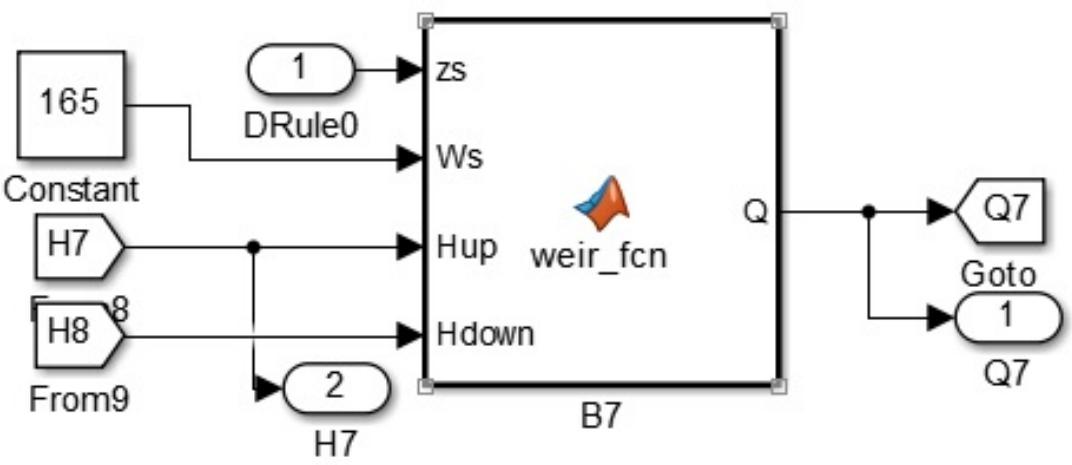

FIGURE 4.35: Simulink scheme for Grey-box Hydraulic Approach - Weir location.

The PI control scheme is implemented by creating a subsystem with the blocks from Figure 4.35 and directly inserting the controller block in the model diagram, configuring the closed loop.

The MPC control is implemented by generating a MATLAB function file that runs the model, and using this function inside an optimization implemented in MATLAB. In the present work, it is used the *fmincon* function, with interior-point algorithm.

4.3.3 Results and discussion

The SOBEK model used is in essence the same from the subsection 4.1.1, with the difference that the 5 weirs were inserted along the reach, with a distance of 20'000m between each other, in such a way that the last weir is settled at the end of the reach. Regarding spatial discretization, it is used 207 nodes where mass continuity is calculated. The time step used was of 60 seconds. The simulation of 1 year period took 175 seconds.

The inertial model is composed of 40 nodes where mass continuity is calculated. The storage characteristics of each node (the water level - storage relation) is extracted from representative nodes in the full-hydrodynamic model. Also the branches characteristics are obtained from representative branches from the SOBEK model. The time step used was of 20 seconds due to stability issues. A single run of the 1 year period took 341.9 seconds, encompassing preprocessing, simulation itself and post-processing. The last represented 67.5% of this time, and just the simulation itself took 6.24 seconds.

The grey-box model has the same structure of the inertial model, as the latter was used to calibrate it. Different time schemes were tested:

- Forward Euler $\Delta t = 20$ (FE)
- Runge Kutta 4th order $\Delta t = 90$ (RK90)
- Runge Kutta 4th order $\Delta t = 180$ (RK180)
- Backward Euler $\Delta t = 450$ (BE)

The performance results for the training and validation datasets are shown in Table 4.7.

TABLE 4.7: Calibration and Validation results.

Model	**RMSE Calibration**	**RMSE Validation**
Inertial	12.65	13.17
FE	18.45	19.12
RK90	14.94	14.77
RK180	20.54	20.78
BE	18.46	19.14

Best performance for the grey-box model was achieved using a Runge-Kutta scheme with a time step of 90 seconds (RK90). To measure time of simulation, the model is transformed from Simulink to C code using Simulink Coder tool. The simulation for the whole period of 1 year took 5.9 seconds, which means that it is almost 30 times faster than the SOBEK model. A representative part of the training results is shown in Figure 4.36, and part of the validation results is shown in Figure 4.37.

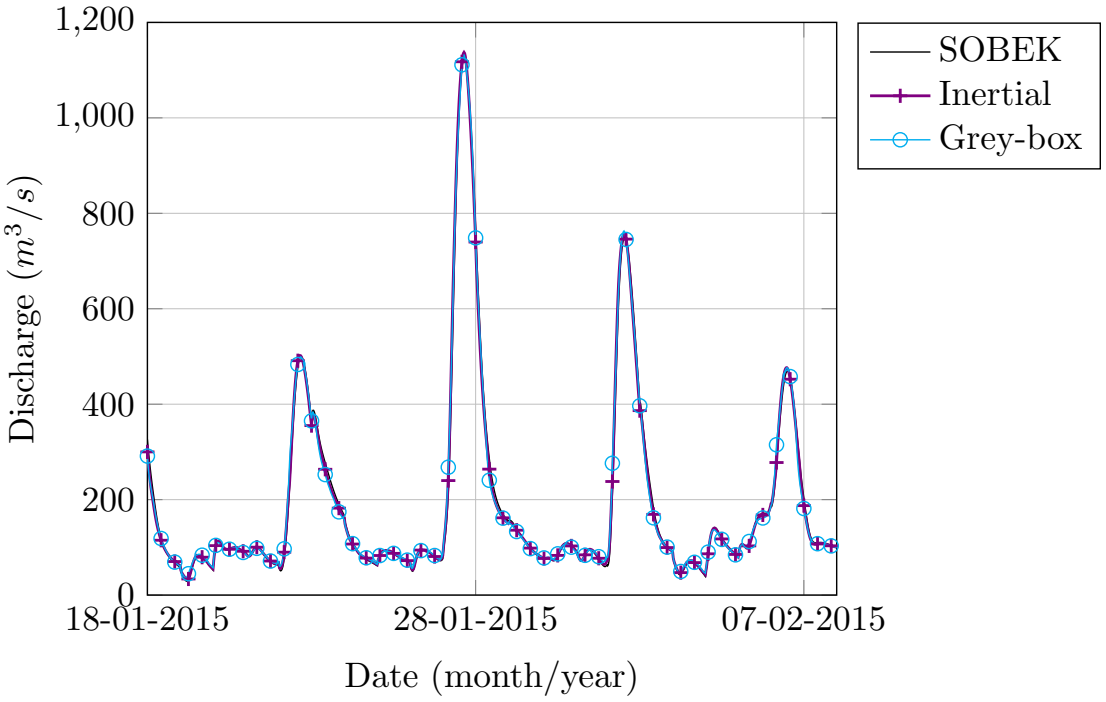

FIGURE 4.36: Training results for the hydraulic academic case.

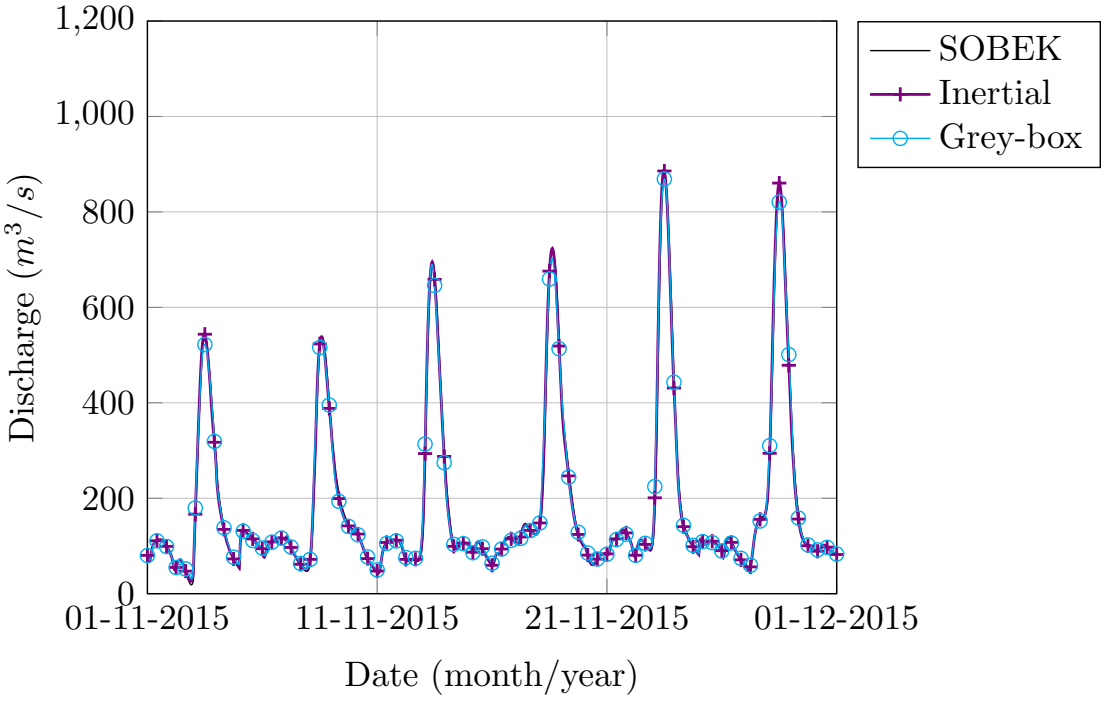

FIGURE 4.37: Validation results for the hydraulic academic case.

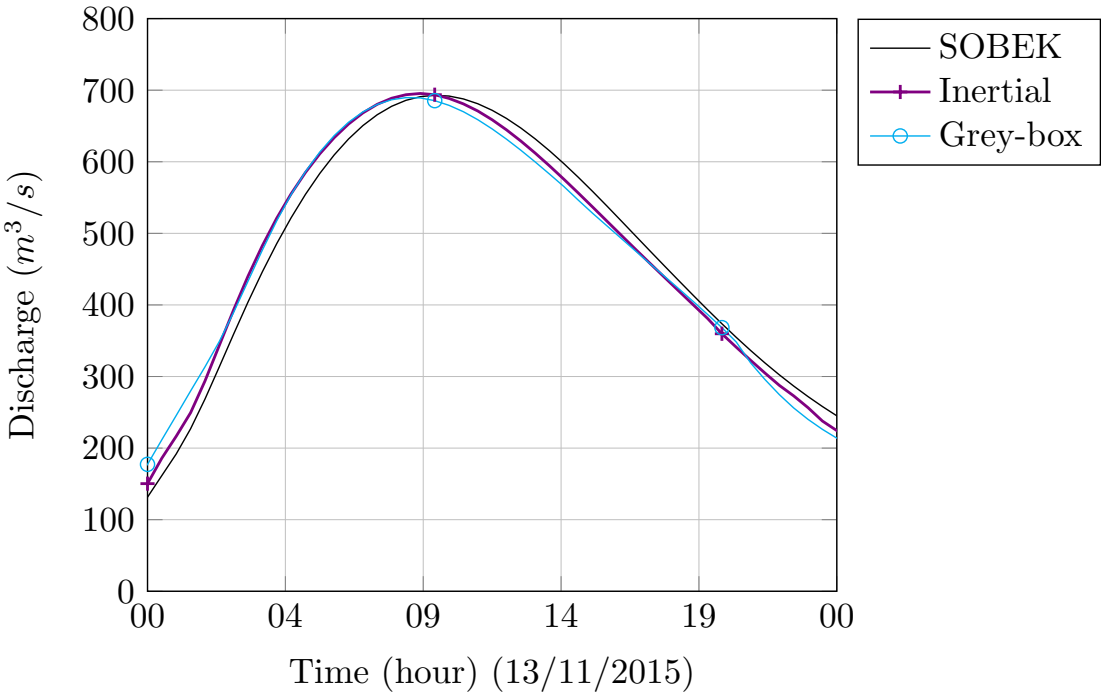

FIGURE 4.38: Validation results for the hydraulic academic case - Zoom in flood event .

The results show that the grey-box model has a very similar performance

with the inertial model, which was used to calibrate it. The limitation is that, as the inertial model is taken as the basis for training, the grey-box model will not get better performance as this model. So a requirement for this approach is to use a model with good accuracy as a basis to calibrate the grey-box model, as the performance that it will reach will be similar, but not better than this one.

Another important point to be discussed is the simulation time. The model was developed and simulated using MATLAB and Simulink, which are high-level languages. It is necessary to implement the model in a lower level language or to use a tool to "translate" the code (as it was done with Simulink Coder), so as to reach the necessary computational performance and to implement the model in frameworks which requires model demanding low computational resources.

4.3.4 Results and discussion - Control

The model was also tested in control schemes. First a control scheme using feedback-control PI was used to keep desired water levels at set point by implementing steps in the crest levels of the weirs. An additional feedforward controller was also implemented, taking as disturbance the discharge downstream the previous weir, so as to control the downstream weir.

The calibration of the PI was done through trial and error, i.e the parameters K_P (proportional gain) and K_I (integrator gain) were disturbed and searched iteratively for a reasonable value which is able to control the water levels with small or no oscillations. For all the five weirs, the following values of parameters were used:

- $K_P = 5$
- $K_I = 0.1$

In order to avoid continuous integration when the PI output is saturated a method called anti-windup through back-calculation is used. According the Simulink documentation, back calculation enables the integrator to discharge when the block output saturates using the integral-gain feedback loop. The discharge level is regulated using a back-calculation coefficient of 0.001.

To illustrate the control results, the Figure 4.39 shows the results for the PI control on the first and last weirs. The obtained results for the grey-box model are compared with the ones obtained with the inertial model.

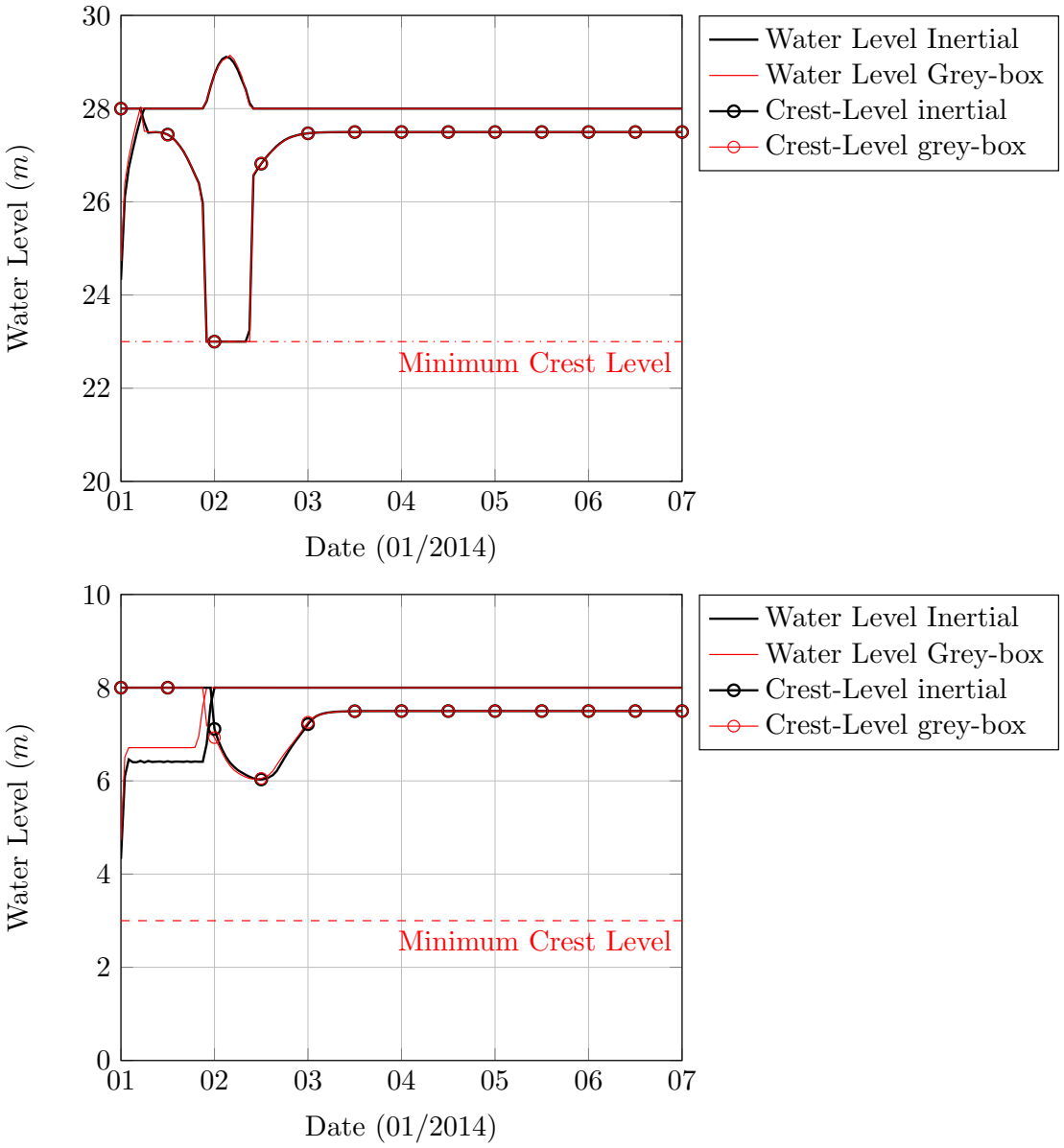

FIGURE 4.39: PI control of the 1st and 5th weir.

One may see that there was good agreement between the PI results for both modelling techniques. Also, the PI controller could keep the water level on set point for the simulated time, except during the peak flow event. In this occasion, the controller saturates in the minimum crest level (23m) and keeps in this level as long as the flow event lasts. The anti-windup term is specially useful during this event, as if the integrator value continued to grow with a saturated controller output, it would lead to a poor performance after the event has taken place. This condition can be seen in the Figure 4.40, where the grey-box performance was compared with and without windup method using PI control.

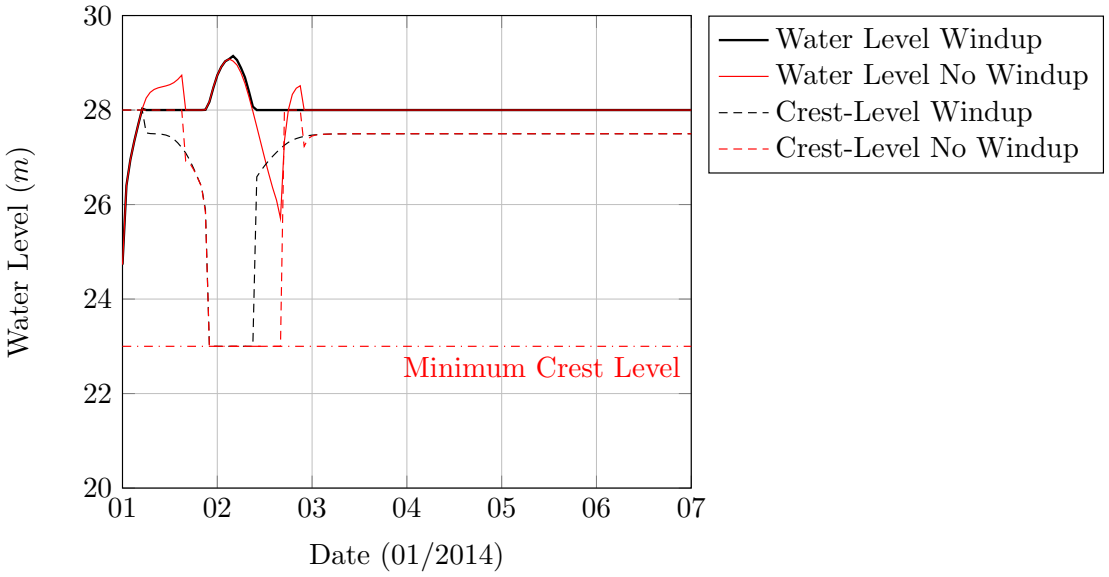

FIGURE 4.40: PI control of the 1st weir.

The next step compromises the use of Model Predictive Control to keep water levels at set point. The optimization problem was defined as:

$$\begin{aligned} \min_{\{u_t\}_{t=1}^{h}} \quad & \sum_{t=1}^{h-1}\sum_{j=1}^{39}(h_j - sp_j)^2 \qquad for j = 7, 15, 23, 31, 39 \\ \text{subject to} \quad & x^t - f(x^{t-1}, u^t, d^t) = 0 \\ & hmin_j \leq h_j \leq hmax_j \end{aligned} \tag{4.4}$$

where:

$x^t - f(x^{t-1}, u^t, d^t) = 0$ - the model (grey-box or inertial)

h_j - water level in location j

u_j - crest level for the weir downstream location j

sp_j - *setpoint* value for water level in location j

$hmin_j$ - lower bound for the water level in location j

$hmax_j$ - upper bound for the water level in location j

The equation above shows that the optimization problem objective is to minimize the term $(h_j - sp_j)^2$ that refers to the difference between the actual water level h_j and the desired set point value sp_j.

The Figures 4.41 to 4.45 illustrate the control of the 5 weirs using the MPC scheme. A comparison between the inertial model and the grey-box model is provided.

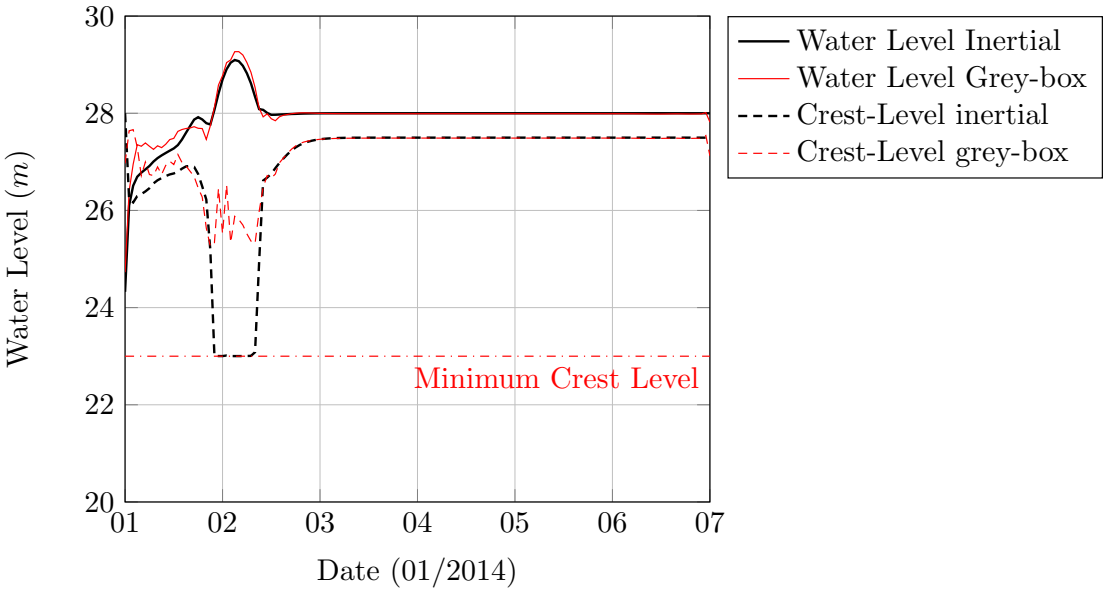

FIGURE 4.41: MPC control of the 1st weir and waterlevel h_7.

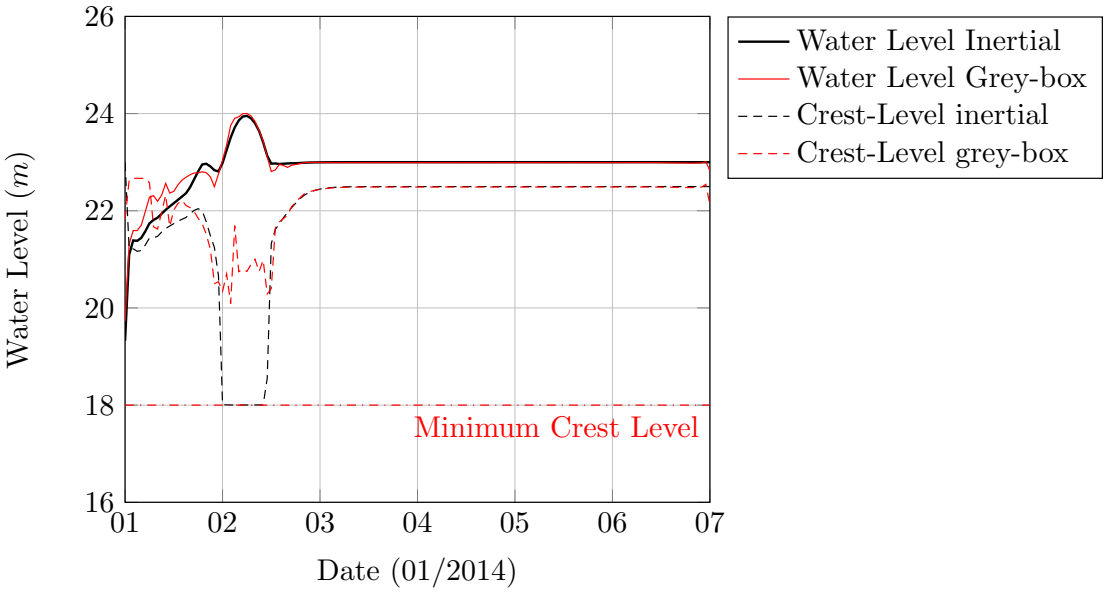

FIGURE 4.42: MPC control of the 2nd weir and waterlevel h_{15}.

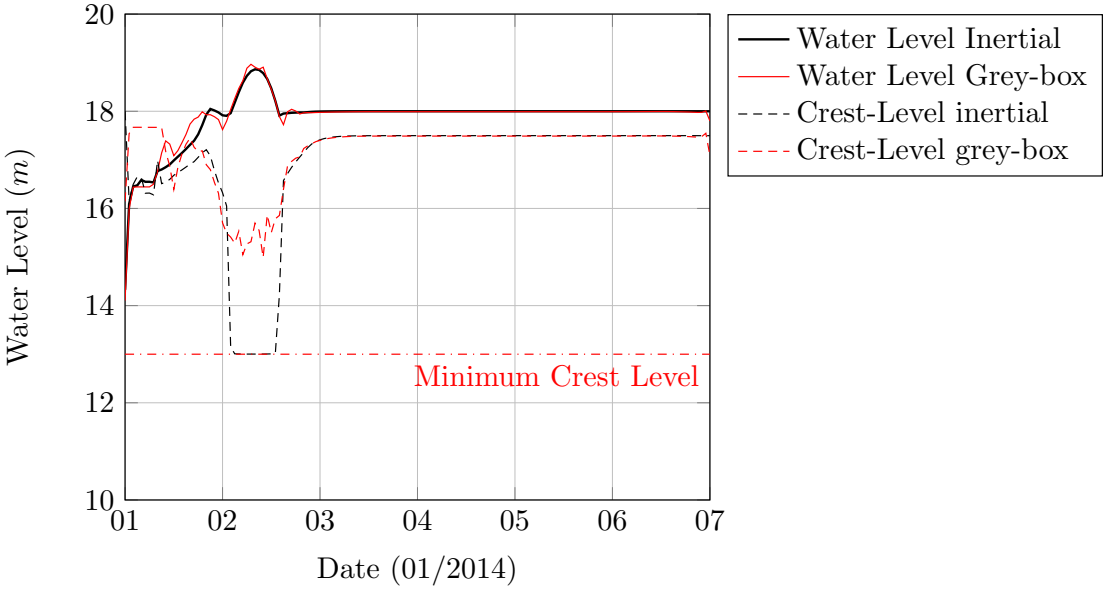

FIGURE 4.43: MPC control of the 3rd weir and waterlevel h_{23}.

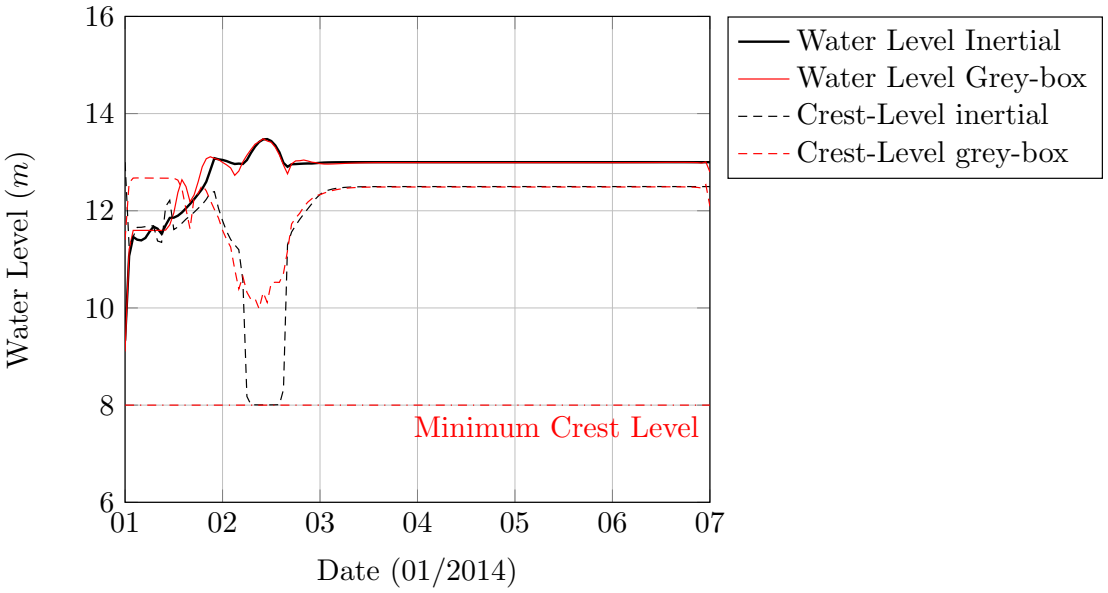

FIGURE 4.44: MPC control of the 4th weir and waterlevel h_{31}.

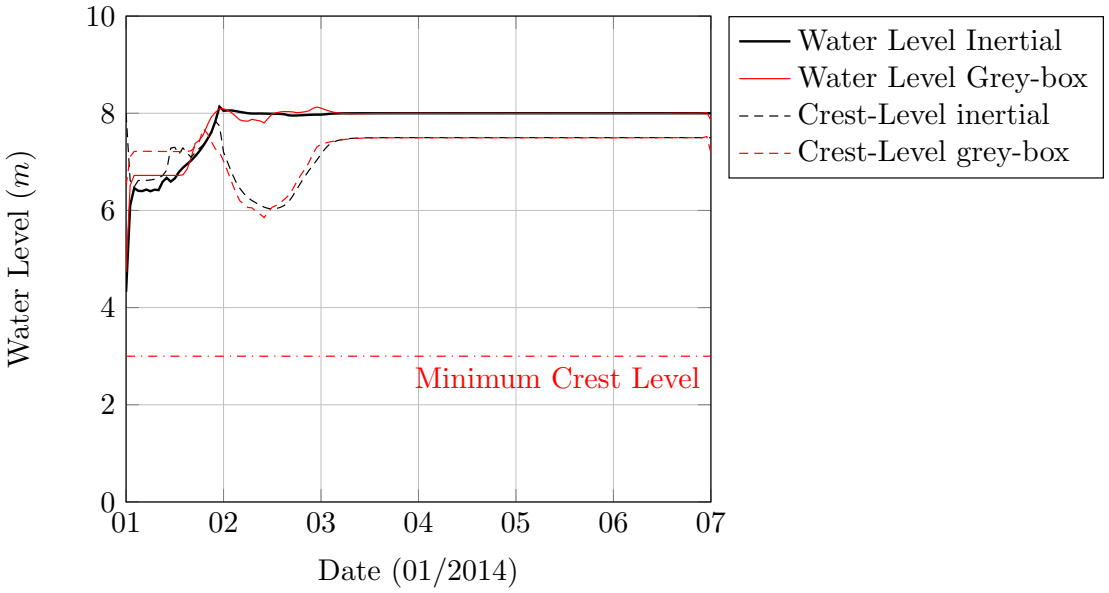

FIGURE 4.45: MPC control of the 5th weir and waterlevel h_{39}.

The figure shows that there was relatively good agreement between the two models regarding using the MPC control scheme to maintain the water level at set point. Nevertheless, the behaviour of the crest levels differed significantly.

Special attention is given to the beginning of the 2nd day, when a peak flow arrives. The MPC using inertial model saturated the controller output by reducing the crest level to the minimum bound, while the grey-box model with MPC this does not happen. Nevertheless, the water levels were similar, which reveals some difference in the dynamics of the models. To examine such difference, the following Figure illustrates the discharge values for the outflow of the first upstream weir.

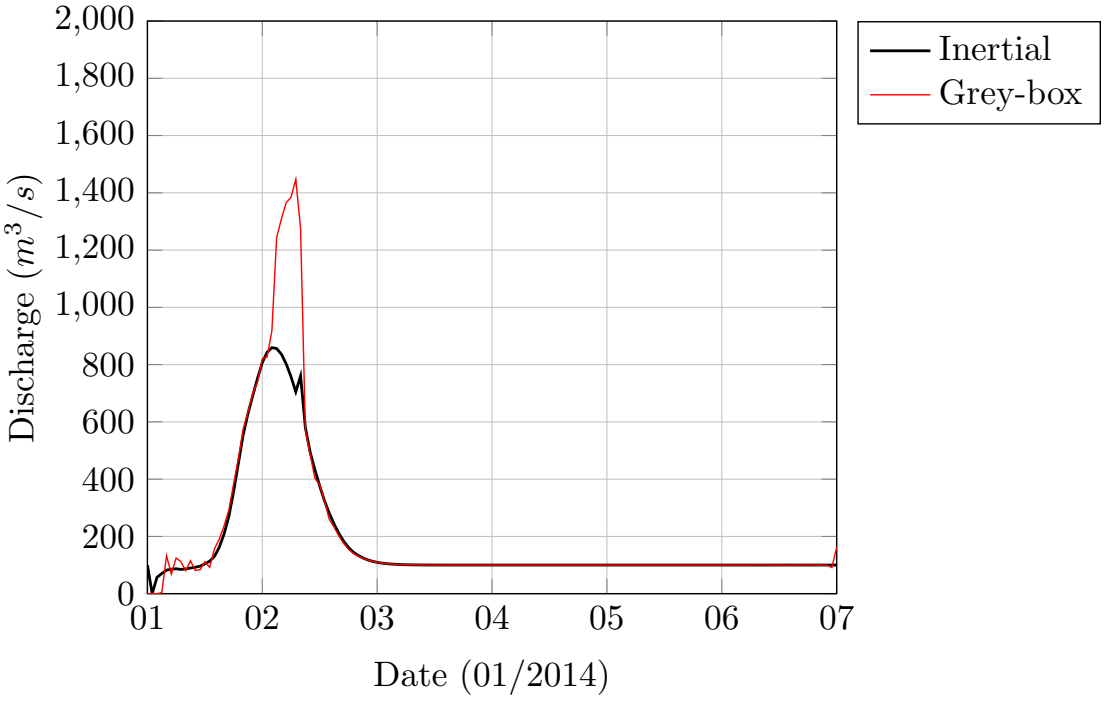

FIGURE 4.46: Discharge for the MPC control of the 1st weir.

It is visible in Figure 4.46 that there is an excessive increase in the outflow of the 1st weir, and due to that, the crest level do not reduces to the bottom level, as the outflow produced by the weir is enough to the controller to pursue the set point tracking.

This difference on the crest levels obtained for each model motivated the investigation and comparison of the full-hydrodynamic model with the results obtained by the models. The following Figure illustrates the comparison between the water levels obtained by the SOBEK full-hydrodynamic model and the inertial one.

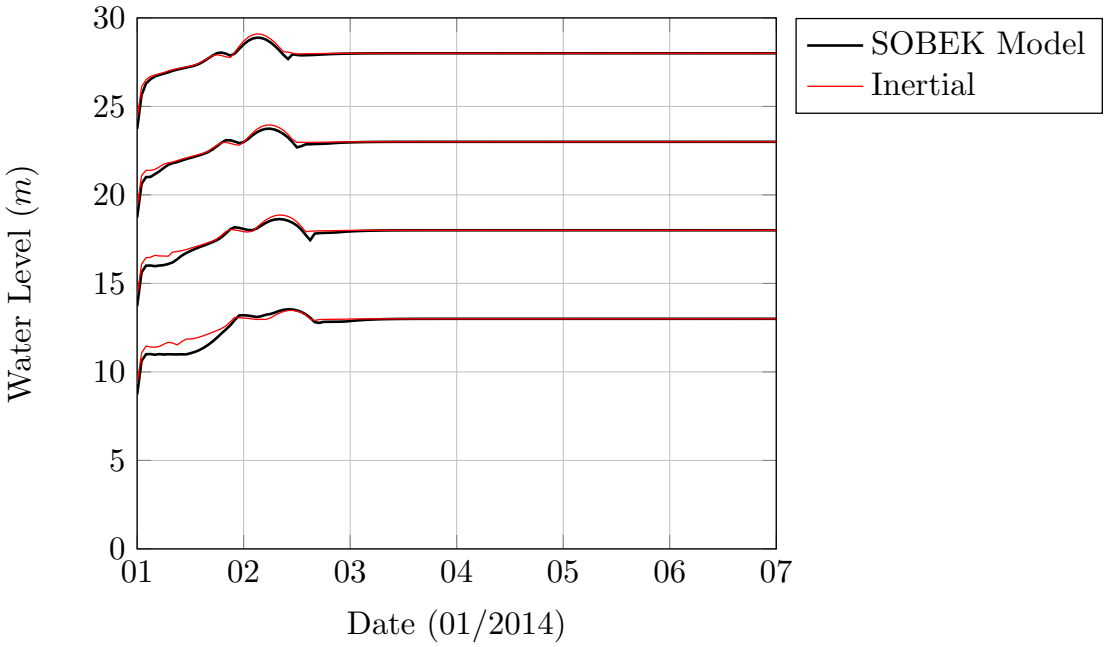

FIGURE 4.47: Comparison between water levels using SOBEK model and inertial model, with crest level obtained by the MPC optimization using the inertial model.

There is good agreement between the obtained water levels for both models. The inertial model slightly over estimated the water levels at the flood event on the beginning of the 2nd day, which may have caused the optimizer to saturate the crest level at the minimum, so as to avoid increasing the distance between the level and the set point.

Next, the result of the crest levels using MPC control with the grey-box model is compared on the SOBEK model. The results are illustrated in the Figure that follows:

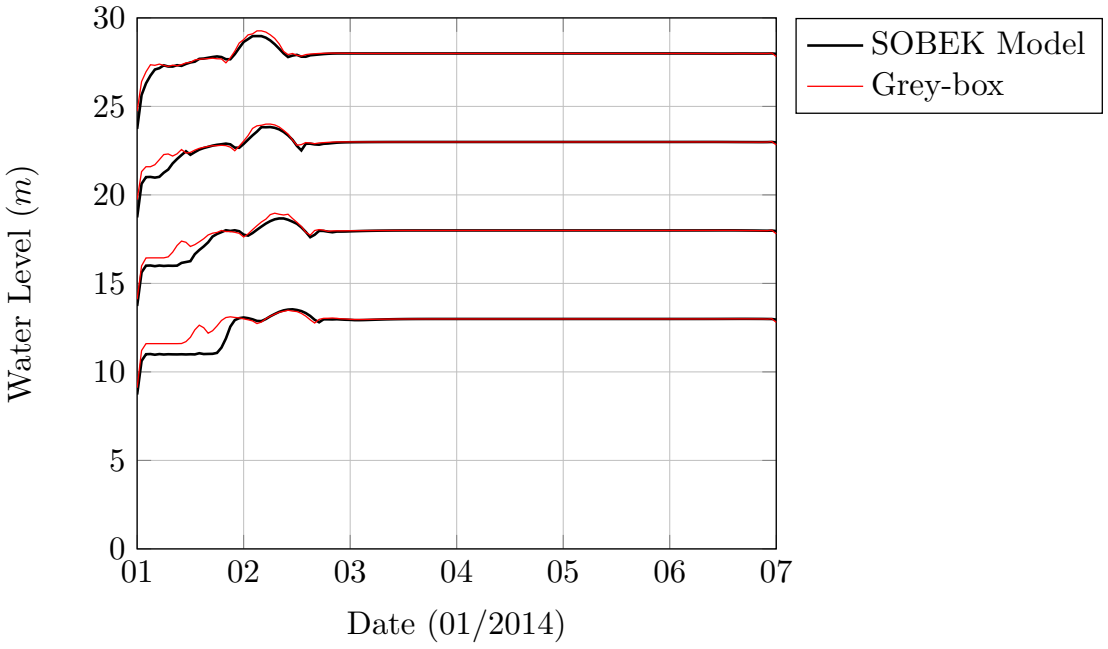

FIGURE 4.48: Comparison between water levels using SOBEK model and grey-box model, with crest level obtained by the MPC optimization using the grey-box model.

Once again, there is reasonable agreement between the results obtained by the full-hydrodynamic model and by the grey-box model. As the inertial model, the grey-box tended to over estimate the water levels. Nevertheless, it does not saturate the crest levels at the minimum, a fact that may be attributed to some non-linearity of the black-box component of the model, i.e., the extrapolation capabilities of the grey-box model are not well-defined, and the dynamics on points outside the calibration range may issue non-expected results.

Regarding the difference between MPC and PI control, one may also notice that, while the PI control of the 1st weir was able to move the water level to setpoint by the middle of the 1st day, the MPC control only reaches this steady condition by the middle of the 2nd day. This is due to the fact that, the PI as a feedback controller, cannot see conditions outside the location where it measures the errors. On the other hand, a MPC controller can minimize the **total** deviation of the setpoint by looking for all the measured locations at the same time. This feature can be seen by the improvement of the last weir in reaching the setpoint. In Figure 4.39b, it can be seen that the water level reaches set point by the beginning of the 2nd day, while before reaching it the water level stays in a steady condition of around 1.5m deviated from the setpoint. On the other side, the MPC controller could gradually provide a rising water level, until it reaches the desired setpoint by the beginning of the 2nd day. The

fact that the water level does not stay in a highly deviated steady condition decreases the **total** deviation of the setpoint when looking through all the weirs.

The Table 4.8 resumes the performance comparison for the PI and MPC control, for both, the inertial and the grey-box models.

TABLE 4.8: Control Performance for Hydraulic academic Case. Values in each cell corresponds to SSE and the values under parenthesis are MAE.

	Inertial		Grey-box	
	PI	MPC	PI	MPC
h_7	27.274 (0.117)	37.543 (0.193)	22.579 (0.107)	29.679 (0.186)
h_{15}	40.546 (0.176)	42.173 (0.208)	30.915 (0.149)	31.118 (0.192)
h_{23}	54.177 (0.234)	44.662 (0.220)	49.932 (0.211)	44.837 (0.221)
h_{31}	61.797 (0.254)	45.898 (0.214)	50.393 (0.215)	42.313 (0.205)
h_{39}	69.057 (0.268)	49.307 (0.212)	43.961 (0.202)	37.586 (0.194)
TOTAL	252.852 (–)	219.584 (–)	197.780 (–)	185.533 (–)

This performance is better visualized graphically. The Figure 4.49 shows the performance results for the inertial and the grey-box model, using the PI and the MPC control techniques.

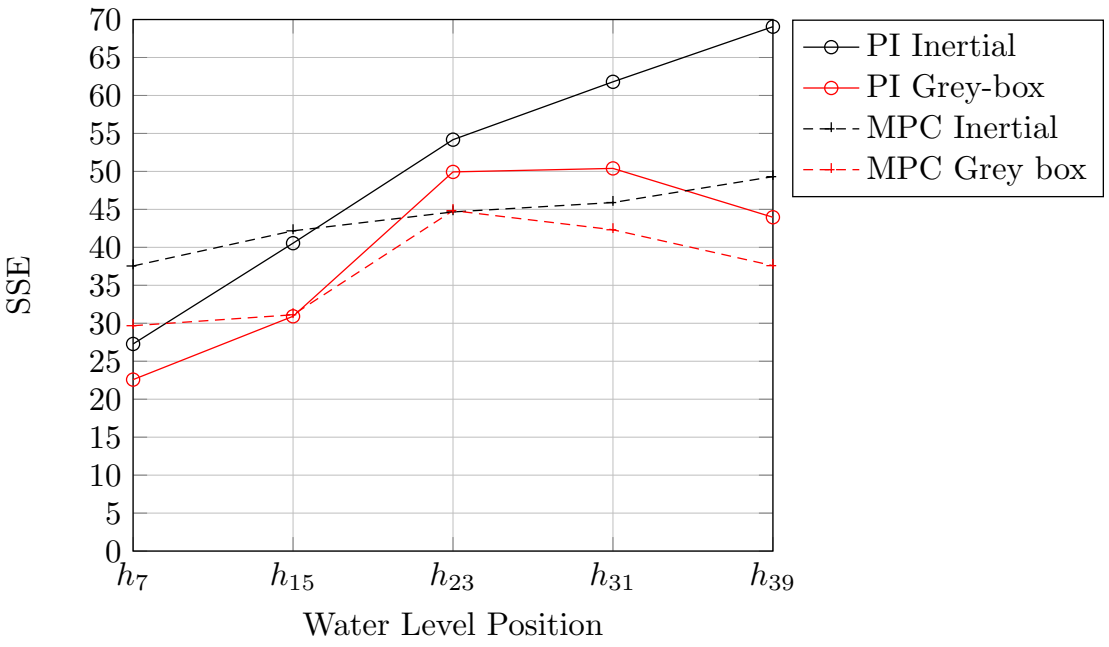

FIGURE 4.49: Performance results for the PI and MPC control using inertial and grey-box models.

As it can be visualized in the Figure above, by sacrificing the performance of the upstream water levels (h_7 and h_{15}), the MPC control can reduce the general deviation of water levels from the desired set point, especially for the downstream ones. One may also observe that the control of the grey-box model showed better performance when compared with the inertial model, although for the PI control the same parameters were used, and for the MPC the same algorithm was also used (interior-point). So this increased performance was not expected, and can be due to the difference in solvers or controllers details between RTC-Tools and Matlab/Simulink.

4.3.5 Comparison with other models

The performance of the developed grey-box model was compared with other modelling techniques. The results obtained for the validation dataset are shown in Table 4.9.

TABLE 4.9: Calibration and Validation results.

Model	**RMSE Validation**
Inertial	13.17
Grey-box(RK90)	16.25
Diffusive	13.84

Results show that, because the diffusive model has a similar performance as the inertial model, the grey-box can not perform better, as was already expected due to the reasons explained in the previous section. In this case, a better approach would be to use the SOBEK model directly to calibrate the grey-box model. This was not done here due to the lack of real observed data, so the SOBEK was used only as the common standard for comparison.

4.4 Grey-box for hydraulic flow routing - Main river, Germany

4.4.1 Case description

The most important tributary of the river Rhein, the Main river extents from the confluence of the Weisser Main with the Roter Main near Kulmbach, passing through regions such as Bamberg, Würzburg,the forests Spessart and Odenwald until its junction with the Rhine after 524 km (Britannica, 2008).

An important infrastructure of the Main river, the so called Main-Danube Channel (Main-Donau-Kanal in German), is a reach upstream up to Bamberg was fully canalized, with 11 structures (weirs, locks and hydroplants), and the upstream path up to Danube was canalized with 5 structures. The construction of the path until Nuremberg, called North Route (in German: Nordstrecke) was concluded in 1962, and the termination of the South Route (Südstrecke) was reached by 1992, with a total length of 171 km. The authority resposible for the management of the channel is the Wasser- und Schifffahrtsamt Nürnberg (Wasserstrassen und Schifffahrtverwaltung des Bundes, 2010).

The climate and vegetation conditions of the basin are intrinsically correlated with the climate of Bavaria state, which is shown in Table 4.10.

TABLE 4.10: Hydroclimatic characteristics of Main river.

Characteristic	
Predominant climate	Cfa (Köppen-Geiger system)
Average Annual Rainfall(mm)	1016 mm
Average Temperature (°C)	12.7 °C

The estimated hydro energy potential of the Main-Danube Channel is estimated in 2.7 Mio. kWh (RMD). Besides that, the pump storage capacity makes possible to cover peaks of 200 Mio. kWh in the energy network. The whole Main-Danube Channel produces energy enough to feed one quarter of the Bavarian state.

The modelled reach consists of 100 km of the river reach, from a small part upstream Bamberg (located in river Regnitz, next to the confluence with the Main), downstream to Kitzingen located in the Main-km 283.979. The Figure 4.50 shows the am aerial schematic view of the Main river, highlighting the

Danube-Main Channel, the path modelled by the full-hydrodynamic model, and the path modelled using the inertial model and the grey-box model. The Figure 4.51 shows the same path, but using a profile view.

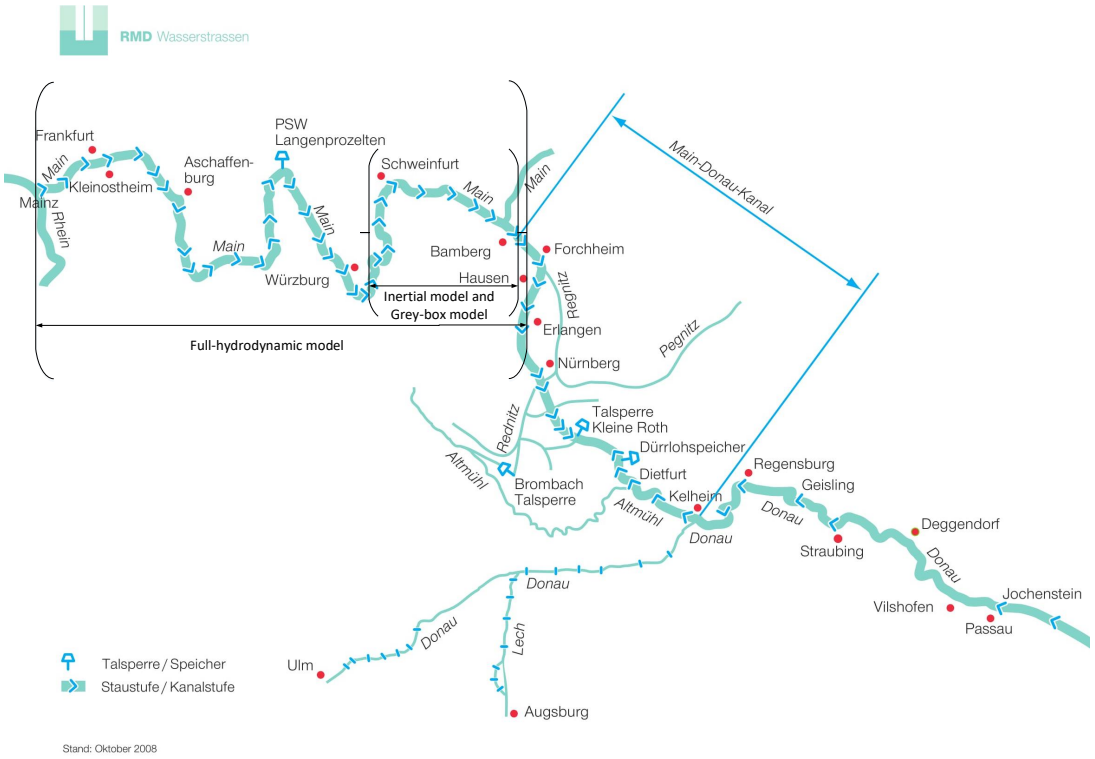

FIGURE 4.50: Aerial schematic view of the Main river. Adapted from http://www.rmd-wasserstrassen.de/main-donau-kanal/

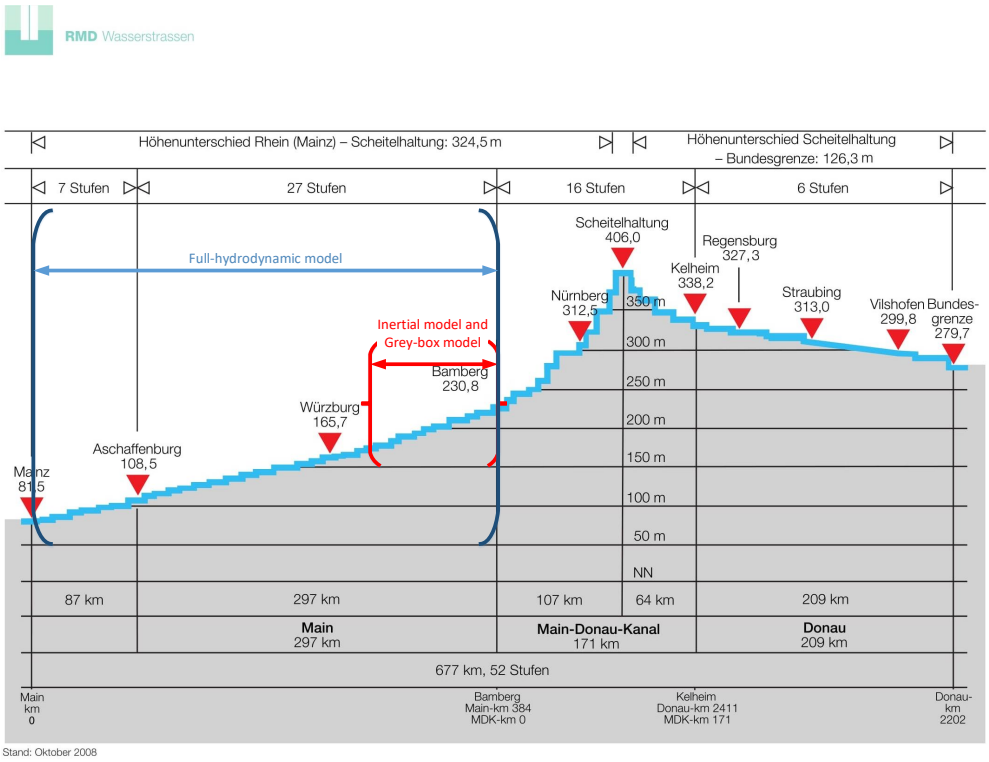

FIGURE 4.51: Profile schematic view of the Main river. Adapted from http://www.rmd-wasserstrassen.de/main-donau-kanal/

The data available for this reach corresponds to the one obtained using the full-hydrodynamic model SOBEK, developed by the German Federal Institute of Hydrology (BfG). The available model is subdivided into branches and nodes, with a total of 2258 nodes. The input data for the model are the flows upstream weir Bamberg and coming from Main before the confluence with the Regnitz river. The period of available data corresponds to 01.01.1999 until 20.06.2013. Table 4.11 shows some statistics of the available data.

TABLE 4.11: Dataset statistics.

Gauge	**Mean**	**Maximum**	**Minimum**	**STD**
Lat Caste	2.11	33.90	0.00	3.67
Lat Ebels	5.38	42.75	0.00	6.84
Lat Flutm	1.50	61.40	0.00	3.36
Lat Marie	2.47	19.95	0.00	3.54
Lat Nassa	3.94	186.00	0.00	5.92
Lat Rauhe	6.79	52.90	0.00	6.88
Lat Schwa	1.31	20.60	0.00	1.94
Lat Seeba	2.51	19.95	0.00	3.19
Lat Stein	2.51	19.95	0.00	3.19
Lat V2	0.00	0.00	0.00	0.00
Lat Volka	0.00	205.00	0.00	3.96
Node 1	135.55	1800.00	0.00	108.83
Node 17	94.80	1200.00	0.00	66.73

An inertial model was developed taking some of the morphological data of the river from the full-hydrodynamic model, corresponding to approximately 25% or $\frac{1}{4}$ of the total length of the full-hydrodynamic model. This model was simulated in order to generate data to train the developed grey-box hydraulic model. The dataset for training corresponds to the period of 15.11.2010 to 26.02.2011. The validation dataset corresponds to the period of 01.12.2012 to 01.03.2013.

Both models were also tested using different control techniques. A classical PI control was implemented in both inertial and grey-box models. The inertial and the grey-box hydraulic models were also tested in a MPC control open loop. The objective of the predictive controller is not only to keep certain water levels at set point, but also to avoid floods and/or droughts in other locations. In this specific case, the water level at the gauge Trunstadt has a list of potential problems which can happen if the water level raises to a certain degree. Some of these characteristics are shown in Table 4.12.

TABLE 4.12: Trunstadt water level rules

Water level(cm)	**Water height(cm)**	**Problem**
223.4	0	Gauge zero point
224.86	146	Trunstadt:Normal water level
226.8	340	Highest Navigable Level
228	460	Oberhaid: blockage of street
229.1	570	Viereth: flooded walking path.
229.1	570	Viereth: Access to the power plant flooded.
230.2	680	Flooding in the Railway Bamberg - Rottendorf km 34,2.

Since the maximum navigable level is 226.2m and from 228m on a series of raising problems are reported in Trunstadt itself and the neighbouring cities, the controller should be the water level at this gauge below 228 m, by controlling the neighbouring weirs (Viereth and Limbach weirs) crest levels.

4.4.2 Model implementation

The model implementation for the Main river case follows the same procedures as the hydraulic academic case, as describes in the section above.

4.4.3 Results and discussion

The developed inertial model consists on 53 nodes, in which mass continuity is calculated, 41 flow branches in which the inertial flow equation is used to calculate the discharge, and 11 composite hydraulic structures along the reach. The spatial scheme used in each branch was central scheme, and cross section topology as well as storage-level curves were extracted from the SOBEK model.

The grey-box model was developed using the same number of nodes as the inertial one. Each flow branch was calibrated using the data obtained after simulating the inertial model. A representative surface of a flow branch function is shown in Figure 4.52. The scatter plot is the data used for calibrating the surface function.

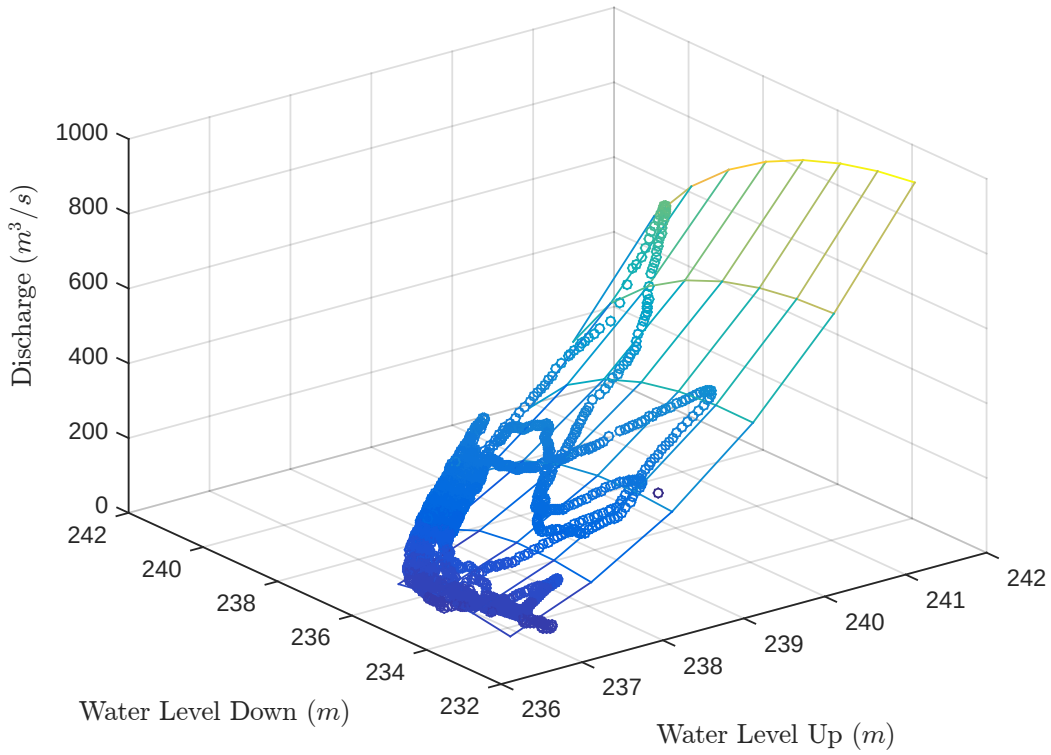

FIGURE 4.52: Example surface for $Q = Q(H_{up}, H_{down})$

The surface above visualizes the non-linearity between the water levels up- and downstream. The surface values are not defined for the case when the upstream water level is lower than the downstream water level, because of the squared root term in the flow equation. It is also clear that the discharge increases as the water level upstream increases and vice-versa, when the downstream water level increases, as expected according the dynamics of the system.

The next Figure shows the results for the calibration of the model regarding the discharge at the last gauge, called Kitz. The number of data points was reduced so as to have a better visualization.

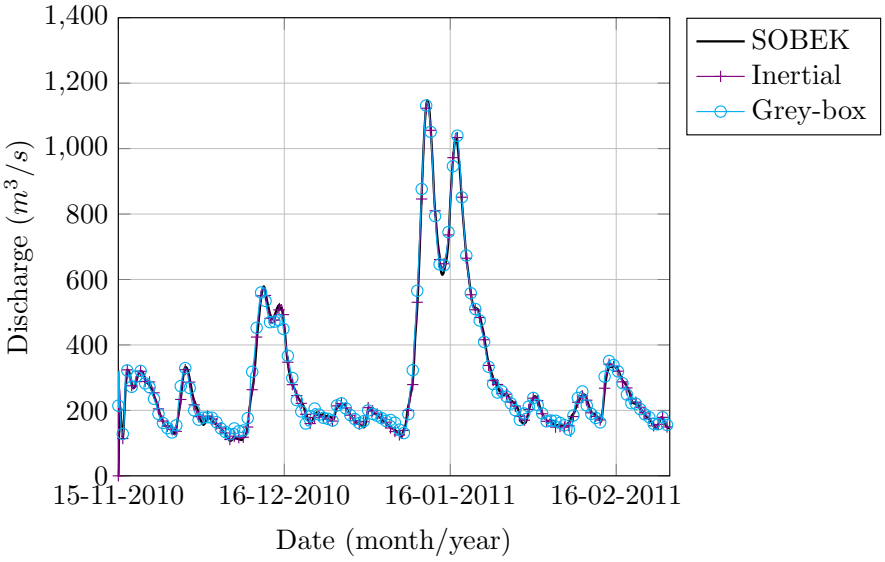

FIGURE 4.53: Training results for the Main river grey-box.

It can be seen that the grey-box model can capture most of the dynamics of the catchment, as there is good agreement between the results from the physically-based model and the results from the grey-box model. The flow peaks are not very well captured by the inertial model, and consequently the grey-box model followed the same pattern.

In order to validate the capabilities of the grey-box model, also when leaving the training data range, the following Figure shows the results at the same location for the validation period. As in the previous graph, the number of data points was reduced so as to have a better visualization.

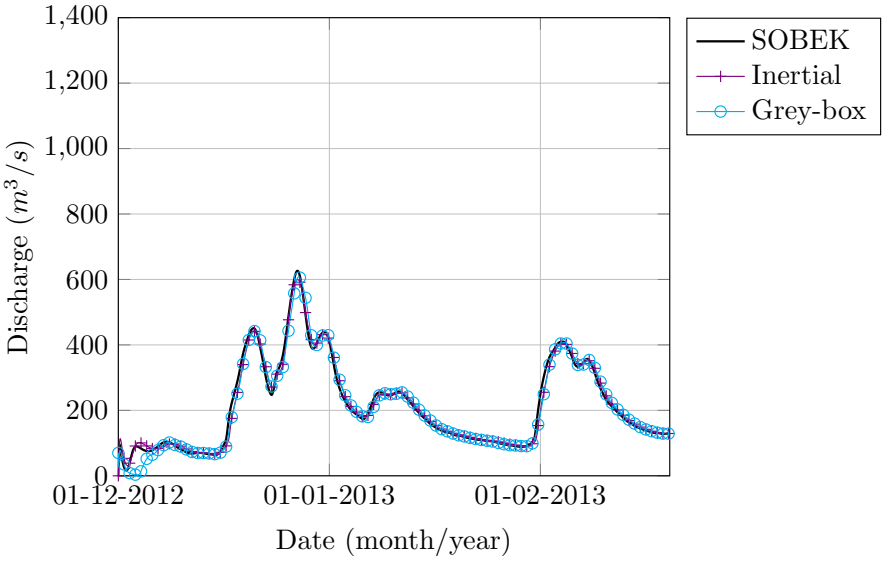

FIGURE 4.54: Validation results for the Main river grey-box.

It can be seen that, while inside the training range,the grey-box can capture with good accuracy the dynamics of the Main river. However a less accurate results is seen when the discharge reaches values outside the range of training. This is to a certain level expected, since data-driven techniques are well-known for their limitations regarding validation outside the expected calibration range. Nevertheless, the performance was reasonable as can also be seen in the Table 4.13, for both, calibration and validation results.

TABLE 4.13: Calibration and Validation results.

	Calibration		**Validation**	
	Inertial	Grey-Box	Inertial	Grey-Box
Bias	6.163	14.168	9.868	13.149
SSE	$1.463 \cdot 10^5$	$8.281 \cdot 10^5$	$4.019 \cdot 10^5$	$8.288 \cdot 10^5$
MSE	59.799	338.429	209.453	431.905
RMSE	7.733	18.396	14.472	20.782
R^2	0.999	0.996	0.994	0.988
NSE	0.999	0.992	0.988	0.975

Although there is a significant increase in the RMSE from the inertial model to the grey-box, the coefficient of correlation shows that both models had a very good performance, and the grey-box could to a reasonable level follow the performance of the inertial model.

4.4.4 Results and discussion - Control

In this section, the implementation of feedback controllers and model predictive control are tested to keep desired water levels at setpoint, and to fulfil some objectives as described below. A section of the inertial model and grey-box model, compromising the first three weirs section (Bamberg - Viereth - Limb) is selected, in order to test the control techniques. This was done to decrease model complexity and to simplify the analysis of the control techniques used, which may be extrapolated to the whole river.

Each of the weirs mentioned above contains one gauge upstream, which can be used to measure the deviation of the water level from desired values. There is one additional gauge dowstream Viereth, called Trunstadt. Figure 4.55 illustrates the scheme of this river section.

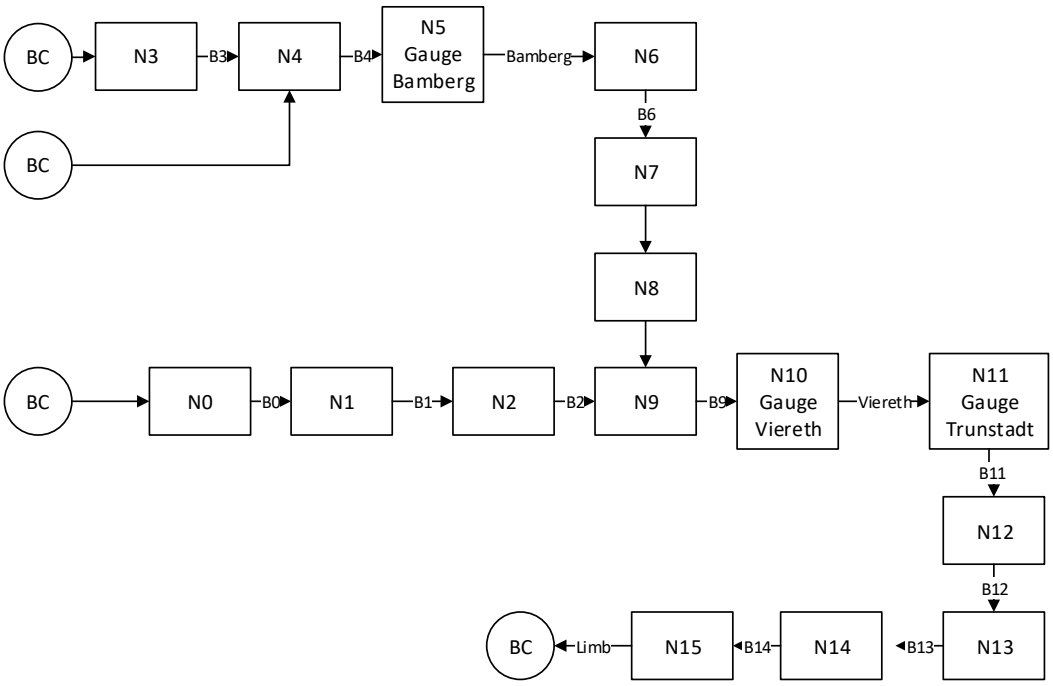

FIGURE 4.55: Schematization of the river Main - control tests.

Feedback control (PI) is used to keep the water level at gauges above weirs controlled in a selected setpoint, according the policy of the current one responsible for the management of the weirs in the Main river. The setpoint of such gauges are shown in Table 4.14.

TABLE 4.14: Setpoint of gauges for PI/MPC control.

Gauge	**Setpoint**
Bamberg	237.9
Viereth	231.16
Limb	225.16

The PI controller is calibrated by trial and error procedure. For all the three weirs, the selected K_P (proportional gain) and K_I (integrator gain) are:

- $K_P = 1$
- $K_I = 0.1$

As it was done in the academic case, anti-windup method through back-calculation was used to avoid continuous integration of the PI controller. The Back-calculation coefficient was fixed in 0.001.

Before applying the control itself, a comparison between the performance of the grey-box model and the inertial one is performed, in order to be able to retrieve any difference in the control results due to difference in the dynamics of each model. The Figure 4.56 shows the water levels obtained at each of the gauges for simulation using both models.

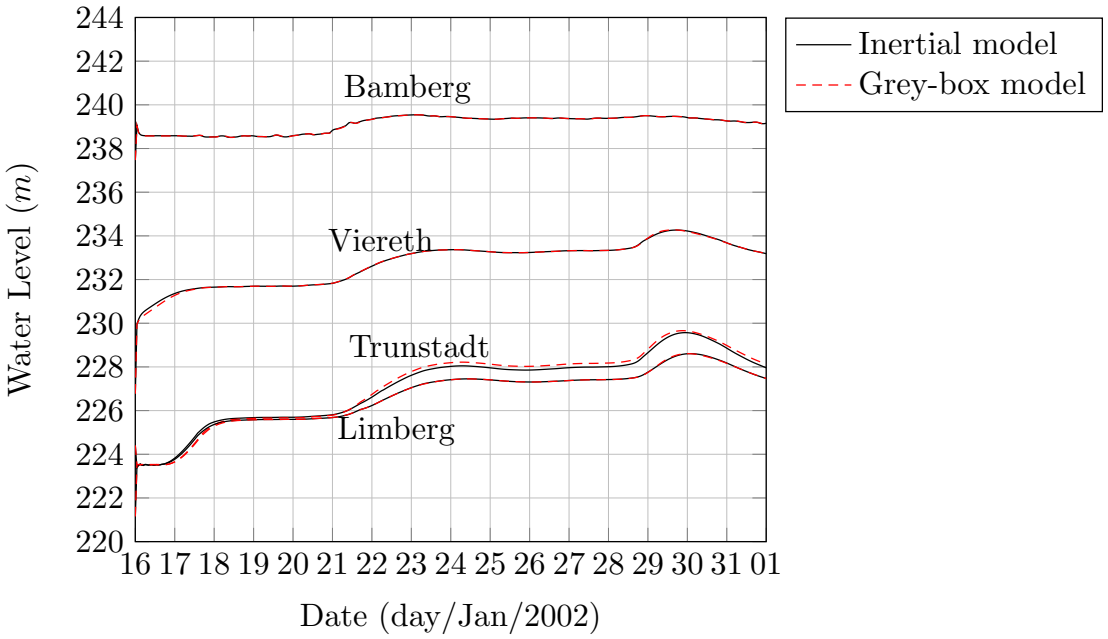

FIGURE 4.56: Water levels at gauges Bamberg, Viereth, Trunstadt and Limb (from up to down).

There is high agreement between the water levels simulated using both models. A slight difference is seen for the gauge Trunstadt, especially in the occasion of high water level. Even being so, one can see that both models have similar performance, so it is expected the same for the applied controlling techniques. The Table 4.15 resumes the performance metrics for such water levels.

TABLE 4.15: Performance metrics for Control Case - fixed crest levels.

	$h_{Bamberg}$	$h_{Viereth}$	$h_{Trunstadt}$	$h_{Limberg}$
Bias	$4.844 \cdot 10^{-3}$	$1.501 \cdot 10^{-2}$	0.123	$1.860 \cdot 10^{-2}$
SSE	$2.544 \cdot 10^{-2}$	0.562	7.596	0.826
MSE	$6.608 \cdot 10^{-5}$	$1.461 \cdot 10^{-3}$	$1.973 \cdot 10^{-2}$	$2.146 \cdot 10^{-3}$
RMSE	$8.129 \cdot 10^{-3}$	$3.822 \cdot 10^{-2}$	0.14	$4.633 \cdot 10^{-2}$
R^2	1	0.999	0.999	1
NSE	1	0.999	0.992	0.999

As a next step, the water levels are controlled using the PI technique as described above. The Figure 4.59 shows the results at all the gauges for the inertial and the grey-box model.

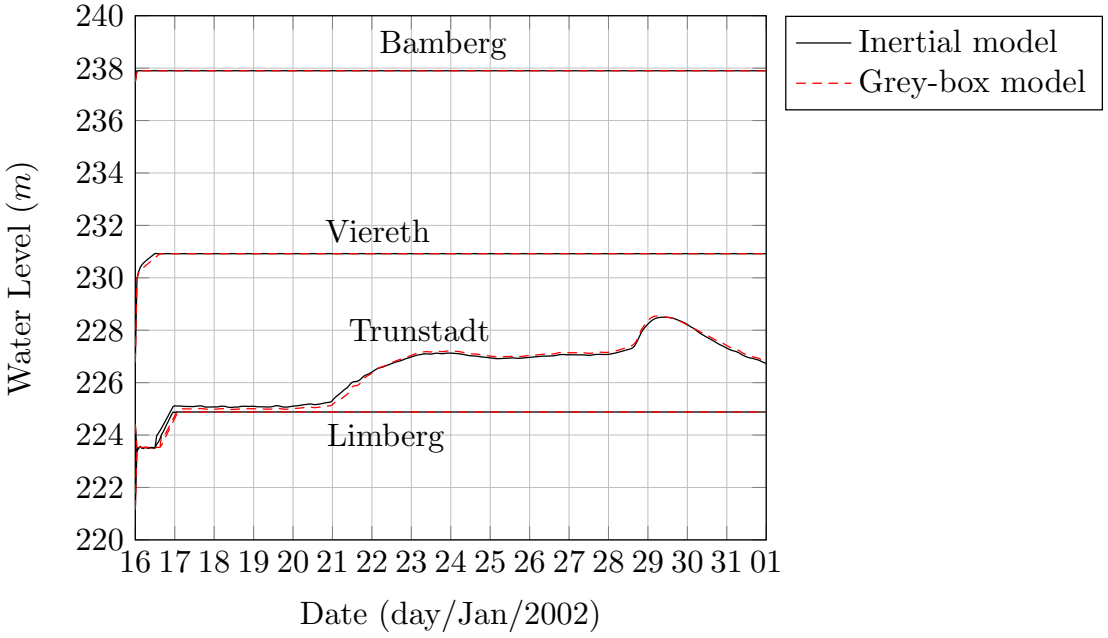

FIGURE 4.57: Results for PI control at the gauges for Main river.

The results show that the PI controller is fully capable of keeping the water levels upstream of the weirs at the desired position for the whole simulation time. There is a small difference in the rising time at the beginning of the simulation, which may be attributed to a difference between the windup method used in the grey-box model (Matlab/Simulink) and the inertial model (RTC-Tools).

However, as can be also seen in the Figure 4.59, the PI control technique can not be used to keep the gauge Trunstadt water level at a set point, since this controlling technique is limited to having as an input one single deviation variable and as output one single manipulated variable. The Trunstadt gauge is located between the Viereth weir and the Limberg weir, and has a set of water level marks, for navigation levels and flood protection. The Figure 4.58 shows only the results with PI control for the Trunstadt gauge, plotted with some of these water level marks.

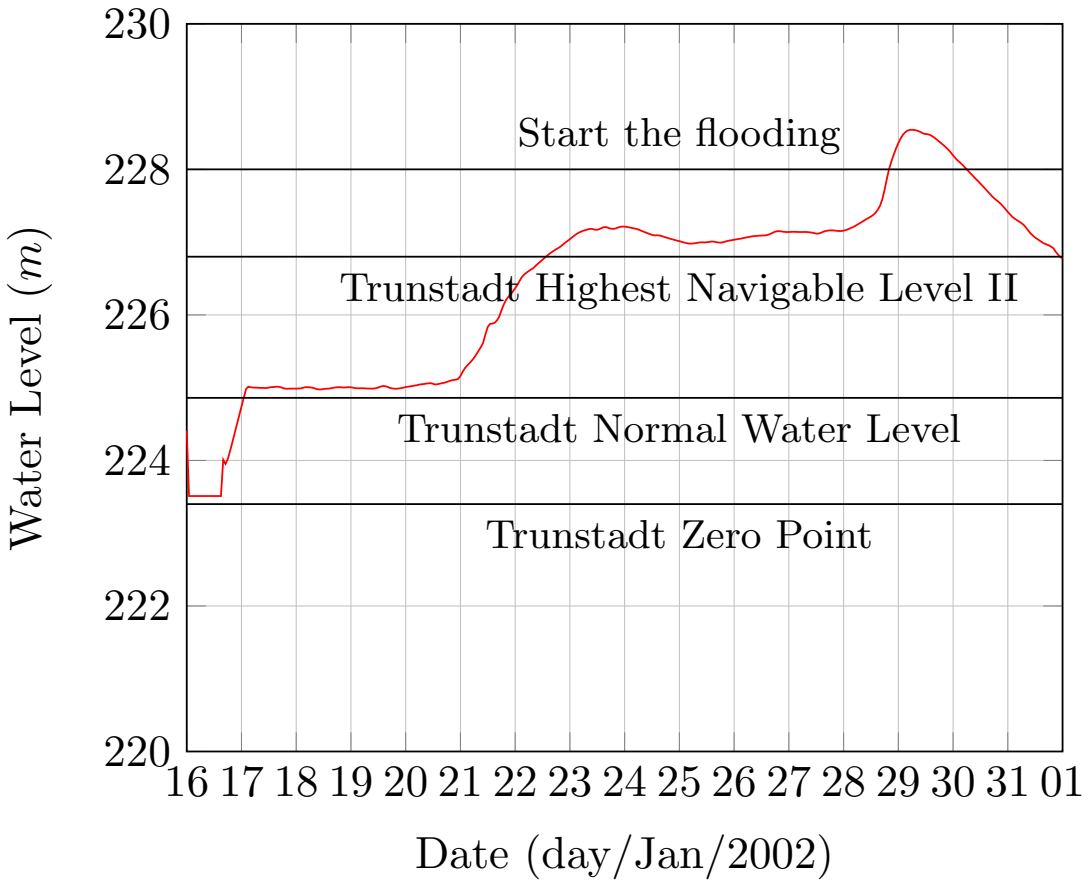

FIGURE 4.58: Trunstadt gauge water levels and marks for navigation and flood protection.

As shown in the Figure above, the water level rises above the maximum navigable level by the middle of 22.01.2002, and it keeps rising until it surpasses the mark of 228 meters, when it starts the flooding. This flooding involves the surrounding cities: Trunstadt and Oberhaid, as shown in the Figure below.

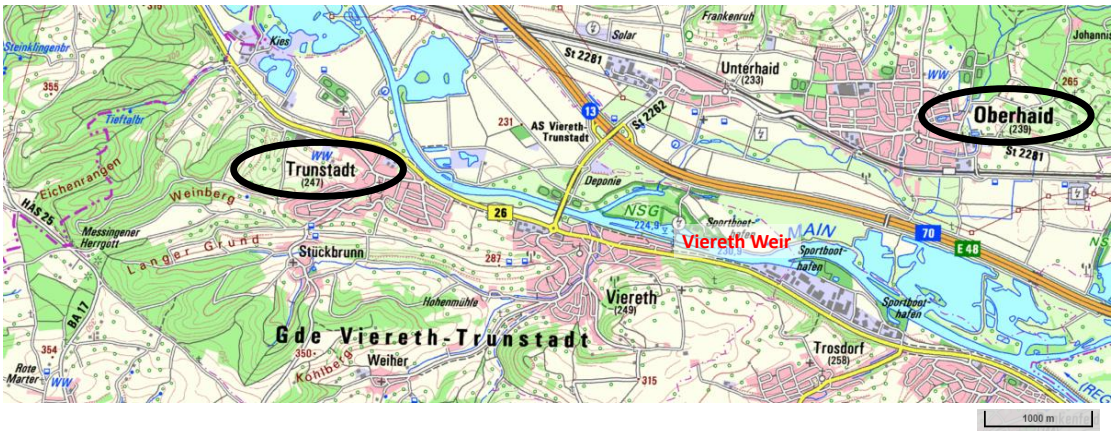

FIGURE 4.59: Location of the potentially flooded cities. Modified from: (Bayerisches Landesamt für Umwelt, 2017).

In order to avoid such event, the Model Predictive Control can be implemented, being capable of handling multiple deviations, objectives and output variables. In this specific case, it was chosen to control the weirs, in order to keep the water levels at the set points **as long as** there is no flooding. To do that the following optimization problem was defined:

$$\begin{aligned} \min_{\{u_t\}_{t=1}^{h}} \quad & \sum_{t=1}^{h-1} 1 * T_1 + 1 * T_2 + 100 * T_3 + 1 * T_4 \\ \text{subject to} \quad & x^t - f(x^{t-1}, u^t, d^t) = 0 \\ & hmin_j \leq h_j \leq hmax_j \end{aligned} \tag{4.5}$$

where:

$x^t - f(x^{t-1}, u^t, d^t) = 0$ - the grey-box model

h_j - water level in location j

u_j - crest level for the weir downstream location j

$hmin_j$ - lower bound for the water level in location j

$hmax_j$ - upper bound for the water level in location j

The terms T_1, T_2, and T_4 refer to deviations from the setpoint for the water levels above the weirs Bamberg, Viereth and Limberg. The term T_3 is a soft constraint terms, i.e., it is just accounted in the objective function if the water level at Trunstadt gauge reaches levels above 227.5 meters. The mathematical description of these terms is given as follows:

$$
\begin{aligned}
T_1 &= (h_{bamberg} - 237.9)^2 \\
T_2 &= (h_{viereth} - 231.16)^2 \\
T_3 &= \begin{cases} (h_{trunstadt} - 227.5)^2 & \text{if} \quad h_{trunstadt} \geq 227.5 \\ 0 & \text{if} \quad h_{trunstadt} < 227.5 \end{cases} \\
T_4 &= (h_{limberg} - 225.16)^2
\end{aligned} \tag{4.6}
$$

The terms T_1,T_2 and T_4 refer to the squared deviation from the water level upstream the weirs to a fixed setpoint. The highlighted term which the PI control would not be able to accommodate is the introduction of the term T_3 which refers to a penalty on the control of the weirs in the case that the water level at the gauge Trunstadt ($h_{trunstadt}$) rises above 227.5 meters. This value was chosen to give some gap until 228 meters, in the case the controller can not avoid raising the water level above the violation level. A weighting factor before T_3 of 100 was used to guarantee that the most important factor in the control is to avoid flood, which could cause material and life damages.

The Figure 4.60 shows the MPC control results at the for 4 gauges for the water levels and Figure 4.61 shows the Crest levels of the weirs. A comparison is performed between the results of the inertial model and the optimization done using RTC-Tools, against the grey-box model and the optimization done using Matlab/Simulink.

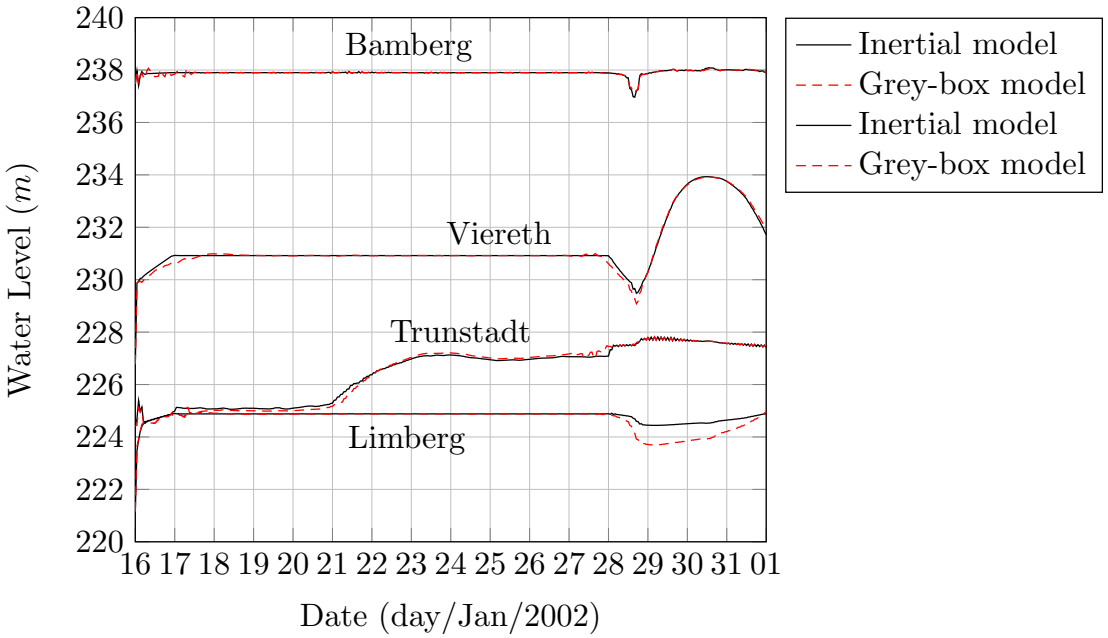

FIGURE 4.60: MPC control of the weirs Bamberg, Viereth and Limberg - Water Levels.

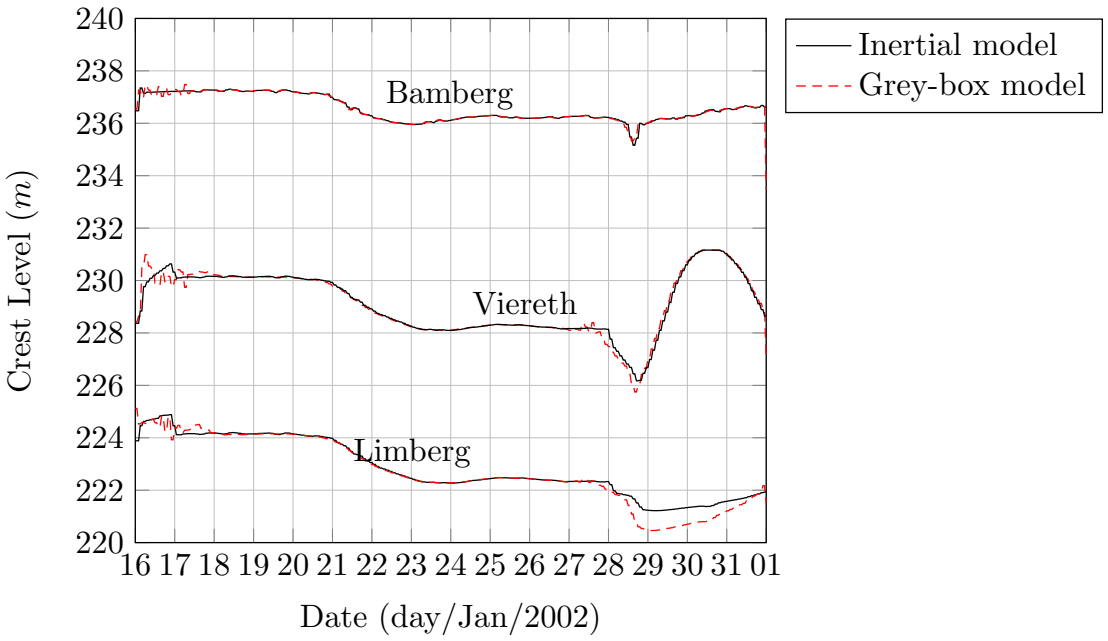

FIGURE 4.61: MPC control of the weirs Bamberg, Viereth and Limberg - Crest Levels.

The results show that, in order to avoid the flood that took place in 29.01.2002, the MPC control starts to decrease the upstream water level one day before (28.01.2002), as well as the water level downstream starts to decrease more

smoothly. By the end of 28.01.2002, the water level upstream Trunstadt increases steeply, and the weir downstream keeps the water level slightly below the set point. This actions could avoid the flood in the region of Oberhaid, Trunstadt by sacrificing the deviation of the water levels upstream and downstream from the desired set point. The gap left between the real flooding level (228 meters) and the level used in the optimization problem (227.5 meters) showed to be useful as the water level in Trunstadt surpasses 227.5 meters, but does not reach 228 meters.

The performance metrics was evaluated and summarized in the Table 4.16. In order to compare equal terms, the water level violation at Trunstadt was also used as a performance value when evaluating the PI.

TABLE 4.16: Control Performance for Main River case. Values in each cell corresponds to SSE and the values under parenthesis are MAE.

	Inertial		Grey-box	
	PI	MPC	PI	MPC
T_1	0.022 (0.001)	0.110 (0.039)	0.022 (0.001)	0.107 (0.045)
T_2	0.225 (0.021)	1.053 (0.489)	0.231 (0.021)	1.077 (0.532)
T_3	70.295 (0.625)	16.682 (0.140)	70.760 (0.583)	16.448 (0.138)
T_4	0.332 (0.070)	0.264 (0.092)	0.350 (0.070)	0.465 (0.216)
TOTAL	70.874 (–)	18.109 (–)	71.363 (–)	18.097 (–)

The performance of the Inertial model and the grey-box are similar, for the PI control technique and also the MPC control. In the table above, the terms T_1, T_2, T_3 and T_4 refers to the terms in Equation 4.6. Although the PI control could keep the water levels upstream the gauges at set point, it could not avoid an increase on the level at Trunstadt, possibly having caused floods in the region.

On the other hand, the MPC control sacrifices the maintenance of the water levels upstream and downstream to a certain degree, but still enough to decrease in an order of 4 the penalty in the term T_2, possibly reducing severely the flood in the region. This is achieved because the MPC is a central controller while the PI is a local controller. Local controllers are aware of one deviation variable and one control variable, while central controllers incorporate into their algorithm any amount of deviation and control variables, thus being able to compensate at different points of the system in order to achieve one or

multiple objectives. The Figures 4.62 and 4.63 show a better visualization of these results.

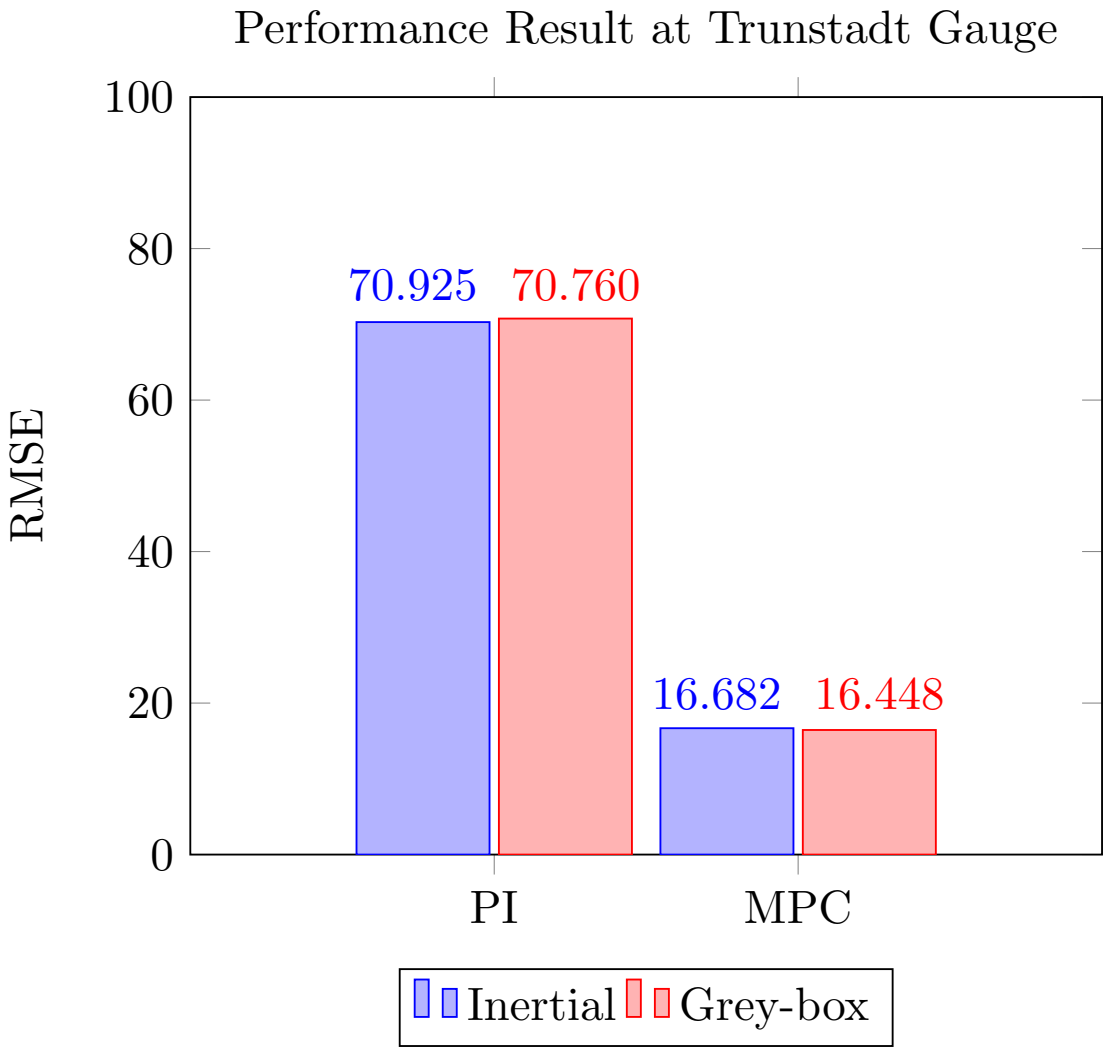

FIGURE 4.62: Comparison of control performances between the two control techniques (PI and MPC) using inertial and grey-box model in Trunstadt gauge.

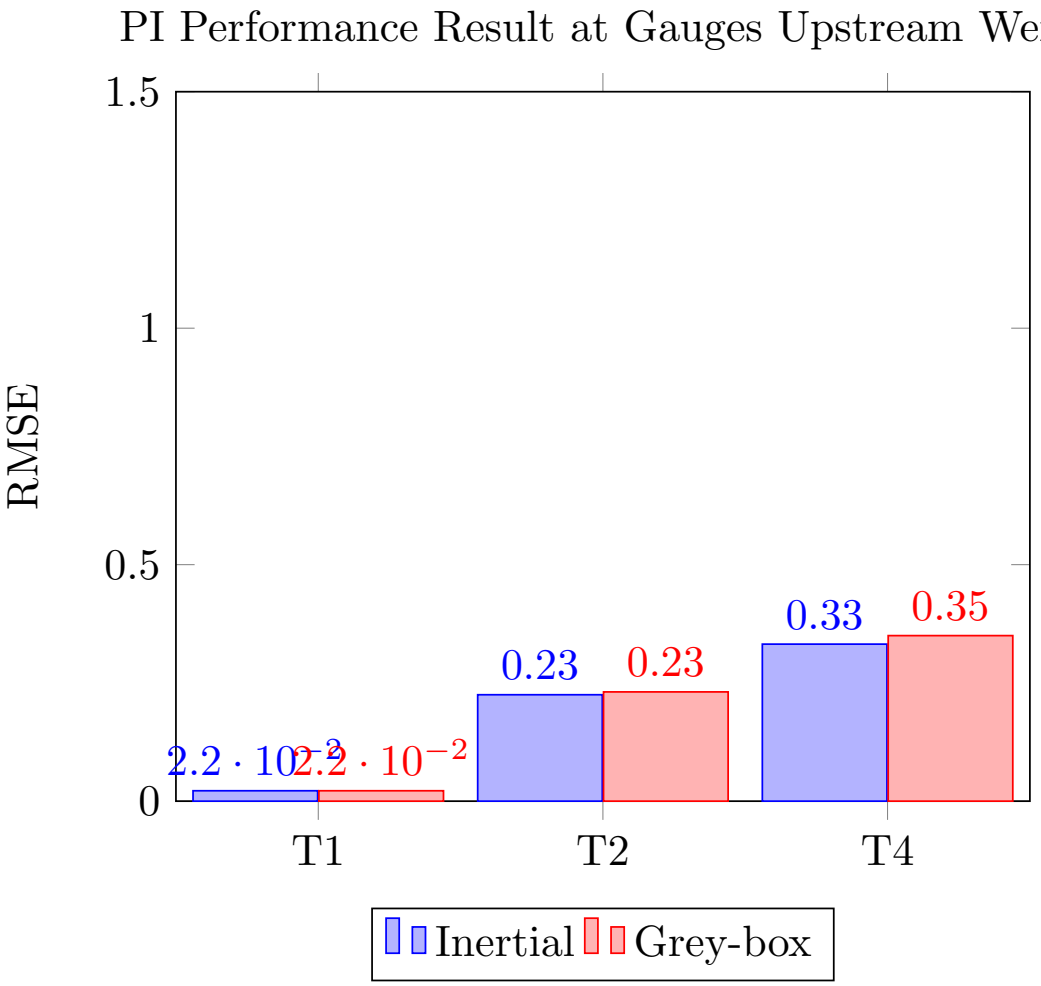

FIGURE 4.63: PI control performances using inertial and grey-box model in gauges upstream the weirs.

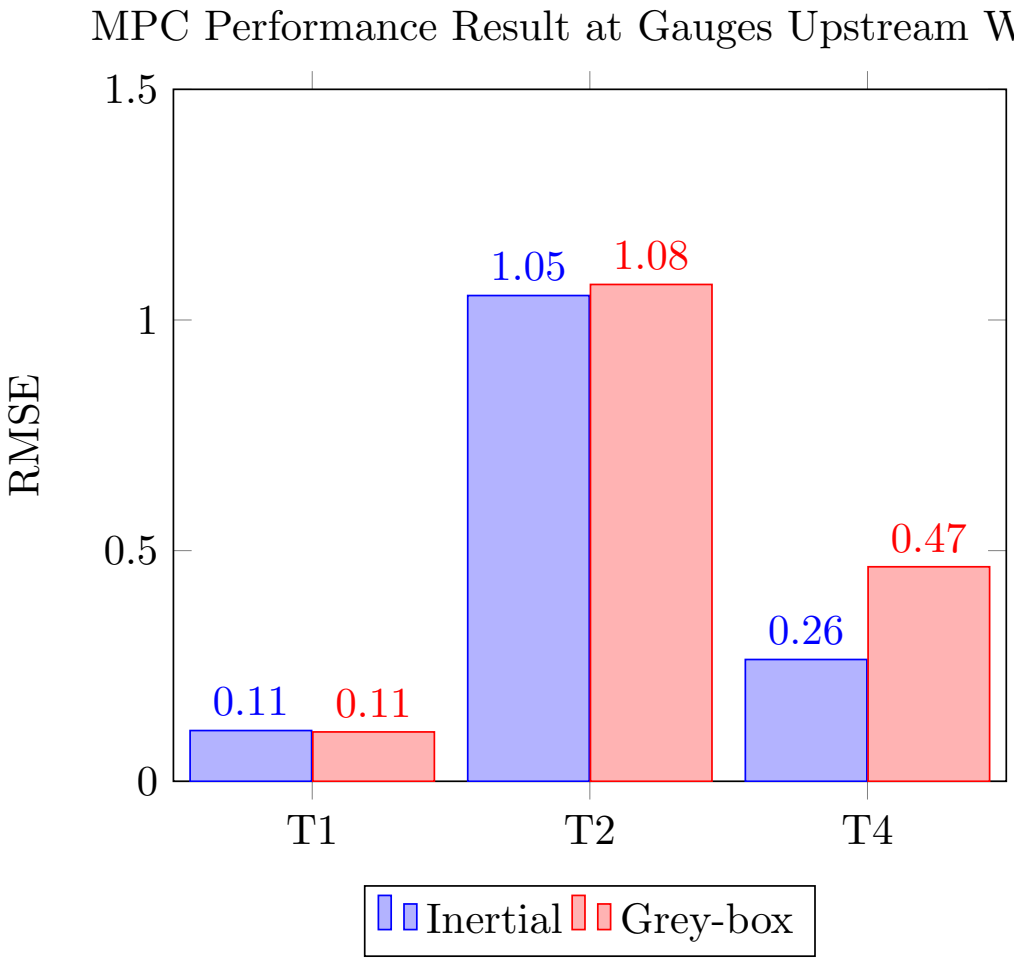

FIGURE 4.64: MPC control performances using inertial and grey-box model in gauges upstream the weirs.

In Figure 4.62, one can see that there is a drastic reduction on the error in Trunstadt gauge, i.e., the amount of water which surpasses 227.5 meters. This is reached through the increase in the error on the water levels upstream the weirs, as can be seen in Figures 4.63 and 4.64. But this compensation is still advantageous, as avoiding floods can reduce material and life losses.

The Figure 4.65 shows the different results obtained using no control, the PI control and MPC control at Trunstadt gauge at the event of the flood, with special attention to the interval between 27.01.2002 and 01.02.2002, when the water level reaches its highest values in the control horizon.

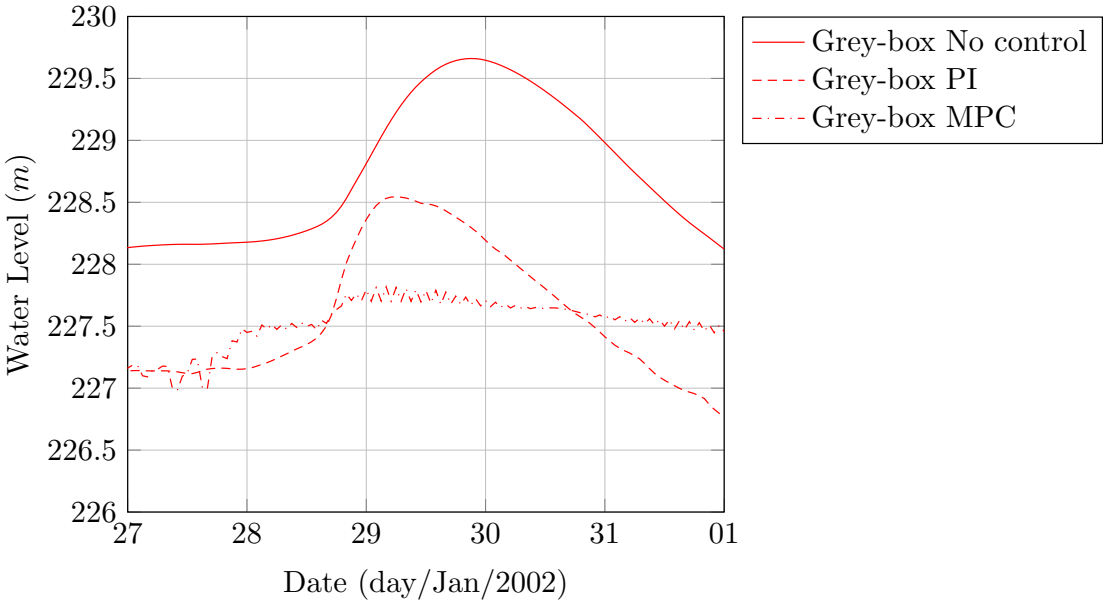

FIGURE 4.65: Comparison between No control (crest levels at maximum), PI control and MPC control results for the flood event in Trunstadt gauge.

From the Figure 4.65, it can be seen that the water level at Trunstadt gauge was 70 cm lower through the use of MPC controller than with the use of PI control. The worst scenario would be the use of no control technique, in which case the water level would rise above 229.5 meters. This scenario shows that the use of predictability could prevent (or reduce) the flood especially in positions along a stream where a manipulated variable, such as the crest level, can not be directly linked to a desired controlled variable, such as the water level at Trunstadt gauge.

A next step using MPC controller is to investigate the effect of aggregation, i.e, to increase the time step between each change in the controller input, in order to reduce the number of decision variables consequently reducing the required time to run the optimization. Three different aggregation steps were implemented: 2 hours, 4 hours, 8 hours and 12 hours. The Figures 4.66 and 4.67 shows the results obtained for each aggregation step on the water levels under control, as well as on the crest levels.

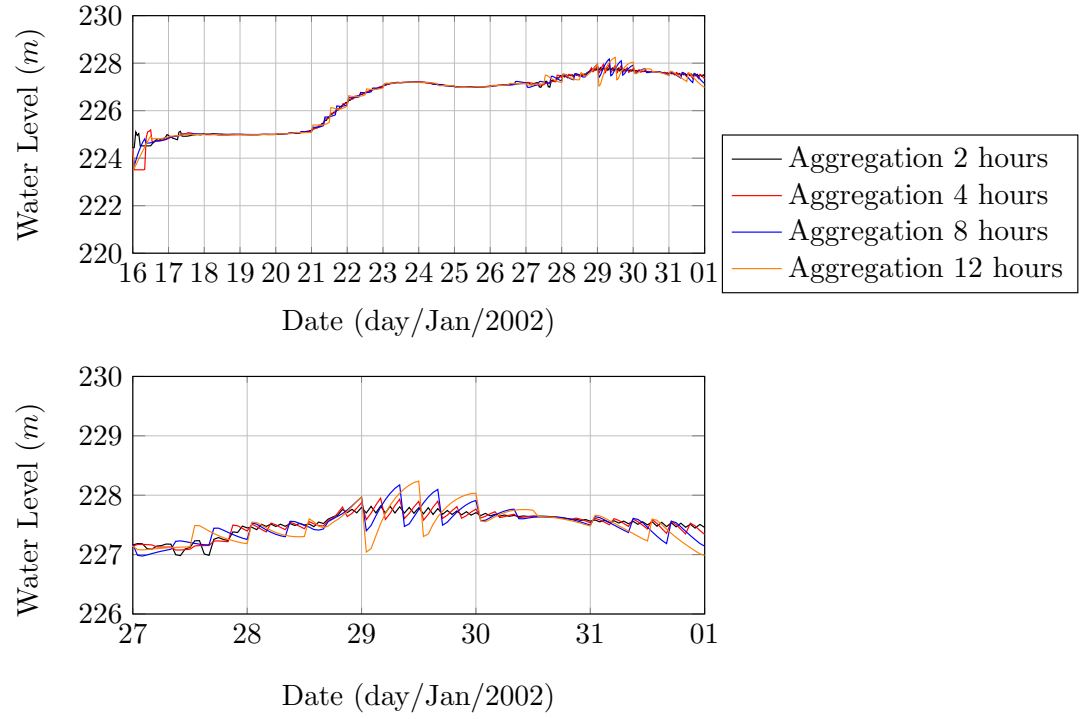

FIGURE 4.66: Comparison between MPC control and Grey-box model with different aggregation time steps at the Trunstadt gauge, with special focus on the flooding event.

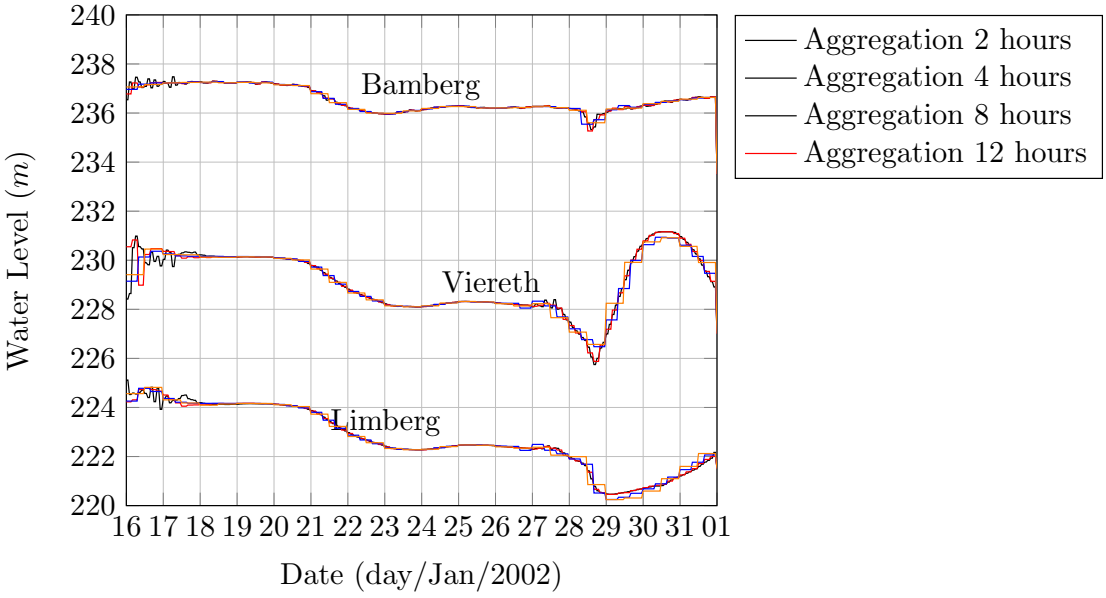

FIGURE 4.67: Comparison between MPC control with different aggregation time steps at the Trunstadt gauge - Crest Levels.

As the aggregation steps increase, the oscillation during the high flooding event as can be seen in Figure 4.66. The reason for that can be retrieved from

the Figure 4.67. As the aggregation increases, the difference between each step taken in the crest level increases. This causes instabilities in the calculation of the discharges at the weirs, highly increasing the discharge at the instant of change in the crest level.

For that reason, one approach to reach the optimum water levels, still reducing the number of optimization variables, is to interpolate between each step given at the crest level, creating smooth transitions between each time of change. This approach was tested for the 2 extreme aggregation steps used (2 hours and 12 hours), and the results obtained can be seen in the Figure 4.68.

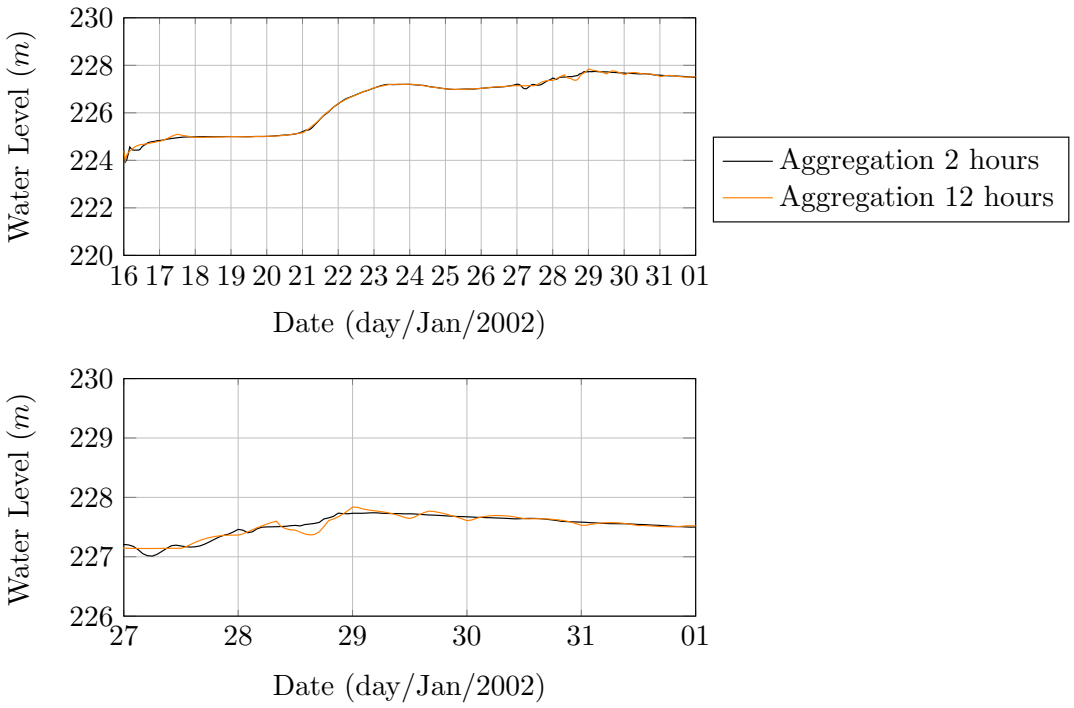

FIGURE 4.68: Comparison between MPC control with different aggregation time steps and using interpolation at the Trunstadt gauge, with special focus on the flooding event.

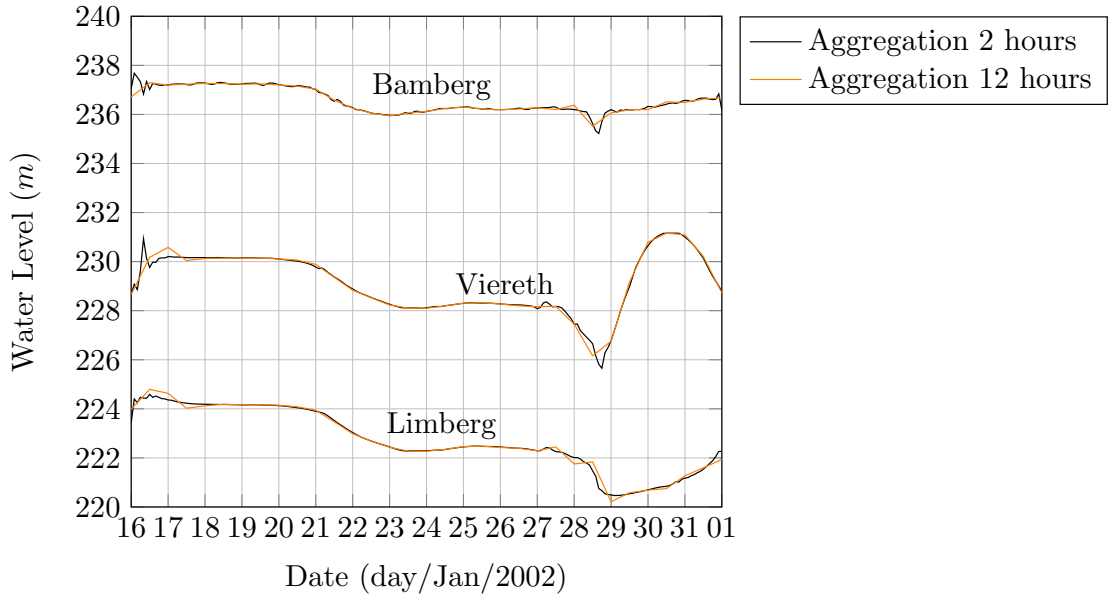

FIGURE 4.69: Comparison between MPC control with different aggregation time steps and using interpolation at the Trunstadt gauge, with special focus on the flooding event - Crest Levels.

By using the interpolation technique, the results for the different time steps were smoother, and more similar to each other. However, by using the 12 hours aggregation step the results at the crest levels (Figure 4.69) show still some peaks, behavior not desired, as smoother transitions produces less oscillations in the water level and are better for navigational purposes. The use of 2 hours aggregation with an interpolation generated smooth transitions, while still highly reducing the flood in the region, which is the desired result.

Chapter 5

Conclusions and Outlook

5.1 Conclusions

The current limitation and disadvantages of both data-driven models (no physical characteristics and limited range of validity) and physically-based models (high computational resources usage) can be reduced by the implementation of grey-box models. Such models use data-driven techniques to reduce computational costs of models, and posses additionally physically-based components, which can deal with physical characteristics such as mass conservation, momentum conservation or other physical properties.

The main contribution of the present work regarding flow forecasting comes with the development of grey-box models. Such models couple ANN or algebraic equation with the mass continuity equation, in order to create computationally inexpensive model with good accuracy. The focus is flow routing modelling, and two approaches are validated. The first one is hydrological modelling and the second one hydraulic modelling, both tested first in a simple academic case and later on applied on a real-world test case. The hydrological approach is used in cases without hydraulic structures and the backwater effects can be neglected. On the other hand, the hydraulic approach is implemented in cases where some hydraulic structures (weirs specifically) are present, therefore having strong backwater effects and requiring the use of hydraulic models.

Regarding the hydrological cases, two different spatial schemes are tested. The first one is a low resolution scheme, namely non-discrete approach, in which the whole catchment is represented by a single node in which the mass balance is calculated and one single downstream branch in which the ANN is used to calculate discharge. The second approach is a high-resolution scheme, namely the discrete approach, in which a series of nodes and branches represents the system under study. Both approaches are validated in the numerical case as well as in the real-world case (Pirapora - Brazil) and the results show

that the grey-box model with discrete approach can outperform some other classical hydrological approaches, such as Linear Reservoir and Muskingum.

From the numerical case, it is clear that the spatial discretization is necessary for the model to be able to capture fast dynamics that can be caused by fast reacting inflows. Nevertheless, the real-world case shows a better performance for the discrete-approach, which reveals that it is possible that an error accumulation on the propagation of the flow from node to node can cause a decay in the performance of the model. So it is necessary to evaluate the level of discretization, i.e, the number of nodes used, so as to be enough to be able to capture the system dynamics, but still avoiding error accumulation.

Another limitation lies in the values near the calibration boundaries of the Artificial Neural Networks. It is important to do some analysis of the generated surface after calibration, in order to guarantee that there are no negative values neighbouring the calibration range. As long as these negative values does not start to appear in the simulation, the model is stable.

Concerning the hydraulic models, they consist into using an algebraic function as a substitute for the momentum equation. Hydraulic structure equations are used for the weirs. The full-hydrodynamic model represents the observed data, and the grey-box model is calibrated using inertial model, built in RTC-Tools. The model performance is compared with other hydraulic models, such as kinematic wave and diffusive wave, showing comparable results.

This approach shows that a polynomial function can be used as a replacement of the momentum equation with good accuracy, as long as the function is calibrated using a reasonable range of data. The validation results, especially for the Main River case, show that the model is even able to extrapolate, i.e, it is stable even outside the calibration range. The limitations of this polynomial function are in the presence of negative values even with the positive difference of the water levels, which can cause negative flows and make the model unstable. Due to this, it is better to replace the polynomial function by a lookup table with the same values, but replacing the negative ones using linear extrapolation, for instance.

The investigation performed in the current work shows that the grey-box models have good stability, and can be used for extrapolation to a certain range.

The experiments using non-discrete and discrete approach with the hydrological grey-box model shows that this type of grey-box models is better implemented using high spatial resolution in order to properly represent the dynamics of the river. Nonetheless the discretization can also lead to error accumulation, as shown in the experiments for the real-world case Pirapora, Brazil. So a balance is necessary between number of nodes, as the lack of them may lead to a model which can not assimilate the system dynamics, and the excess of these ones may lead to error accumulation.

The experiments with the hydraulic grey-box models shows that these models succeed to give optimal results of the control procedures that must be taken in order to keep water levels in a certain operating point, or to avoid floods by compensating the water levels upstream and downstream the endangered area. The fact that these models converged to a result similar to the detailed model shows that the extrapolation capabilities are reasonable and the model results are reliable in a real-world case application.

Regarding computational performance, there are clear differences between the grey-box models and the full-hydrodynamic one. For instance, the simulation of the full-hydrodynamic Pirapora for the whole period of data available (4 years) took 64 seconds, wile the discrete grey-box model using ANN with 15 hidden neurons and C compiled code took approximately 6 seconds, or 10 times faster. The simulation of Main River full-hydrodynamic model, for the period of 01.01.2002 until 01.02.2002 took approximately 20 minutes. On the other hand, the grey-box model using C compiled code took approximately 0.4 seconds to simulate a path that corresponds to 1/4 of the full-hydrodynamic model, meaning that it was more than 700 times faster.

5.2 Outlook

Some suggestions for future research as well as some research topics are highlighted, which may broaden the application and knowledge of grey-box models in hydrology and hydraulics, focusing in the flood forecasting:

- To test grey-box models validity using stochastic forecasts.
- Currently, the grey-box models depend on the existence of another model for calibration. This may be improved by making the grey-box dependable only on observed data, instead of on the existence of a highly accurate model.

- Evaluation of the limits of validity of the grey-box model, as the calibration range is increased or reduced, by limiting the calibration data.
- Evaluation of the applicability of the hydrological grey-box model as an adjunct model in the operation process of hydro-reservoirs. Specifically, evaluate the coupling of the Pirapora case grey-box model for the operation of the TrêsMarias Reservoir.

Bibliography

Rhein-Main-Donau: Daten und Fakten. URL `http://www.rmd.de/daten.php`.

M. Abbott, J. C. Bathurst, J. a. Cunge, and J. L. Rasmussen. An introduction to the European Hydrological System - Systeme Hydrologique Europeen, "SHE", 2: Structure of a physically-based, distributed modelling system. *Journal of Hydrology*, 1-2:61–77, 1986.

T. S. Abdulkadir, a. W. Salami, a. R. Anwar, and a. G. Kareem. Modelling of hydropower reservoir variables for energy generation: neural network approach. *Ethiopian Journal of Environmental Studies and Management Vol.*, 6(3): 310–316, 2013.

N. A. Abebe, F. L. Ogden, and N. R. Pradhan. Sensitivity and uncertainty analysis of the conceptual HBV rainfall–runoff model: Implications for parameter estimation. *Journal of Hydrology*, (389):301–310, 2010.

R. J. Abrahart, F. Anctil, P. Coulibaly, C. W. Dawson, N. J. Mount, L. M. See, a. Y. Shamseldin, D. P. Solomatine, E. Toth, and R. L. Wilby. Two decades of anarchy? Emerging themes and outstanding challenges for neural network river forecasting. *Progress in Physical Geography*, 36(4):480–513, 2012. ISSN 0309-1333. doi: 10.1177/0309133312444943.

T. Ackermann, D. P. Loucks, D. Schwanenberg, and M. Detering. REAL-TIME MODELING FOR NAVIGATION AND HYDROPOWER IN THE RIVER MOSEL. *JOURNAL OF WATER RESOURCES PLANNING AND MANAGEMENT*, 126(October):298–303, 2000.

G. Acuña, F. Cubillos, J. Thibault, and E. Latrille. Comparison of Methods for Training Grey- Box Neural Network Models. *Process Engineering*, 2003.

H. Ajami, U. Khan, N. K. Tuteja, and A. Sharma. Development of a computationally efficient semi-distributed hydrologic modeling application for soil

moisture, lateral flow and runoff simulation. *Environmental Modelling & Software*, 85:319–331, 2016. ISSN 13648152. doi: 10.1016/j.envsoft.2016.09.002. URL http://dx.doi.org/10.1016/j.envsoft.2016.09.002.

ANA. Projeto de gerenciamento Integrado das atividades desenvolvidas em terra na bacia do São Francisco. *Agência Nacional de Águas*, page 140, 2003.

M. Aqil, I. Kita, A. Yano, and N. Soichi. Decision Support System for Flood Crisis Management using Artificial Neural Network. *International Journal of Intelligent Technology*, 1(1):70–76, 2006. URL http://search.ebscohost.com/login.aspx?direct=true{&}profile=ehost{&}scope=site{&}authtype=crawler{&}jrnl=13056417{&}AN=21582790{&}h=/JO2mZlwr+0i+Xtcc4YEaXFc6BflIdNCNvJrTCIhru4Vb+ezjb8Kco3m2fE9ulSitJHy+Qd+bUZLKIin8+SnTw=={&}crl=c.

P. D. Bates, M. S. Horritt, and T. J. Fewtrell. A simple inertial formulation of the shallow water equations for efficient two-dimensional flood inundation modelling. *Journal of Hydrology*, 387(1-2):33–45, 2010. ISSN 00221694. doi: 10.1016/j.jhydrol.2010.03.027. URL http://dx.doi.org/10.1016/j.jhydrol.2010.03.027.

E. Bautista, T. S. Strelkoff, and A. J. Clemmens. General Characteristics of Solutions to the Open-Channel Flow, Feedforward Control Problem. *Journal of Irrigation and Drainage Engineering*, 129(2):129–137, apr 2003. ISSN 0733-9437. doi: 10.1061/(ASCE)0733-9437(2003)129:2(129). URL http://ascelibrary.org/doi/10.1061/{%}28ASCE{%}290733-9437{%}282003{%}29129{%}3A2{%}28129{%}29.

Bayerisches Landesamt für Umwelt. Bayern Atlas, 2017. URL https://geoportal.bayern.de/bayernatlas.

M. Baymani-Nezhad and D. Han. Comparative study of IHACRES model optimisation schemes. *Proceedings of the Institution of Civil Engineers - Water Management*, 167(4):194–205, apr 2014. ISSN 1741-7589. doi: 10.1680/wama.12.00055. URL http://www.icevirtuallibrary.com/doi/10.1680/wama.12.00055.

S. Bergström. Development and Application of a conceptual runoff model fro Scandinavian catchment. (January):153, 1976.

S. Bergström, G. Lindström, and A. Pettersson. Multi-variable parameter estimation to increase confidence in hydrological modelling. *Hydrological Processes*, 16(2):413–421, feb 2002. ISSN 08856087. doi: 10.1002/hyp.332. URL http://doi.wiley.com/10.1002/hyp.332.

K. Beven and J. Freer. A dynamic TOPMODEL. *Hydrological Processes*, 15(10): 1993–2011, 2001. ISSN 08856087. doi: 10.1002/hyp.252.

A. Breinholt, F. Ö. Thordarson, J. K. Møller, M. Grum, P. S. Mikkelsen, and H. Madsen. Grey-box modelling of flow in sewer systems with state-dependent diffusion. *Environmetrics*, (22):946–961, 2011. doi: 10.1002/env.1135.

T. E. o. E. Britannica. Main river, 2008. URL https://www.britannica.com/place/Main-River.

CEMIG. Energia da Gente - 50 Anos de Três Marias. *Informativo Mensal Para Os Empregados Da Cemig*, ANO IX(91):1–12, 2012.

F.-J. Chang and Y. C. Chen. A counterpropagation fuzzy-neural network modeling approach to real time streamflow prediction. *Journal of Hydrology*, 245 (1-4):153–164, 2001. ISSN 00221694. doi: 10.1016/S0022-1694(01)00350-X.

K. W. Chau. Application of the Preissmann scheme on flood propagation in river systems in difficult terrain. *Hydrology in Mountainous Regions*, 193, 1990. URL http://hydrologie.org/redbooks/a193/iahs{_}193{_}0535.pdf.

K.-w. Chau and C.-l. Wu. Hydrological Predictions : Using Data-Driven Models Coupled with Data Preprocessing Techniques. (December), 2010.

Y. M. Chiang, L.-C. Chang, and F.-J. Chang. Comparison of static-feedforward and dynamic-feedback neural networks for rainfall-runoff modeling. *Journal of Hydrology*, 290(3-4):297–311, 2004. ISSN 00221694. doi: 10.1016/j.jhydrol.2003.12.033.

V. Chow, D. R. Maidment, and L. Mays. *Applied Hydrology*. McGraw-Hill Book Company Inc., New York City, USA, 1988.

COIN-OR. Ipopt home page, 2016. URL https://projects.coin-or.org/Ipopt.

G. Corzo, D. P. Solomatine, Hidayat, M. de Wit, M. Werner, S. Uhlenbrook, and R. Price. Combining semi-distributed process-based and data-driven models in flow simulation: a case study of the Meuse river basin. *Hydrology and Earth System Sciences Discussions*, 13(9):1619–1634, 2009. ISSN 1607-7938. doi: 10.5194/hessd-6-729-2009.

B. Croke, F. Andrews, A. Jakeman, S. Cuddy, and A. Luddy. Redesign of the IHACRES rainfall-runoff model. *29th Hydrology and Water Resources Symposium, Water Capital, Engineers Australia*, 2005. URL `https://toolkit.ewater.org.au/Tools/IHACRES/PublicationDetail.aspx?id=1000023{&}publicationID=1000110`.

J. a. Cunge. On The Subject Of A Flood Propagation Computation Method (Musklngum Method). *Journal of Hydraulic Research*, 7(2):205–230, 1969. ISSN 0022-1686. doi: 10.1080/00221686909500264.

A. C. da Cunha, D. C. Brito, A. C. B. Junior, L. A. d. R. Pinheiro, H. F. A. Cunha, E. Santos, and A. V. Krusche. Challenges and Solutions for Hydrodynamic and Water Quality in Rivers in the Amazon Basin. *Hydrodynamics - Natural Water Bodies*, 3:67–88, 2012.

K. M. De Bruijn. *Resilience and flood risk management*. PhD thesis, 2005.

D. S. de Mendonça and F. C. R. de Souza. INUNDAÇÕES: UMA ANÁLISE NA PERSPECTIVA CLIMATOLÓGICA E URBANA. In *Anais XVI Encontro Nacional de Geógrafos*, pages 1–9, 2010. ISBN 9788599907023.

N. J. de Vos. *Computational Intelligence in Rainfall–Runoff Modeling*. 2009. ISBN 9789085595854.

P. Deka and V. Chandramouli. Fuzzy Neural Network Model for Hydrologic Flow Routing. *Journal of Hydrologic Engineering*, 10(4):302–314, 2005.

Deltares. *SOBEK User Manual*. Deltares, Delft, The Netherlands, 2015.

A. Dey and R. Ayyagari. Robust PID Controller design using Fuzzy Pole Placement Techniques. *IFAC-PapersOnLine*, 49(1):789–794, 2016. ISSN 24058963. doi: 10.1016/j.ifacol.2016.03.153. URL `http://linkinghub.elsevier.com/retrieve/pii/S2405896316301537`.

C. Doulgeris, P. Georgiou, D. Papadimos, and D. Papamichail. Evaluating three different model setups in the MIKE 11 NAM model. *Advances in the Research of Aquatic Environment*, 1(Dhi 2009):pp 241–249, 2011. doi: 10.1007/978-3-642-19902-8.

M. Franchini. Use of a genetic algorithm combined with a local search method for the automatic calibration of conceptual rainfall-runoff models. *Hydrological Sciences Journal*, 41(1):21–39, 1996. ISSN 0262-6667. doi: 10.1080/02626669609491476.

M. Franchini, J. Wendling, C. Obled, and E. Todini. Physical interpretation and sensitivity analysis of the TOPMODEL. *Journal of Hydrology*, 175(1-4):293–338, 1996. ISSN 00221694. doi: 10.1016/S0022-1694(96)80015-1.

C. A. Guimarães Santos and G. B. L. D. Silva. Daily streamflow forecasting using a wavelet transform and artificial neural network hybrid models. *Hydrological Sciences Journal*, 59(2):312–324, 2014. ISSN 0262-6667. doi: 10.1080/02626667.2013.800944. URL http://dx.doi.org/10.1080/02626667.2013.800944.

M. H. Kashani, M. A. Ghorbani, Y. Dinpashoh, and S. Shahmorad. Integration of Volterra model with artificial neural networks for rainfall-runoff simulation in forested catchment of northern Iran. *Journal of Hydrology*, 540:340–354, sep 2016. ISSN 00221694. doi: 10.1016/j.jhydrol.2016.06.028. URL http://linkinghub.elsevier.com/retrieve/pii/S0022169416303791.

M. Hafezparast. A Conceptual Rainfall-Runoff Model Using the Auto Calibrated NAM Models in the Sarisoo River. *Journal of Waste Water Treatment & Analysis*, 04(01):1–6, 2013. ISSN 21577587. doi: 10.4172/2157-7587.1000148.

A. Hassan, T. Norio, and T. Nobuyuki. Distributed water balance with river dynamic-diffusive flow routing model. *Journal of Hydrodynamics, Ser. B*, 21(4):564–572, aug 2009. ISSN 10016058. doi: 10.1016/S1001-6058(08)60185-7. URL http://linkinghub.elsevier.com/retrieve/pii/S1001605808601857.

J. Hauth. Grey-Box Modelling for Nonlinear Systems. page 357, 2008. URL https://kluedo.ub.uni-kl.de/frontdoor/deliver/index/docId/2045/file/diss.pdf.

H. Jaeger. A tutorial on training recurrent neural networks , covering BPPT , RTRL , EKF and the " echo state network " approach. *ReVision*, 2002:1–46, 2005.

M. R. Khazaei, B. Zahabiyoun, B. Saghafian, and S. Ahmadi. Development of an Automatic Calibration Tool Using Genetic Algorithm for the ARNO Conceptual Rainfall-Runoff Model. *Arabian Journal for Science and Engineering*, 39(4):2535–2549, apr 2014. ISSN 1319-8025. doi: 10.1007/s13369-013-0903-8. URL http://link.springer.com/10.1007/s13369-013-0903-8.

D. F. Kibler and D. A. Woolhiser. The Kinematic Cascade as a Hydrologic Model. *Hydrologic Papers*, 1970. URL https://dspace.library.colostate.edu/bitstream/handle/10217/61319/HydrologyPapers{_}n39.pdf?sequence=1.

Ö. Kişi. Streamflow forecasting using different artificial neural network algorithms. *Journal of Hydrologic Engineering*, (October):532–539, 2007. ISSN 10840699. doi: 10.1061/(ASCE)1084-0699(2007)12:5(532). URL http://ascelibrary.org/doi/abs/10.1061/(ASCE)1084-0699(2007)12:5(532).

N. N. Kourgialas and G. P. Karatzas. A hydro-sedimentary modeling system for flash flood propagation and hazard estimation under different agricultural practices. *Natural Hazards and Earth System Sciences*, 14(3):625–634, 2014. ISSN 16849981. doi: 10.5194/nhess-14-625-2014.

C. T. Kwin, A. Talei, S. Alaghmand, and L. H. Chua. Rainfall-runoff Modeling Using Dynamic Evolving Neural Fuzzy Inference System with Online Learning. *Procedia Engineering*, 154:1103–1109, 2016. ISSN 18777058. doi: 10.1016/j.proeng.2016.07.518. URL http://dx.doi.org/10.1016/j.proeng.2016.07.518.

A. Lacasta, M. Morales-Hernández, P. Brufau, and P. García-Navarro. Simulation of PID Control Applied to Irrigation Channels. *Procedia Engineering*, 70:978–987, 2014. ISSN 18777058. doi: 10.1016/j.proeng.2014.02.109.

D. Lawrence, I. Haddeland, and E. Langsholt. *Calibration of HBV hydrological models using PEST parameter estimation*. 2009. ISBN 9788241006807. URL http://www.google.de/url?sa=t{&}rct=j{&}q={&}esrc=s{&}source=web{&}cd=1{&}ved=0CCAQFjAA{&}url=http://www.nve.no/

Global/Publikasjoner/Publikasjoner2009/Report2009/report1-09.pdf{&}ei=eVXaU4uGEsn04QTptoHQCA{&}usg=AFQjCNE344Hd3c7Ln76DRQWqDVmv-U-oVQ{&}bvm=bv.72185853,d.bGE.

R. A. Letcher, S. Y. Schreider, A. J. Jakeman, B. P. Neal, and R. J. Nathan. Methods for the analysis of trends in streamflow response due to changes in catchment condition. *Environmetrics*, 12(7):613–630, nov 2001. ISSN 1180-4009. doi: 10.1002/env.486. URL http://doi.wiley.com/10.1002/env.486.

G. C. Liang and J. E. Nash. Linear models for river flow routing on large catchments. *Journal of Hydrology*, 103(1-2):157–188, 1988. ISSN 00221694. doi: 10.1016/0022-1694(88)90012-1.

G. Lindström, B. Johansson, M. Persson, M. Gardelin, and S. Bergström. Development and test of the distributed HBV-96 hydrological model. *Journal of Hydrology*, 201(1-4):272–288, 1997. ISSN 00221694. doi: 10.1016/S0022-1694(97)00041-3.

X. Litrico and D. Georges. Robust continuous-time and discrete-time flow control of a dam–river system. (II) Controller design. *Applied Mathematical Modelling*, 23(11):829–846, 1999. ISSN 0307904X. doi: 10.1016/S0307-904X(99)00013-X.

Z. Liu and E. Todini. Towards a comprehensive physically-based rainfall-runoff model. *Hydrology and Earth System Sciences*, 6(5):859–881, 2002. ISSN 16077938. doi: 10.5194/hess-6-859-2002.

J. López, F. Gimena, M. Goñi, and U. Agirre. Analysis of a unit hydrograph model based on watershed geomorphology represented as a cascade of reservoirs. *Agricultural Water Management*, 77(1-3):128–143, aug 2005. ISSN 03783774. doi: 10.1016/j.agwat.2004.09.025. URL http://linkinghub.elsevier.com/retrieve/pii/S0378377405000958.

J. Mateo Lázaro, J. Á. Sánchez Navarro, A. García Gil, and V. Edo Romero. A new adaptation of linear reservoir models in parallel sets to assess actual hydrological events. *Journal of Hydrology*, 524:507–521, may 2015. ISSN 00221694. doi: 10.1016/j.jhydrol.2015.03.009. URL http://linkinghub.elsevier.com/retrieve/pii/S0022169415001808.

C. Mathworks. Simulink User's Guide R 2014 b. 2014.

R. A. Montero, D. Schwanenberg, M. Hatz, and M. Brinkmann. Simplified hydraulic modelling in model predictive control of flood mitigation measures along rivers. *Journal of Applied Water Engineering and Research*, 1(November):17–27, 2013. ISSN 2324-9676. doi: 10.1080/23249676.2013.827897. URL http://www.tandfonline.com/doi/abs/10.1080/23249676.2013.827897.

J. E. Nash. The form of instantaneuous unit hydrograph. *Int Assoc Sci Hydrol*, 51:546–557, 1958.

R. C. D. Paiva, W. Collischonn, and D. C. Buarque. Validation of a full hydrodynamic model for large-scale hydrologic modelling in the Amazon. *Hydrological Processes*, 27(3):333–346, 2013. ISSN 08856087. doi: 10.1002/hyp.8425.

R. Peters, G. Schmitz, and J. Cullmann. Flood routing modelling with Artificial Neural Networks. *Advances In Geosciences*, 9:131–136, 2006.

F. Petrone. Model Predictive Control of a Hydro Power Valley. (June), 2010.

L. Raso, D. Schwanenberg, N. V. D. Giesen, and P. J. V. Overloop. Short-term Management of Water Systems using Ensemble Forecasts in Tree-Based Model Predictive Control. *Advances in Water Resources*, 2013.

Z. Ren-Jun. The Xinanjiang model applied in China. *Journal of Hydrology*, 135 (1-4):371–381, 1992. ISSN 00221694. doi: 10.1016/0022-1694(92)90096-E.

I. d. M. A. e. d. R. N. Renováveis. São Francisco - Caderno da Região Hidrográfica, 2006.

J.-D. Rinaudo. Long-Term Water Demand Forecasting. In Q. Grafton, K. A. Daniell, C. Nauges, J.-D. Rinaudo, and N. W. W. Chan, editors, *Understanding and Managing Urban Water in Transition*, pages 239–268. Springer Netherlands, Dordrecht, 2015. ISBN 978-94-017-9801-3. doi: 10.1007/978-94-017-9801-3_11. URL http://dx.doi.org/10.1007/978-94-017-9801-3{_}11.

R. Rojas. Neural Networks. In *Springer-Verlag*, Berlin, 1996.

P. Roy, P. S. Choudhury, and M. Saharia. Dynamic ANN modeling for flood forecasting in a river network. In *International Conference on Modeling, Optimization, and Computing*, volume 1298, pages 219–225, 2010. ISBN 9780735408548. doi: 10.1063/1.3516305.

N. Sajikumar and B. S. Thandaveswara. A non-linear rainfall-runoff model using an artificial neural network. *Journal of Hydrology*, 216(1-2):32–55, 1999. ISSN 00221694. doi: 10.1016/S0022-1694(98)00273-X.

J. Sand and S. Skelboe. Stability of backward Euler multirate methods and convergence of waveform relaxation. *BIT Numerical Mathematics*, 32:350–366, 1992. ISSN 15729125. doi: 10.1007/BF01994887.

D. Schwanenberg and B. Becker. RTC-Tools, 2014.

D. Schwanenberg, B. Becker, and B. Becker. Real Time Control Tools User Manual, 2012.

J. Shiri and O. Kisi. Short-term and long-term streamflow forecasting using a wavelet and neuro-fuzzy conjunction model. *Journal of Hydrology*, 394(3-4):486–493, 2010. ISSN 00221694. doi: 10.1016/j.jhydrol.2010.10.008. URL http://linkinghub.elsevier.com/retrieve/pii/S0022169410006098.

B. Sohlberg and E. W. Jacobsen. Grey Box Modelling - Branches and Experiences. In *17th World Congress The International Federation of Automatic Control*, 2008. doi: 10.3182/20080706-5-KR-1001.0607. URL http://folk.ntnu.no/skoge/prost/proceedings/ifac2008/data/papers/0607.pdf.

STFC Rutherford Appleton Laboratory. The HSL Mathematical Software Library, 2016. URL http://www.hsl.rl.ac.uk.

J. Szilagyi, G. Balint, B. Gauzer, and P. Bartha. Flow routing with unknown rating curves using a state-space reservoir-cascade-type formulation. *Journal of Hydrology*, 311(1-4):219–229, 2005. ISSN 00221694. doi: 10.1016/j.jhydrol.2005.01.017.

A. Szöllösi-Nagy. The discretization of the continuous linear cascade by means of state space analysis. *Journal of Hydrology*, 58(3-4):223–236, sep 1982. ISSN 00221694. doi: 10.1016/0022-1694(82)90036-1. URL http://linkinghub.elsevier.com/retrieve/pii/0022169482900361.

X.-N. Tang, D. W. Knight, and P. G. Samuels. Volume Conservation in Variable Parameter Muskingum-Cunge Method. *Journal of Hydraulic Engineering*, 125 (6):610–620, 1999.

The World Bank and United Nations. *Natural Hazards, UnNatural Disasters*. 2010. ISBN 9780821380505.

E. Todini. The ARNO rainfall—runoff model. *Journal of Hydrology*, 175(1-4):339–382, 1996. ISSN 00221694. doi: 10.1016/S0022-1694(96)80016-3. URL http://linkinghub.elsevier.com/retrieve/pii/S0022169496800163.

E. Todini. A mass conservative and water storage consistent variable parameter Muskingum-Cunge approach. *Hydrology and Earth System Sciences Discussions*, 11:1645–1659, 2007. ISSN 1812-2116. doi: 10.5194/hessd-4-1549-2007.

E. Toth and A. Brath. Flood Forecasting Using Artificial Neural Networks in Black-Box and Conceptual Rainfall-Runoff Modelling. *The International Environmental Modelling and Software Society*, pages 166–171, 2002.

M. Vafakhah, S. Janizadeh, and S. K. Bozchaloei. Application of Several Data-Driven Techniques for Rainfall-Runoff Modeling. 2(1):455–469, 2014.

B. Van den Zegel, E. Vermuyten, V. Wolfs, P. Meert, and P. Willems. Real-time control of floods along the Demer River, Belgium, by means of MPC in combination with GA and a fast conceptual river model. *Proceedings of 11th International Conference on Hydroinformatics (HIC 2014)*, pages 1–8, 2014.

P. J. Van Overloop, R. R. Negenborn, D. Schwanenberg, and B. De Schutter. Towards integrating water prediction and control technology. *2011 International Conference on Networking, Sensing and Control, ICNSC 2011*, (April):80–85, 2011. doi: 10.1109/ICNSC.2011.5874940.

S. C. van Pelt, P. Kabat, H. W. ter Maat, B. J. J. M. van den Hurk, and A. H. Weerts. Discharge simulations performed with a hydrological model using bias corrected regional climate model input. *Hydrology and Earth System Sciences*, 13(12):2387–2397, dec 2009. ISSN 1607-7938. doi: 10.5194/hess-13-2387-2009. URL http://www.hydrol-earth-syst-sci.net/13/2387/2009/.

A. Wächter and L. T. Biegler. *On the Implementation of a Primal-Dual Interior Point Filter Line Search Algorithm for Large-Scale Nonlinear Programming*, volume 106. 2006. ISBN 1010700405.

W. Wang. *Sochasticity, nonlinearity and forecasting of streamflow processes*. 2006. ISBN 1586036211.

Wasserstrassen und Schifffahrtverwaltung des Bundes. Generaldirektion Wasserstraßen und Schifffahrt -Außenstelle Süd-, 2010. URL http://

www.wsd-sued.wsv.de/wasserstrassen/bundeswasserstrassen/main/index.html.

L. J. Weber. The Hydraulics of Open Channel Flow: An Introduction. *Journal of Hydraulic Engineering*, 127(3):246–247, 2001. ISSN 0733-9429. doi: 10.1061/(ASCE)0733-9429(2001)127:3(246).

V. Wolfs. *Conceptual model structure identification and calibration for river and sewer systems*. PhD thesis, 2016.

V. Wolfs and P. Willems. Development of discharge-stage curves affected by hysteresis using time varying models, model trees and neural networks. *Environmental Modelling and Software*, 55:107–119, 2014. ISSN 13648152. doi: 10.1016/j.envsoft.2014.01.021. URL http://dx.doi.org/10.1016/j.envsoft.2014.01.021.

R. Wooding. A hydraulic model for the catchment-stream problem: I-Kinematic Wave Theory. *Journal of Hydrology*, 3(3-4):254–267, nov 1965. ISSN 00221694. doi: 10.1016/0022-1694(65)90084-3. URL http://linkinghub.elsevier.com/retrieve/pii/0022169465900843.

World Meteorological Organization. *Integrated Flood Management - Concept Paper*. Number WMO-No. 1047. 2009. ISBN 978-92-63-11047-3.

M. Xu, P. J. van Overloop, and N. C. van de Giesen. Model reduction in model predictive control of combined water quantity and quality in open channels. *Environmental Modelling and Software*, 42:72–87, 2013. ISSN 13648152. doi: 10.1016/j.envsoft.2012.12.008.

H. Yonaba, F. Anctil, and V. Fortin. Comparing Sigmoid Transfer Functions for Neural Network Multistep Ahead Streamflow Forecasting. *Journal of Hydrologic Engineering*, 15(4):275–283, 2010. ISSN 1084-0699. doi: 10.1061/(ASCE)HE.1943-5584.0000188.

X.-q. Zhang and W.-m. Bao. Modified Saint-Venant equations for flow simulation in tidal rivers. *Water Science and Engineering*, 5(2008):34–45, 2012. ISSN 16742370. doi: 10.3882/j.issn.1674-2370.2012.01.004. URL http://dx.doi.org/10.3882/j.issn.1674-2370.2012.01.004.

Appendix A

Modelling Technical Information

A.1 Cascade of linear reservoirs model

The model was written in RTC-Tools©(Schwanenberg and Becker, 2014), and the minimization problem was solved by coupling Pyhton and using pyswarm, which is a module for optimization using Particle Swarm Algorithm.

A.2 Muskingum model

The model was written in RTC-Tools©(Schwanenberg and Becker, 2014). The parameters C_0, C_1 and C_2were calibrated by coupling Pyhton and using pyswarm, which is a module for optimization using Particle Swarm Algorithm.

A.3 Inertial hydraulic model

An Inertial hydraulic model was developed using RTC-Tools©(Schwanenberg and Becker, 2014), which is an open-source, modular tool for development of models and real-time control of water systems. It may be also integrated into Matlab, Pyhton, Delft-FEWS or OpenDA. The model schematization, as well as the controller(s) configuration and parameters are written in XML format, but internal calculations are made in C++ language.

A.4 Grey-box for hydraulic flow routing

The block *weir fcn* calculated the discharge by using the weir equation as shown below.

```
function Q = weir_fcn(zs,Ws,Hup,Hdown)
```

```
Q=0;
if Hup<zs
     Q=0;
elseif (Hup-zs)>3/2*(Hdown-zs) % Free flow
     us = sqrt(2/3*9.81)*sqrt(Hup-zs);
    As = Ws*2/3*(Hup-zs);
     Q = us*As;
elseif (Hup-zs)<=3/2*(Hdown-zs) %Submerged flow
     us = sign(Hup-Hdown).*sqrt(2*9.81.*abs(Hup-Hdown));
    As = Ws.*(Hdown-zs);
    Q = us*As;
end
end
```